A STUDY ON AGE-HARDENABLE ALLOYS BY MEANS OF MÖSSBAUER EFFECT AND NUCLEAR MAGNETIC RESONANCE

SABURO NASU

A Thesis Submitted to
Kyoto University
for the Partial Requirements of
the Degree of Doctor of Engineering

August, 1970

ACKNOWLEDGEMENTS

The author would like to thank his supervisor Professor Yotaro Murakami for introducing him to the field of Physical Metallurgy and for continued encouragement and valuable advice throughout this work.

The author is indebted to Professor Yoji Nakamura of Department of Metal Science and Technology for his warmful encouragement for this work.

The author would like to thank Dr. Teruya Shinjo of Institute for Chemical Research for introducing him to the Mössbauer works and for valuable discussions.

The author is indebted to Dr. Hiroshi Yasuoka for introducing him to the study of Nuclear Magnetic Resonance in magnetic materials and for valuable discussions.

The author is also indebted to Dr. Masayuki Shiga, Mr. Michitaka Nishio and Mr. Yutaka Nishio for their helpful discussions and earnest contributions throughout this work.

Thanks are also due to Dr. Yutaka Maeda and Mr. Hiroyuki Yoshida for their assistance in the experimental works at the Research Reactor of Kyoto University.

Mr. Satoru Yamamoto supplied a experimental assistance in the preparation of one of specimens.

SUBJECT INDEX

SUBJECT INDEX(CONT.)

SUBJECT INDEX(CONT.)

SUBJECT INDEX(CONT.)

SUBJECT INDEX(CONT.)

CONTENTS

CONTENTS (CONT.)

CONTENT(CONT.)

CONTENT(CONT.)

INDEX OF FIGURES

INDEX OF FIGURES (CONT.)

INDEX OF FIGURES (CONT.)

INDEX OF FIGURES (CONT.)

INDEX OF FIGURES (CONT.)

INDEX OF TABLES

INDEX OF PHOTOGRAPH

CHAPTER I

GENERAL INTRODUCTION

Age-hardened alloys have been the subject of intensive theoretical and experimental studies in the field of physical metallurgy since on old time[1]. A considerable body of research work in the age-hardened alloys are devoted to the study of thermodynamics and kinetics of precipitation. There have been developed in progress of research techniques for the study of precipitation in alloys. The precipitates structures were firstly deduced by using X-ray diffraction techniques[2,3] and the electron microscope study of thin alloy foils reveals directly the microstructure of the alloy, i.e. it gives information on the number, size, shape and distribution of precipitates[4]. Several other techniques has been developed in the last ten years to provide valuable information on various aspects of precipitation phenomena in metal and alloys[1]. For instance, careful measurements of electrical resistance of quenched alloys have offered a powerful method for studying the decomposition of supersaturated solid solutions since large changes in resistivety can be unambigously attributed to the clustering of precipitation of solute atoms[5].

Many fruitful results from age-hardened alloys have been obtained by many investigators using the X-ray diffraction techniques, thin foil electron microscopic observations and the electrical resistivity measurements, however the accurate and more microscopic investigations, i.e. the direct

measurements of the electronic and vibrational local states of solute atoms and in precipitated particles, cannot be found in those research works. Using the usual techniques, there are a few alloy system in which the measurements for the precipitation are very difficult. Namely, the direct observation of the ultra-fine precipitated particles does not be possible and also it is very difficult even to determine the solid solubility of solute atoms in a few alloy system such as Al-Fe alloys containing small amounts of iron.

However, more microscopic investigations can be made possible by the observation of the hyperfine interactions between the nucleus of the solute atoms and their outer electrons[6], since the hyperfine interactions attributed to the gathering information about the solid. There are conveniently two experimental techniques to estimate the hyperfine interactions in metals and alloys:

1. Mössbauer effect
2. Nuclear magnetic and quadrupole resonance.

These measurements are well recognized to be powerful methods for the investigations on the solid states physics[7,8,9]; especially their measurements have been extremely developed in the field of magnetism. The first group of measurements, the Mössbauer effect, utilizes a rather special property of the excited or isomeric states of certain nuclei like Fe^{57}. The energy widths of the ground state and the excited state are extremely sharpe and a fraction, e^{-M}, of the gamma-rays,

emitted by the excited state, Fe^{57*}, are just the right energy for resonance absorption by Fe^{57} in the ground state. If the absorber is moved relative to the emitter with a velocity of only a few cm/sec, then the relative energy of the 14.4 KeV γ-ray is altered by about 10^{-7} eV and this is enough to eliminate the resonance absorption. Thus other small energy shifts such as the hyperfine interaction of the nuclear magnetic moment with local magnetic fields are sufficient to alter the resonance conditions. In such a case one determines the relative velocity necessary to re-establish the resonance condition and thus measure the energy shift and effective magnetic field at the nucleus. In the second group of measurements one measures the magnitude of the magnetic fields or electric field gradients created by the magnetic fields the position of the nucleus. pnce the nucleus is in effect a point at the center of the atom the information is limited to the magnetice of the fields at this point. In spite of this restriction it is possible to gain some information about the electron wave functions.

In this study, we attempt to apply the $Fe^{57}(Co^{57})$ Mössbauer effect and Co^{59} pulsed NMR measurements to investigate of some age-hardened alloys; Al-dilute Fe alloys, Cu-dilute Co alloys, and Cu-2wt.%Be alloy containing small amount of cobalts. From the results obtained about the hyperfine interactions, we discuss it in a view of metallurgical stand points. However, it is fact that the relative energy

shifts in Mössbauer resonance and the magnitude of the effective hyperfine field of Fe^{57} and Co^{59} nuclei are only noticed throughout this work.

In Chap. II, the Mössbauer effect study is applied the determination of the solubility of iron in solid aluminum and the precipitation in Al-dilute Fe alloys are discussed by the analysis of the Mössbauer spectra.
In Chap. III, the isomeric shifts and the second-order Doppler shifts in Mössbauer effect are estimated for the Fe solute atoms dissolved in Al matrix. In Chap. IV, the Mössbauer measurements applied to the investigation on Cu-dilute Co alloy systems; the solubility of cobalts in solid copper, a size distribution of the Co-rich particles precipitated in copper matrix, a precipitation of cobalts from copper matrix and a transformation of precipitates structure induced by cold rolling are discussed.
The Mössbauer effect study of the small additional cobalts elements in Cu-2wt.%Be alloy is discussed in Chap. V, since the Mössbauer spectrum of Fe^{57} produced by decay of Co^{57} represents the situations of the mother nucleus, Co^{57}.
In Chap. VI, the pulsed Co^{59} NMR technique is firstly applied in the most accurate estimation of the hyperfine fields of Co nucleus in the Co-rich particles precipitated in copper matrix, since the accurate values of the hyperfine fields offer new information about precipitated particles.

REFERENCES

1. A. Kelly and R. B. Nicholson; "Precipitation Hardening" in Progress in Material Science, vol. 10, edited by B. Chalmers, (Pergamon Press, 1961).

2. A. Guiner; Ann. Physique, 12 (1939) 161.

3. G. D. Preston; Proc. Roy. Soc., A-167 (1938) 526.

4. P. W, Hirsch, A. Howie, R. B. Nicholson, D. W. Pashley and M. J. Whelan; "Electron Microscopy of Thin Crystals", (Butterworths, London, 1965).

5. D. Turnbull, H. S. Rosenbaum and H. N. Treaftis; Acta Met., 8 (1960) 277.

6. A. J. Freeman and R. E. Watson; "Hyperfine Interactions in Magnetic Materials" in Magnetism, vol. II, Part A, edited by G. T. Rado and H. Suhl, (Academic Press, 1965).

7. H. Frauenfelder; The Mössbauer Effect, (W. A. Benjamin, New York, 1963).

8. G. K. Wertheim; Mössbauer Effect: Principles and Applications, (Academic Press, New York, 1964).

9. A. M. Portis and R. H. Lindquist; Magnetism, vol. II Part A, edited by G. T. Rado and H, Suhl, (Academic Press, 1965).

CHAPTER II

MÖSSBAUER EFFECT STUDY ON IRON DILUTE Al-Fe ALLOYS

II-1. Introduction

Recently, Fe^{57} Mössbauer effect studies for the aging phenomena in iron-based alloys are variously reported[1,2] and many fruitful results were obtained from these investigations. The analysis of the Mössbauer spectra is shown to be very useful and new tool for the study of the precipitation in alloy systems. The measurement of the Mössbauer spectra obtained by the solute Fe^{57} atoms dissolved in age-hardened iron dilute alloy systems is seemed to be more powerful method for the investigations of the precipitation phenomena in these alloys, since the solute atom Mössbauer effects are directly observed after the diffusive motion of the solute atom and show the properties of the precipitated second phase which was formed by Mössbauer active atoms.

For the experimental side, the Fe^{57} Mössbauer spectra have been able to easily obtain using the iron-based alloy specimens as a gamma-ray absorber, since there are many Mössbauer active nucleus of Fe^{57} in these alloy specimen. However, an Al-Fe alloy containing small amounts of iron atoms can be, of cource, used as a gamma-ray absorber in Fe^{57} Mössbauer effect experiments and the Mössbauer spectra may be observed easily, if all of the iron solute atoms in the specimen are prepared by Fe^{57}.

Small amounts of the iron impurities are usually contained in a aluminum ingot and have played considerable important parts for the properties of commercial aluminum and its alloys[3,4]. The Fe^{57} Mössbauer spectra show clearly the individual states of Fe solute atoms in Al matrix and its measurements are useful tool for the study in dilute iron in aluminum alloys. The values of solid solubilities of iron in aluminum at the various temperatures are reported to be quite small[5] and it is very difficult to determine its value as a function of temperature, because of its being quite small. The Fe^{57} Mössbauer spectra of the Al-Fe alloys containing small amounts of iron can be separated into two parts; i.e. one arising from the solute iron atoms in the aluminum matrix and the other from the precipitated second phase. The values of solid solubility of iron in aluminum at various temperatures can be estimated by the analysis of Mössbauer spectra obtained from the specimens annealed for long periods at various temperatures, enough to complete the precipitation of the equilibrium phase. The changes of the thermodynamic properties resulted from the solution in this alloy can be estimated from the relation between the values of solid solubility and the temperatures. Furthermore, the complete investigations for the diffusion of iron in aluminum can not be finished. The temperature dependence of the diffusion coefficient for these Al-dilute Fe alloy specimens are reported in previous two papers[6,7], but the results obtained by

these two papers are not in good agreement in values.

Mössbauer effect study of the precipitation phenomena in Al-0.01at.%Fe^{57} alloy can be made possible by the analysis of the Mössbauer spectra, as above mentioned. The effects of cold working on the precipitation kinetics in this alloy is one of the most interesting subject suggested previously by Hirano et al.[6], since the diffusive motion might be interpreted in terms of the pipe diffusion along dislocations.

In Sec. II-2 are described the sample preparation and experimental procedures in this study. Experimental results and its interpretations are given by Sec. II-3. The values of the solid solubility obtained from the Mössbauer spectra and the discussion for the thermodynamic properties in this solution are presented in Sec. II-3-1 and Sec. II-3-2, respectively. In Sec. II-3-3 are described the precipitation study in Al-0.01at.%Fe alloy and the effects of cold working for this alloy specimen are also reported in Sec. II-3-4.

II-2. Sample Preparation and Experimental Procedures

The tools required for a demonstration of the Mössbauer effect are fundamentally those encountered in gamma-ray spectroscopy. The experiments in this chapter were performed in transmission geometry and required a radio-active source, Co^{57} in Cu plate, an absorber which was made up as a specimen and a gamma-ray detecter and a energy modulation system which consists of commercial Mössbauer apparatus; T. M. C. set (Gammascope 102, Drive Unit 306 and Transducer 305)

operated in a time mode.

Al-0.01∿0.05at.%Fe^{57} alloys were prepared by melting from 99.999%Al and Fe^{57} powders which were obtained by deoxidation of $Fe_2^{57}O_3$ powders (ORNL Stable Isotope, Fe^{57} 90% Up) in hydrogen atmoshpere. This ingots were homogenized for 1 day at 643°C after rolling of 50% reduction in thickness at room temperature. The resultant grain size is estimated to be about 2 mm and does not change its value during subsequent theat treatments. For the discussion in the Sec. II-3-3 and II-3-4, the grain size is large enough to eliminate grain boundary diffusion and we made it negligible. The platellet alloy specimens of various thickness are cut out from this alloy ingots. The thickness of the specimen at the Mössbauer measurements is selected to be 0.5 mm because of the best condition for the 14.4 KeV gamma-rays by the specimen. Detailed discussions and the determination of the specimen thickness for the Mössbauer measurements are presented in CHAPTER III.

All of the alloy specimens were annealed for 1 day at 643°C as a solution heat treatment and then quenched into water. For the determination of the solid solubility of iron in aluminum, Al-0.01∿0.05at.%Fe alloys were used as a specimens. These alloy specimens were annealed for 30 days at the temperatures above 450°C. The measurements of the Mössbauer spectra were always carried out at room temperature. For the precipitation study, a typical alloy composition of Al-0.01at.%Fe^{57} was used as a alloy specimen.

The solution heat treatment was done by annealing for 1 day at 643°C and quenching into water samely in the study of solid solubility determination. For the subsequent aging treatments the specimens were annealed for various time at 300°C, 450°C and 500°C. For cold working prior to the aging treatments, the several specimens were rolled or pressed at room temperature and also pressed in the liquid nitrogen bath. The Mössbauer measurements for the specimen rolled at 77°K were carried out at 95°K using the coolant being shown in Fig. 1. The procedure of the pressing at 77°K is shown in Fig. 2. The values of the isomer shift are always estimated relative to that of Fe^{57} in α-iron. The analysis of the Mössbauer spectra was carried out by the aid of the computer (Kyoto University Degital Computer No. 2 : commercial name is HITAC-5020).

II-3. Experimental Results and Interpretations

II-3-1. Solubility of Iron in Solid Aluminum

Observed Mössbauer spectrum is represented by the linear combination of the Loretzian functions associated with the various environments of Fe^{57} nucleus, if the different phase containing Fe^{57} atoms exists in the specimen. In these spectra, the magnitude of the resonant absorption Y(X) as a function of Doppler velocity X is given by

$$Y(X) = \sum_i \frac{A_i}{1+4(B_i-X)^2/C_i^2} , \qquad \text{(II-1)}$$

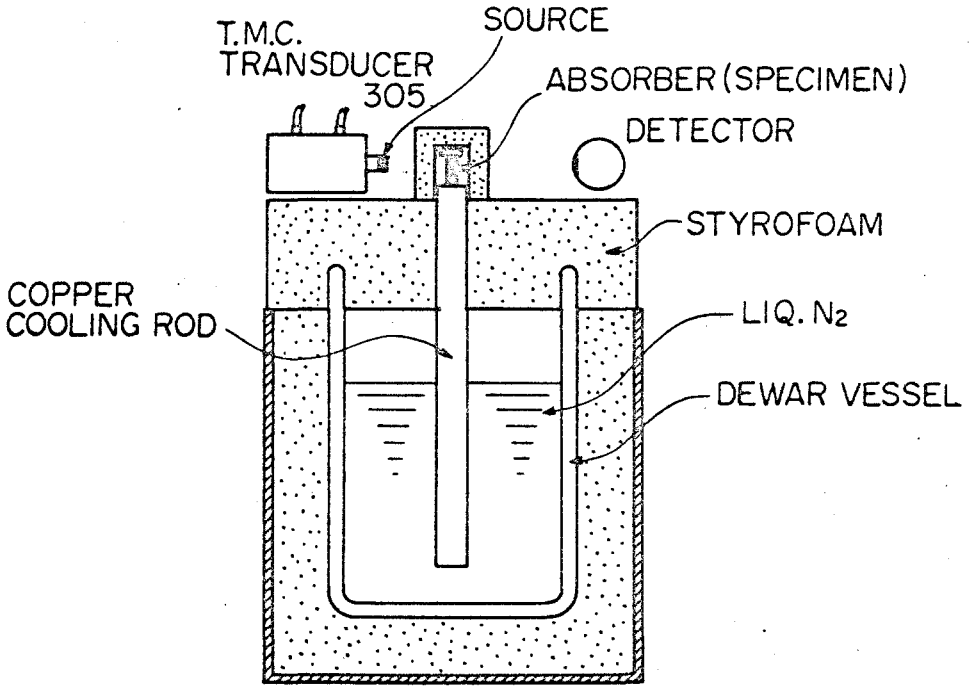

FIG. 1 Constitution of the cryostat for cooling the absorber.

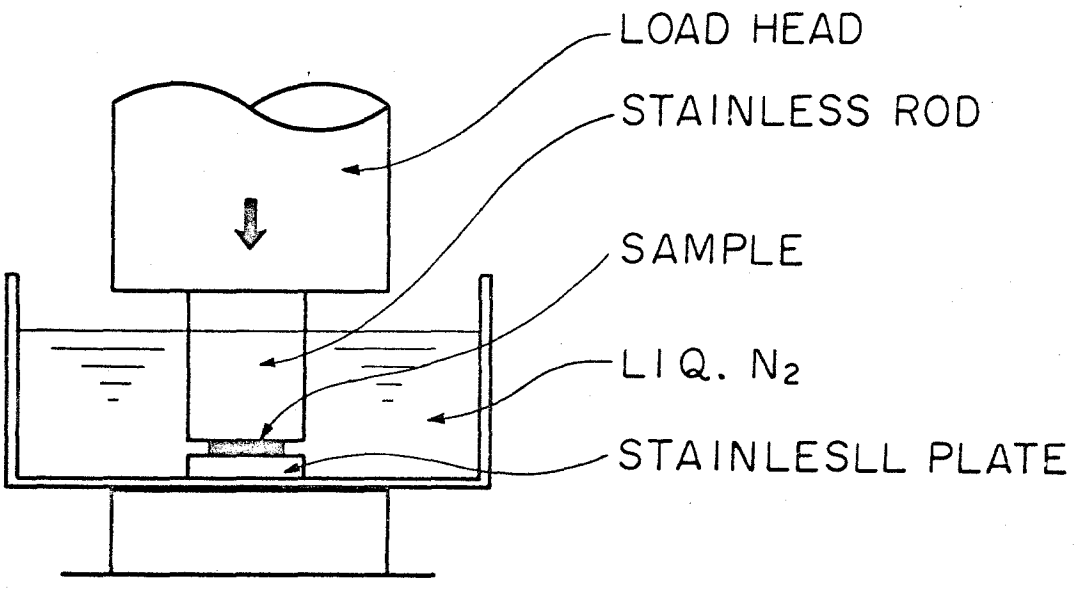

FIG. 2 Illustration for the procedure of pressing of specimen in the liquid nitrogen bath.

where A_i, B_i and C_i show the maximum cross section, peak position and the half-width of the absorption curve associated with the Fe^{57} nucleus in i-th phase. Therefore, if the Al-Fe alloy specimen are annealed for a long time enough to reach the eqilibrium state, the Mössbauer spectrum measured by these alloy specimens should be shown as a superposition of the spectrum arising from the Fe^{57} nucleus dissolved in Al matrix and the Fe^{57} atoms constructed the precipitated second phase Al_3Fe. From Eq. II-1, the Mössbauer spectra expected by Al-Fe alloy specimens containing small amounts of Fe^{57} atoms are written as a next form of

$$Y(X) = \left[\frac{A_o}{1+4(B_o-X)^2/C_o^2} \right]_{\text{Fe in Al}} + \left[\frac{A_1}{1+4(B_1-X)^2/C_1^2} + \frac{A_2}{1+4(B_2-X)^2/C_2^2} \right]_{Al_3Fe}, \qquad \text{(II-2)}$$

where suffix "o" is given by the Fe^{57} nucleus in the Al-Fe alloy matrix and "1" & "2" show that of the precipitated second phase Al_3Fe, since the Fe^{57} Mössbauer spectrum results obtained by Al_3Fe shows as a superposition of two Lorentzian absorption curve having the same parameters except for the peak position[8]. In Eq. II-2, the first term in the right members represents the single Lorentzian curve obtained by the Fe^{57} atoms in solid solution and the second and third terms show the double Lorentzian curve arising

from the Fe^{57} atoms in Al_3Fe. Figure 3 shows the Mössbauer spectrum analized by the aid of computer. This spectrum was obtained by the Al-Fe alloy specimen which contains small amounts of the Fe^{57} atoms and was annealed for 11 days at 450°C prior to the measurement. Results obtained by the least-square fit of data to the individual Lorentz function in Eq. II-2 represent as "$_*$" and experimental results are given by white circles and also large black dot indicates a superposition of analysed doublet curve and a single one.

Assuming the value of Mössbauer fraction for the Fe^{57} nucleus indicate the same value in each of alloy phases, that is, in Eq. II-2 the magnitudes of A_o, A_1 and A_2 are simply proportional to the amounts of Fe^{57} atoms; the amounts of Fe atoms in each alloy phases can be estimated by the integrated intensity ratio of the individual Lorentzian type absorption spectra, since the total integrated absorption area, $\int Y(X)dX$, is attributed to the total amounts of Fe^{57} atoms in the specimen.

If the values of the Mössbauer fraction are different in each other, the corrected integrated intensity ratio can be estimated by the production of the inverse of the Mössbauer fraction to the observed integrated intensity ratio. From the simple arguments, the total iron concentration C_o in the alloy being reached at the equilibrium state can be easily calculated by the values

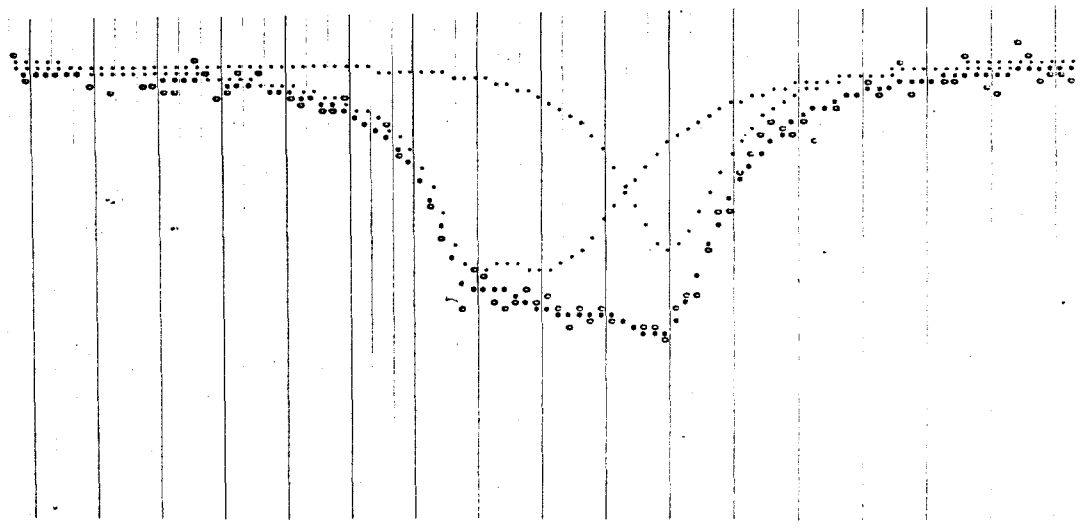

FIG. 3 Analysed Mössbauer spectrum which was plotted by compute.

O : experimental results

● : amalysed doublet and single line; doublet indicates the Al_3Fe phase and single line shows the dissolved iron atoms in aluminum matrix

• : superposition of analysed doublet and single line.

of Fe concentration in the alloy matrix C_1 and in the precipitated second phase C_2. Then C_o is given by

$$C_o = C_1(1 + r)/\{ 1 + (C_1/C_2) \cdot r \}, \quad \text{(II-3)}$$

where r indicates the ratio of the numbers of Fe^{57} atoms in the alloy matrix to that of Fe^{57} in the precipitated second phase. Using the two alloy specimens which have two different values only for C_o, the values of C_1 and C_2 are experimentally determined from the value of r which can be estimated by the integrated intensity ratio in the Mössbauer spectra as being described in Eq. II-2.

Figure 4 shows the two Mössbauer spectra obtained from the Al-0.01at,%Fe^{57} alloy specimen. Upper spectrum in Fig. 4 was measured by the specimen which was quenched into water immediately after the solution heat treatment at 650°C. A completes single line is shown in the upper spectrum and it is resulted from the isolated Fe^{57} atoms in alloy matrix. However, the lower spectrum was measured by the specimen whose composition is same as that for the upper spectrum, but that specimen was aged for 30 minutes at 450°C. Its spectrum shows the superposition of a single component and a double component. Double component indicates the Fe^{57} atoms which constructs the precipitated second phase Al_3Fe. The values of γ-ray absorption per cent of the individual spectrum in Fig. 4

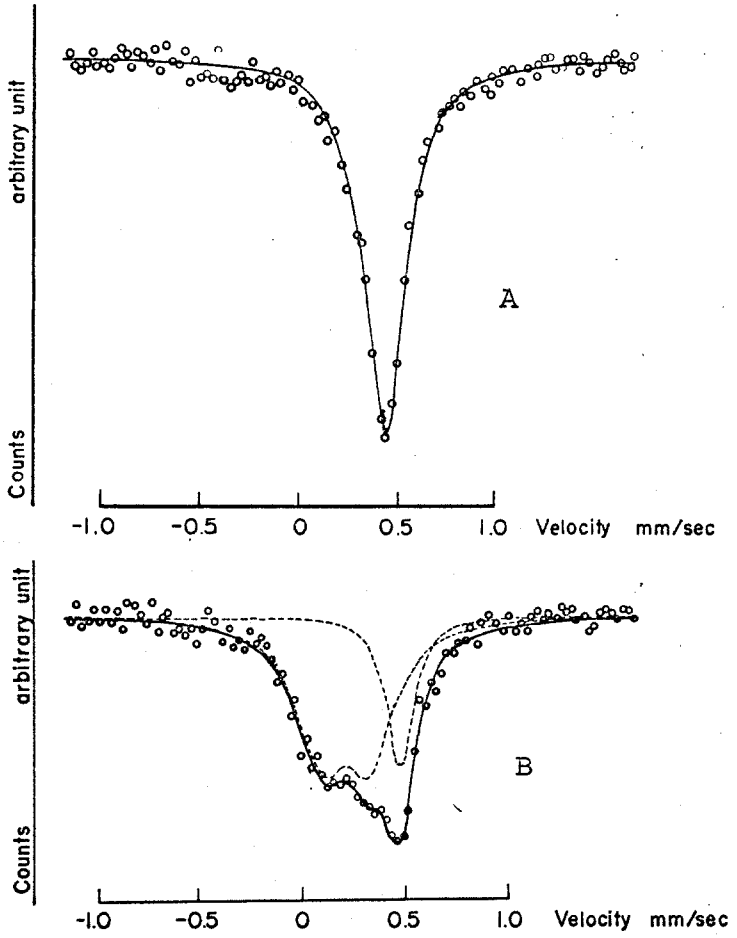

FIG. 4 Typical Fe^{57} Mössbauer spectra obtained from a Al-0.01at.%Fe.

A. quenched specimen

B. annealed specimen

indicate the same value as large as 0.3 ± 0.1 % .
The individual spectrum in Fig. 4 were measured at constant condition; that is , the same thickness of the specimen and same geometry of apparatus involving same distance to the detector from a mono-chromatic γ-ray source. This fact implies that the value of Mössbauer fraction for the Fe^{57} dissolved in alloy matrix is nealy equal to that of Fe^{57} in the precipitated second phase Al_3Fe. Therefore, the integrated intensity ratio of the second component to the double component indicates the ratio of the amounts of iron atoms in alloy matrix to that of iron atoms in the precipitated second phase.

Using the specimens containing 0.01∿0.04at.%Fe^{57} which were annealed for 30 days at various temperatures above 450°C, the Mössbauer spectra were measured and analysed by the least-square method to fit for Eq. II-2. The values for C_1 and r in Eq. II-3 could be estimated from the results obtained by the least-square fit of data and then evaluated values are tabulated in Table 1, since the precipitated second phase is Al_3Fe and C_2 is equal to 0.25 in this case.

Figure 5 shows the solidus curve resulted by the present estimations of the values of the solid solubility as compared with the values of obtained previously by Edgar[5]. In Fig. 5 it has been found that the solidus curve obtained by using the Mössbauer technique is slightly

TABLE 1 Solid solubility limit of Fe in Al at various temperatures.

Annealing Temperature (°C)	Specimen Composition (at. %)	Value of r	Solubility Limit of Fe in Al (at. %)
640	0.031 ± 0.001	0.24	0.0250 ± 0.0008
630	0.031 ± 0.001	0.45	0.0214 ± 0.0007
600	0.031 ± 0.001	0.89	0.0164 ± 0.0005
570	0.036 ± 0.001	2.45	0.0102 ± 0.0003
538	0.019 ± 0.001	1.35	0.0081 ± 0.0004
500	0.010 ± 0.001	0.82	0.0055 ± 0.0005
450	0.010 ± 0.001	3.00	0.0025 ± 0.0003

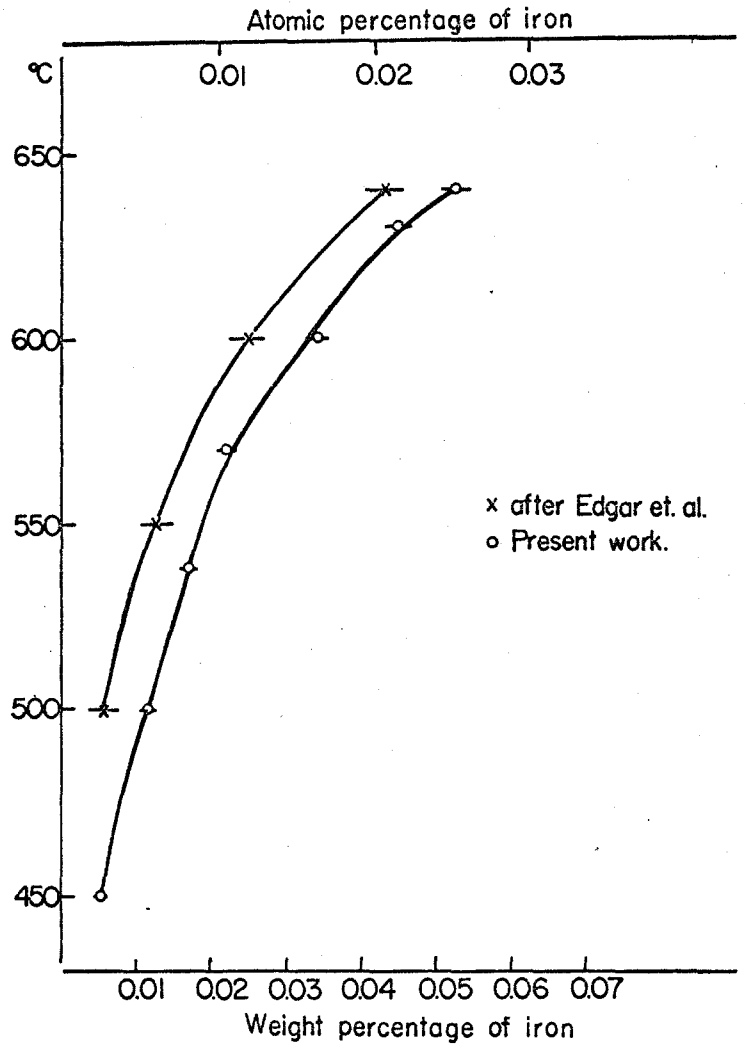

FIG. 5 The solvus curves in Al-Fe alloy system at Al-rich side.

differ from that of the results from Edgar[5]. In the determination of the solid solubility by way of the Mössbauer technique, the accuracy in the obtained values always shows to be same and is not depend on the alloy composition of the specimens even if the alloy composition is extremely small for the iron atoms, since the Mössbauer spectra directly represent the individual states of the solute Fe^{57} atoms. On the contrary, the electrical resistivity measurements have been employed by Edgar[5] for the method to determine the solubility of iron in solid aluminum. Using the Al-Fe alloy specimens containing various amounts of iron, Edgar observed the changes of the electrical resistiviy as a function of alloy composition after the annealing at various temperatures, and decides for the values of solid solubility to the minimum alloy compositions indicating the constant value of the electrical resistance. In this method, the iron concentration in alloy matrix is assumed to be proportional to the value of the electrical resistivity indicating after the alloy specimens annealed for 5 days at that temperatures and also the contribution of the precipitated second phase Al_3Fe to the electrical resistivitymeasurements employed by Edgar[5] is one of the most general methods and techniques to determine the solidus curve in various alloy systems. However, the amount of scatter in the values of electrical resistivity resulted by Edgar[5] is larger than that of present Mössbauer results as shown together in Fig. 6.

It implies that the change in the values of the electrical resistivity as a function of amounts of solute atoms is relatively small in the case of the measurements for the alloy specimen containing extremely small amounts of solute atoms and its linear proportionality for the concentration of the solute atoms is not close approximation. Morever, the contribution of the second phase to the electrical resistance was assumed to be zero in this alloy, but in general if the alloy contains some meta-stable precipitates such as clusters of solute atoms and G. P. zones, these contributions to the electrical resistivity are well known to be quite large compared with that of the isolated Fe atoms[9].

Therefore, the Mössbauer technique to determine the values of solid solubility seems to be more accurate method than the electrical resistivity measurements, especially for the alloy specimen containing very small amounts of the solute atoms. Present results obtained by the Mössbauer technique show the solubility of iron in solid aluminum at the equilibrium states of the alloy system. The amounts of Fe atoms dissolved in alloy matrix at the meta-stable condition, by the analysis of the Mössbauer spectra.

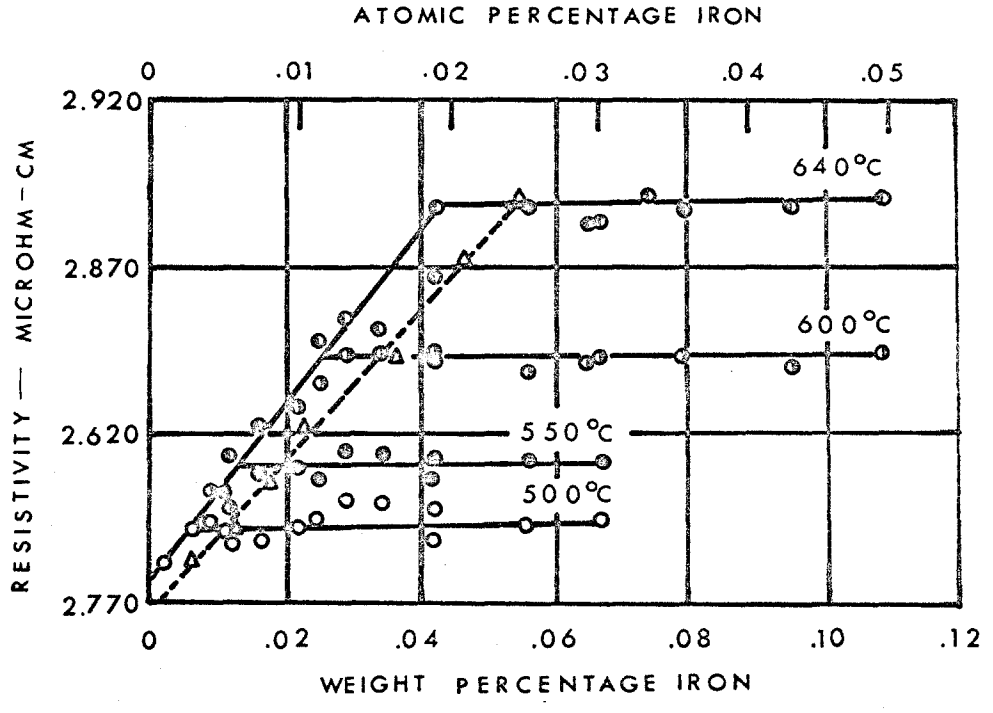

FIG. 6 Comparison of our result with that by Edgar. Dashed line indicate the expected line from our result.

II-3-2. The Change of the Thermodynamic Properties by Solution of Fe Atoms in Al Matrix

In this section, we attempt to discuss the change of the thermodynamic properties by the solution of iron atoms in aluminum matrix, using the values of solubility of iron in solid aluminum which were estimated from the analysis of the Mossbauer spectra (as described in Sec. II-3-1).

It is well known that at a sufficient dilution the variation of the equilibrium concentration of solute with temperature is given by[10)]

$$\ln X_B = \Delta S_i/K - \Delta h/KT, \qquad \text{(II-4)}$$

where X_B is the mole fraction of solute and the quantities Δh and ΔS_i are the appropriate enthalpy and excess entropy, respectively. K is Boltzmann constant. From Eq. II-4 it is clear that Δh and ΔS_i are readily obtained from the slope and intercept, respectively, of a plot of $\ln X_B$ versus T^{-1}. Figure 7 shows a logarithmic plot of $\ln X_B$ versus T^{-1} using the results obtained by the present investigation. In Fig. 7 the quantities of $\Delta S_i/K$ and $\Delta h/K$ could be estimated 1.5±0.5 and 9000°K, respectively. For the quantities of those variations in the thermodynamic properties are discussed in following sections using the

simple models.

(i) Intrinsic Entropy Change

Entropy change of the solution of iron atoms in solid aluminum matrix can be interpreted in terms of the variations of the configurational entropy and the intrinsic entropy. In this alloy system, the configurational entropy terms can be negligible for a sufficient dilution of the solution. The intrinsic entropy can be interpreted in three terms, that is, avibrational entropy change, a elastic contributions, contributions from the change of the electronic states and the correlation terms between them. In general, the intrinsic entropy change is attempted to discuss by the vibrational entropy change[11], since above three terms could not be separate to individual contribution.

The presence of a impurity serves to change the vibrational frequencies such that the frequency changes from ν to ν', and then the intrinsic entropy change, ΔS_v , is given by[11]

$$\Delta S_v = - K \ln(\nu'/\nu). \qquad \text{(II-5)}$$

Frequencies of the atoms in crystal lattice are derived by the Einstein model and are represented by

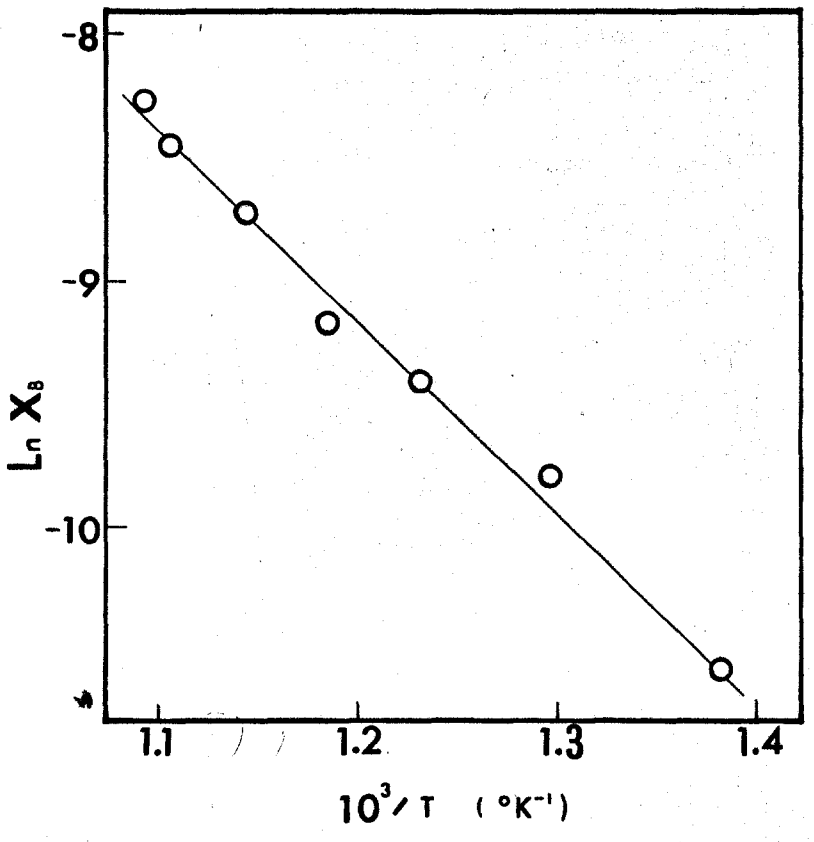

FIG. 7 Logarithmic representation of X_B vs. 1/T.

$$\nu^2 = 1/(4\pi^2 M) \cdot \lambda, \qquad \text{(II-6)}$$

where M is given by the mass of the atoms and λ is a force-constant for the atoms in the crystal. According to Eq. II-6, the vibrational entropy change can be rewritten by the next form of

$$\Delta S_v = -(3/2)\cdot K \cdot \ln[(M_{Al}/M_{Fe})\cdot(\lambda'/\lambda)], \qquad \text{(II-7)}$$

where λ'/λ is the force-constant ratio of Al-Fe bonds to Al-Al bonds. From the Mössbauer study on the second order Doppler shifts of Fe^{57} in Al-0.01at.%Fe^{57} solid solution descrived in CHAPTER III, the best fitted value for the force-constant ratio λ'/λ could be estimated to be 0.74[12]. The value of $\Delta S_v/K$ in Eq. II-7 was estimated to be 0.6 using the value of $\lambda'/\lambda = 0.74$ and agree very well with the experimental results of $\Delta S_i/K = 1.5$ whose value was estimated in Fig. 7. This fact implies that the intrinsic entropy change by the solution of the Fe atoms in aluminum matrix should be interpreted mainly in terms of the vibrational change and also its vibrational change is described by the much localized model such as the Einstein model.

(ii) Appropriate Enthalpy Change

The value of $\Delta S_i/K$ is given by 1.5 and thus the Δh in Eq. II-4 is obtained from the equation of

$$\Delta h = K \cdot T \cdot (1.5 - \ln X_B), \qquad \text{(II-8)}$$

where X_B is the obtained values for the solubility of iron in solid aluminum at the temperature T .

The fact that Δh cannot be interpreted as due primarily to the strain energy is well known[13]. For example, on the basis of the strain energy alone one cannot interpret the fact that Δh values for the system Au-Ni are positive, while those for Au-Ni and Au-Ag are negative[13].

In this section we attempt, however, to discuss the the enthalpy of solution at sufficient dilution compared with the elastic strain energy, since the strain energy caused by the different stomic size should one part of the enthalpy change of solution. Thus from the classical elastic theory, the partial enthalpy change per a solute atom is given by [14]

$$\Delta h_B = 6 \cdot \mu_A^\circ \cdot V_B \cdot [\, 1 - (r_B/r_A^\circ)]^2, \qquad \text{(II-9)}$$

where r_A° and r_B are atomic radius of a solvent in pure metal

and a solute in the solid solution, respectively, and μ_A° is a temperature independent term of a shear modulus. Using the values of $\mu_A^\circ = 0.27 \times 10^6$ Kg/cm^2 [15] and $r_B = 2.6$ atomic unit[7] in Eq. II-9, the value of $\Delta h/K$ is estimated to be 2200°K. This estimated value from the strain energy contribution is much smaller than that of the experimental results obtained in Fig. 7, 9000°K.

After all, the partial enthalpy change in solution of Al- dilute Fe alloy system should not be interpreted by the terms of the strain energy contribution.

II-3-3. Precipitation Study on Al-0.01at.%Fe alloy

As mentioned previously in introductory remarks of this chapter, the investigation on the precipitation phenomena for the Fe atoms as a function of the temperatures has considerable importance for the industrial use of Al and its alloys, since the iron impurities are usually contained in solid aluminum. The study on the precipitation in Al- dilute Fe alloys containing small amounts of iron is very difficult by the usual techniques because of the small solubility and low diffusivity of iron in solid aluminum. However, the Mössbauer spectra show clearly the individual states of solute Fe atoms in Al matrix and its measurements are useful tool for the study in Al- dilute Fe alloy system.

We described in this section the Mossbauer study on the precipitation phenomena in Al-0.01at.%Fe^{57} alloy using the specimens which was unrolled and rolled respectively after the water quenching. Amounts of the precipitation reaction, the kinetics of the precipitation and also its dependence on the deformation of the specimen are subjects in this section and also those are discussed using the analysis of the obtained Mössbauer spectra.

(i) Precipitation Measurements

All of the spectra obtained from the specimens aged for 12 hours, 40 hours and 16 days at 300°C after quenching from 643°C showed the same profiles as the spectrum of the specimen quenched from 643°C, which is shown as the upper spectrum in Fig. 8. From this spectrum the isomer shift is estimated to be 0.43±0.03 mm/sec relative to that of Fe^{57} in α-Fe and the estimated half-width is 0.25±0.03 mm/sec. These values agree well with those of previously estimated values of Fe^{57} in Al-Fe solid solution[16]. These facts show that the any clusters of Fe atoms do not exist in Al matrix by the aging treatments being less than that for 16 days at 300°C.

The values of the isomer shift at the constant temperature is related to the electro-static interaction between Fe^{57} nucleus and the electron charge density at

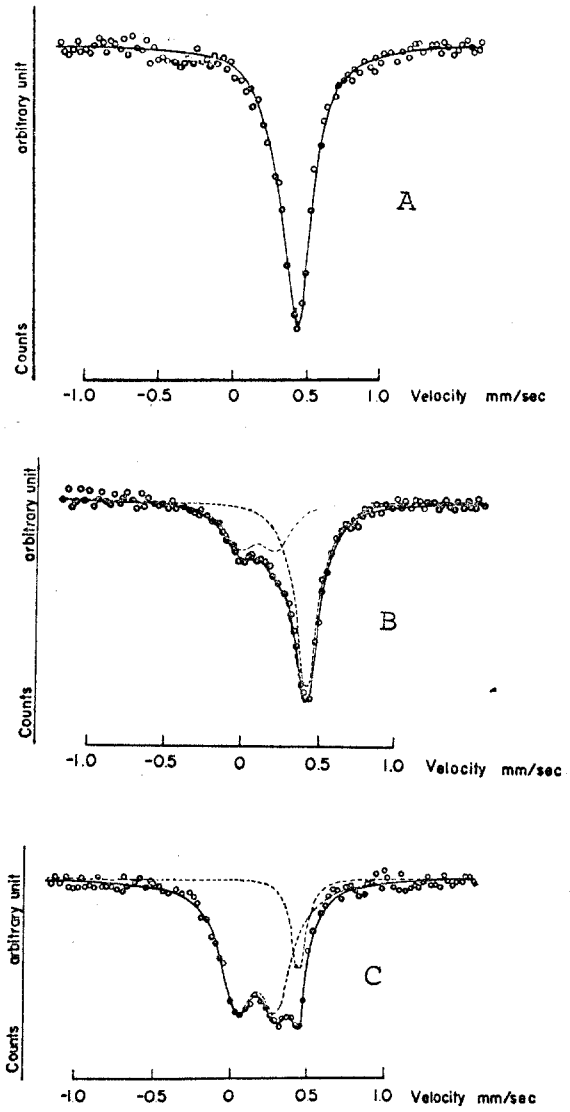

FIG. 8 The Fe^{57} Mossbauer spectra obtained from the dilute Al-0.01at.%Fe alloy specimen by various heat treatments.

A : after quench

B : as deformed after quenching

C : annealed

the nucleus[17,18]. The magnitude of the electron charge density at the nucleus would be different between at the Fe^{57} nucleus in Al matrix and that in some clusters of Fe atoms and the precipitated second phase Al_3Fe. For the clustering or precipitation of Fe atoms the observed values for the isomer shift should show the discrepancy from that of Fe^{57} in Al matrix.

Another Mössbauer spectra were observed for the specimen which were rolled to 95% reduction in thickness at room temperature after solution heat treatment and then aged for various periods at 300°C. The spectrum B in Fig. 8 was measured by the specimen rolled immeadiately after quenching from 643°C. This spectrum consists of a superposition of more than two kinds of peaks, the single peak and other profiles. The value of the isomer shift for the single component of spectrum B in Fig. 8 was estimated to be 0.43±0.03 mm/sec and also indicates the agreement with that of Fe^{57} in Al matrix. Another profile has the smaller isomer shifts than that of Fe^{57} in Al matrix and this would suggest the existence of the cluster of Fe atoms and/or precipitated second phases. The spectrum C in Fig. 8 was measured by the specimen which was rolled and then aged for 16 hours at 300°C and differs from the spectrum B. The magnitude of the single line component indicating Fe^{57} in the Al matrix is reduced by the aging treatments

and the other components probably indicating the Fe^{57} in precipitated second phase is increased. It is able to estimate the quantity of Fe atoms being existed in the precipitated second phase from the integrated intensity ratio between the single line component and the other components, as described in Sec. II-1, the quantity of the Fe atoms in precipitated second phase was estimated as the functions of the aging periods at the temperatures of 300, 450 and 500°C for the both of unrolled and rolled specimens. Figure 9 shows the typical Mössbauer spectra obtained by the specimens which were aged for various periods at 450°C after the solution heat treatment at 643°C. The variations of the quantities of the precipitated solute Fe atoms as a function of aging periods are shown in Fig. 10.

(ii) Precipitated Second Phase

As shown in Fig. 8, the Mössbauer spectrum obtained by the precipitated second phase shows the superposition of two single lines of essentially equal to each other in intensity and the values of those isomer shifts are estimated to be 0.03±0.03 mm/sec and0.32±0.03 mm/sec respectively. Appearing the discrete two kinds of the isomer shifts in the Mössbauer spectrum for the precipitated second phase suggest that this precipitated second phase

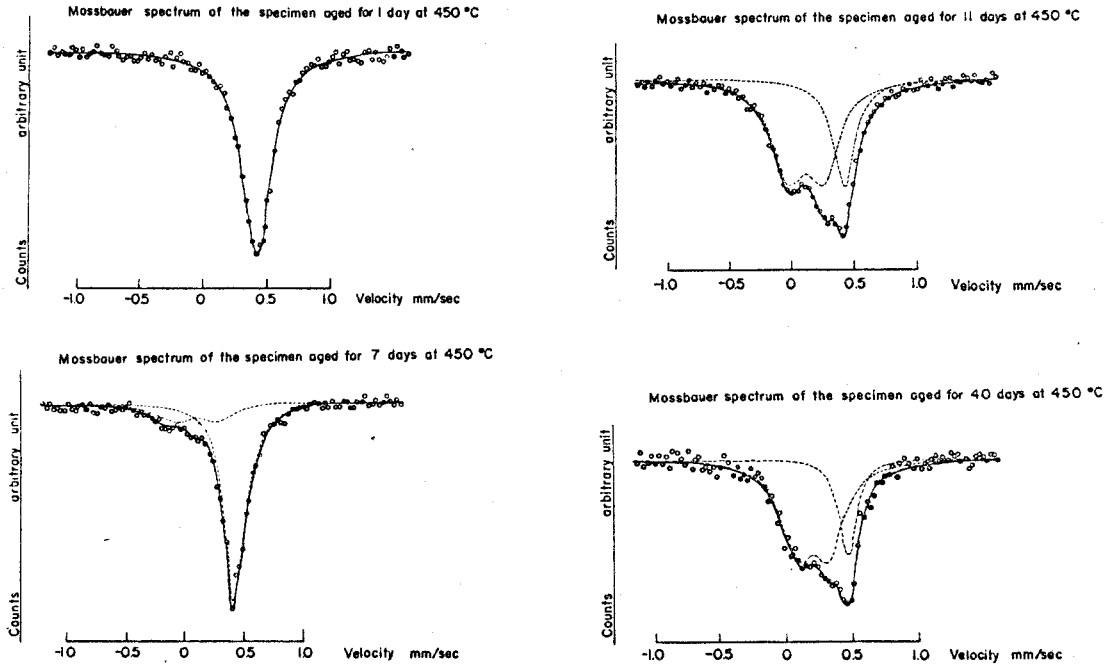

FIG. 9 The Mössbauer spectra of a dilute A-Fe^{57} alloy specimen annealed at 450°C for various aging periods. Obtained data are shown as circle, the solid line indicates the theoretical Lorentzian curve which was obtained by least-square fitting and dotted lines show two cmponents, the single line and the doublet.

would have some ordered structure. The Mössbauer spectra for the intermediate phase in Al-Fe alloy system were measured previously by Nemoshkalenko et al.[8] and the value of the individual isomer shift of the doublet which shows the precipitated second phase coincides with those of Al_3Fe. Therefore, the precipitated second phase in this alloy specimens is considered to be Al_3Fe as has been expected in equilibrium phase diagram of this alloy.

(iii) Kinetics of Precipitation

Figure 10 shows the quantities of the precipitated Fe solute atoms as a function of the various aging time. They were measured by the two kinds of specimens, one is rolled to 95% reduction in thickness at room temperature after the solution heat treatment and then aged subsequently for 40 days at 450°C, the other was only aged for 40 days at the same temperature after quenching from 643°C. Both spectra show the identical superposition of the single line and the doublet. From the integrated intensity ratio in those spectra, the amounts of Fe atoms precipitated in Al matrix by the aging treatment at 450°C is considered to be saturated at 75% of Fe atoms in the alloy specimen. The fact of being identical in the shape of the spectra for the two kinds of specimens suggests that the Fe atoms

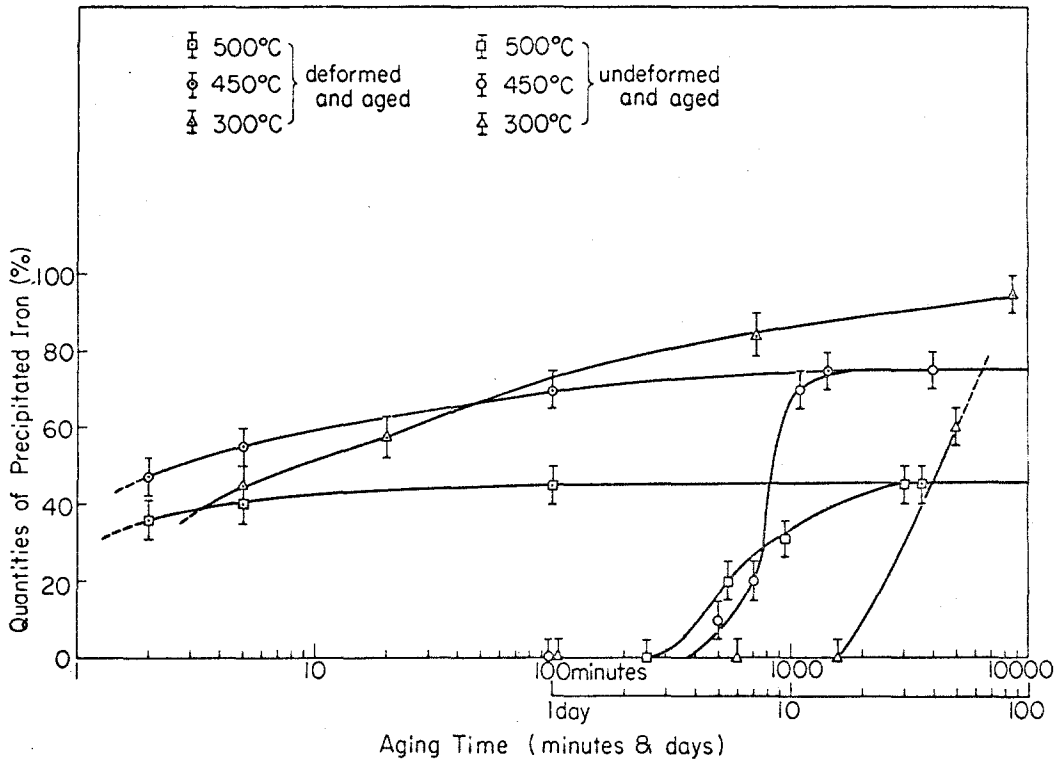

FIG. 10 The change in the amount of precipitated Fe atoms by the annealing periods at various temperatures for two kinds of specimens; undeformed specimen and deformed specimen after quenching.

in both specimens would be situated in the quite similar environments microscopically.

Figure 11 shows the normalized quantity of the degree of the precipitation as a function of the aging temperatures using the results in Fig. 10. To reach the 50% quantity for the degree of the precipitation by the aging treatment at 500°C, 450°C and 300°C the specimen the aging periods were required to 6±1, 7.5±1.0 and 40±10 days respectively in the undeformed specimen, while for the deformed specimen these times were required to 1±1, 2±1 and 20±10 minutes respectively. The rato of precipitation was increased about 10^3 times by the deformation of the specimen. The activation energy for the precipitation was estimated by the cross cut method at 50% degree of the precipitation.

Figure 12 shows a plot of ln t , the time to achieve the 50% degree of the precipitation, versus $10^3/T$, inversed aging temperatures. In both cases, the small activation energies were estimated to be 8.6±1.0 Kcal/mol and 13.4± 2.3 Kcal/mol for the undeformed specimen and the deformed specimen respectively. The activation energy obtained by the increase in the quantity of Fe atoms formed the precipitated second phase. Assuming the nucleation process in this alloy system is not depend on the aging temperatures[19], these activation energies show those for the diffusion of Fe in Al, since the growth of the precipitated

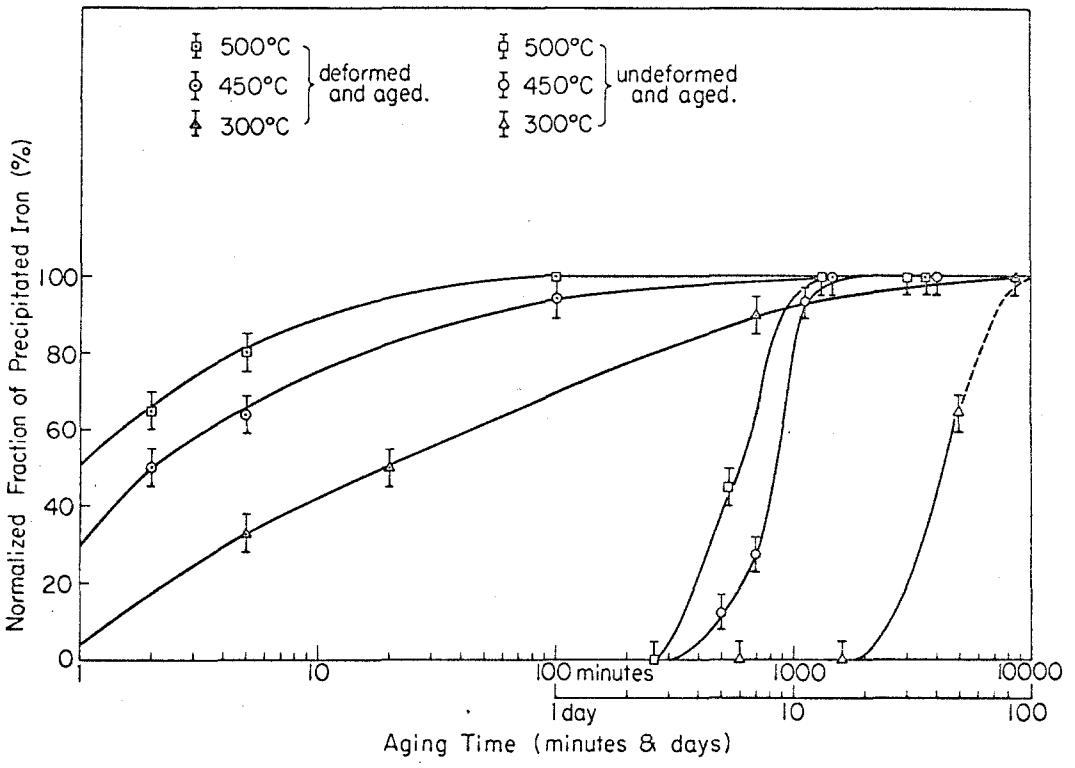

FIG. 11 The normalyzed precipitation presented by plots as amount of precipitated solute Fe atoms as a function of aging time; for the undeformed and deformed specimen.

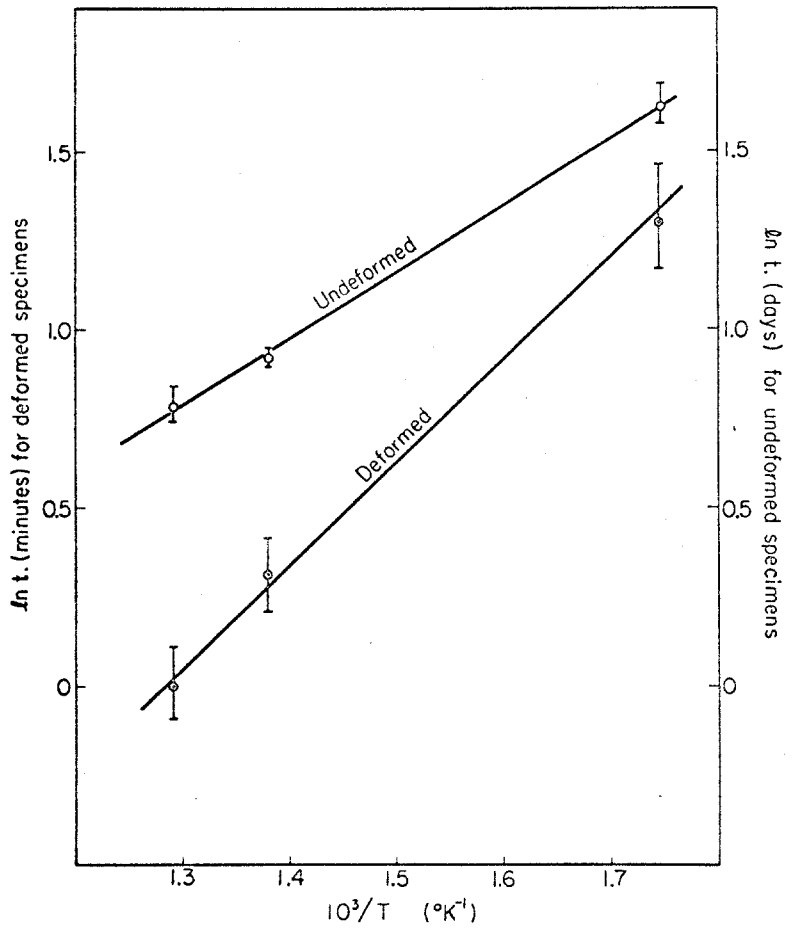

FIG. 12 The plot ln t vs. 1/T. The value of t means the time to achieve at 50% precipitation.

second phase is controlled by the diffusion of the solute Fe atoms.

The activation energy for the diffusion of Fe in Al is determined to be 13.5 Kcal/mol by Hirano et al.[7], which agrees well with that obtained from the present Mössbauer study in the deformed specimen. The deviation of the value in the annealed specimen would be caused from the temperature dependence of the nucleation process of the precipitates. This deviation is not observed in the deformed specimen because of the nucleation is almost completed by the deformation at room temperature and the temperature dependence on the nucleation process does not occur.

From such small activation energies, it may be suggested that the diffusion process for the formation of the precipitated second phase is controlled by the pipe diffusion along the dislocations for the Fe^{57} atoms in Al matrix. The activation energy for the lattice diffusion of the Fe atoms in Al matrix is estimated to be 38 Kcal/mol by Miki et al.[3], using the slope change method in the elecrical resistivity measurements of Al-0.02at.%Fe alloy. The change of the elecrical resistivity in the precipitation process of this alloy indicates the reduction of the amounts of Fe solute atoms in the Al matrix at aging temperatures, even if when the Fe solute atoms segragte along the dislocations.

Therefore, the activation energy estimated by their method means that of Fe atoms diffusion process through the lattice.

The diffusion coefficient of the solute atoms through the lattice and the dislocations is written by[20]

$$D_{eff.} = (1 - f) \cdot D_l + f \cdot D_d \ , \qquad \text{(II-10)}$$

where $D_{eff.}$ is the effective diffusion coeficient of the solute atoms, D_l and D_d are those through the lattice and along the dislocations, respectively. The parameter, f, means the fraction of solute atoms existing on the dislocations. Usually, $D_{eff.}$ is controlled by the value of D_l, since the value of f is quite small comparing with the unity. However, the value of $D_{eff.}$ becomes to be dominated by the value of D_d when the value of D_d/D_l is larger than that of 1/f. If the dislocation density in two kinds of the specimens are 10^8 /cm^2 for the annealed specimens and 10^{10} /cm^2 for the deformed specimens, the values of f are seems to be 10^{-7} and 10^{-4}, respectively. And then the value of $D_{eff.}$ being dominated by the value of D_d is expected to be 10^3 times larger than in the deformed specimen than in the annealed specimen and experimental results agree well with this consideration.

II-3-4. Abnormal Mössbauer Spectra Induced by Cold Working in Al- dilute Fe alloys

In this section, we will discuss about the Mössbauer spectrum obtained at 95°K for the specimen which was deformed at liquid nitrogen temperature.

The spectrum A in Fig. 8 (see in Sec. II-3-3) indicates the profile obtained by the Fe^{57} in Al matrix which shows the single line centered at 0.43±0.03 mm/sec relative to Fe^{57} in α-iron and the spectrum B, which was measured by the specimen rolled to 95% reduction in thickness at room temperature, show the sperposition of the single peak in the spectrum A and the satellite which has the smaller isomer shift than that of the main line. This satellite disappeared by the annealing for 1 day at 643°C and then the satellite is induced by the cold rolling. The magnitude of the satellite is changed by the degree of the deformations. Figure 13 shows the variations of the magnitude in the satellite as a function of the reduction per cent in thickness with rolling. This satellite is considered to be arising from the Fe atoms on the dislocations or in the any precipitates which were constructed during cold working. If it shows the interaction of the Fe^{57} atoms with lattice vacancies, the satellite line would be also observed in the quenched specimen and in the neutron irradiated specimen.

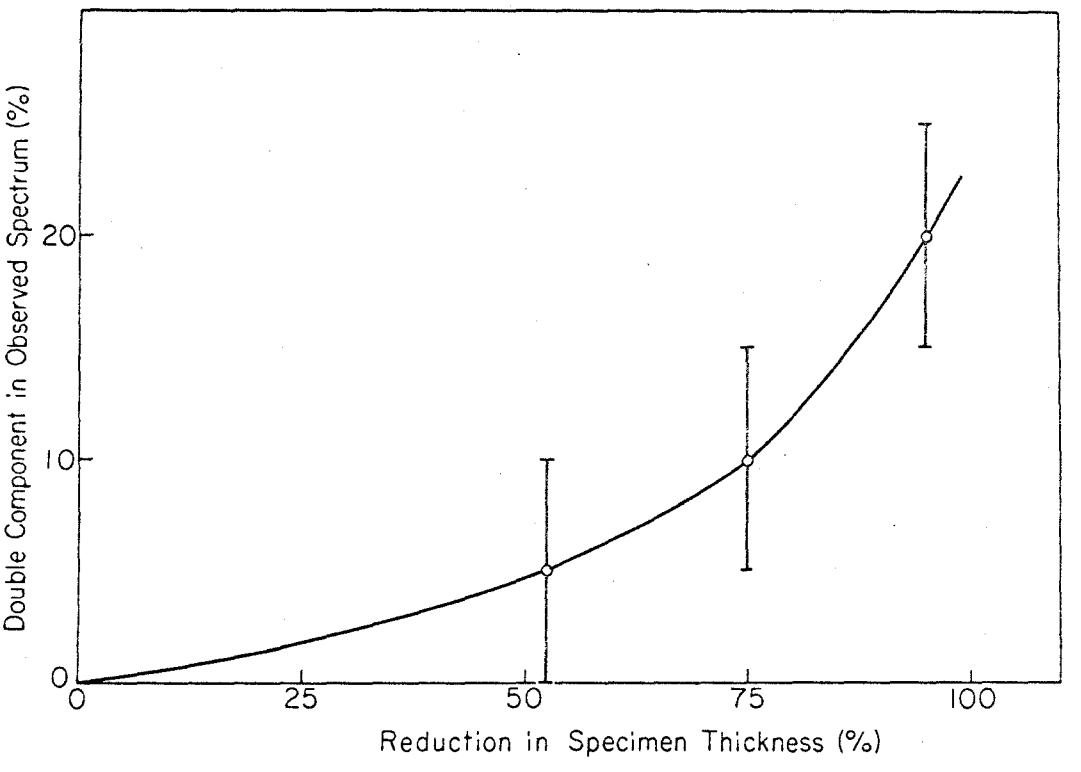

FIG. 13 The change in magnitude of the satellite in Mössbauer spectrum as a function reduction in specimen thickness.

However, it did not appear in the quenched specimen as described in Sec. II-3-1.

Another Mössbauer measurements were carried out using the specimen which was pressed at liquid nitrogen temperature. A spectrum obtained from the specimen pressed to 75% reduction in thickness at liquid nitrogen bath as being shown in Fig. 2 and was measured at 95°K, while the other spectrum was measured by the specimen retained for 1 day at room temperature after pressing. In both spectra, the large satellite were observed. This fact suggested that it would be arising from the Fe atoms pinned on the dislocations, because the Fe atoms cannot move at 95°K by the simple arguments for the jump frequency and it is probably impossible to make a Al-Fe precipitates during the deformation for the sufficient dilution. The magnitude of the satellite relative to that of the single peak as observed in both spectra, which shows Fe in Al matrix, was not changed by the keeping at room temperature, while it was increased by the subsequent aging treatment at 300°C. This fact implies that the movement of the dislocations does not occure at room temperature, but they can be moved at 300°C foe the recrystallization and Fe atoms in the matrix are newly located on the dislocations and can be move along them[4]. The value of isomer shift obtained by the satellite is

estimated to be smaller than that of the main line arising from Fe^{57} atoms in aluminum matrix. This suggests that the electron charge density is larger than that of the Fe^{57} in Al matrix at the center of atom, i.e. at the point of Fe^{57} nucleus[17,18].

II-4. Conclusions

Conclusive remarks in this CHAPTER are following: (1) The values of solubility of iron in solid aluminum hase been determined as a function of various temperatures using the analytical method for the Mössbauer spectra and compared with the results of the previous investigation. It is found that the Mössbauer technique are one of the most powerful methods to determine the phase diagrams about the alloy systems containing extremely small amount of iron atoms. Analytical method in Mössbauer spectra is also discussed for the determination of solid solubility in binary alloy system. (2) From the values of solid solubility of iron in aluminum, the change of the thermodynamic properties by the solution of Fe atoms in Al matrix are estimated to be $\Delta S_i/K = 1.5\pm0.5$ and $\Delta h/K = 9000°K$. These values were compared with a vibrational entropy change and a strain energy by solution which have been calculated using a simple model. It is found that in

this alloy system the intrinsic entropy change can be interpreted by the vibrational entropy term calculated by a simple Einstein model, but the partial enthalpy change cannot be interpreted by the classical strain energy as has been expected. (3) Precipitation phenomena in Al-0.01at.%Fe^{57} alloy specimen are investigated by the analysis of the Mössbauer spectra, using the undeformed specimens and also specimens deformed prior to the aging treatments immediately after the water quenching. Precipitation reaction in deformed Al-0.01at.%Fe alloy indicates extremely rapid as large as 10^3 times than that in undeformed specimens. Activation energy for the 50% precipitation in this alloy can be estimated to be 13.4±2.3 Kcal/mol by the cross cut method and its values agree with one of the other results previously reported. (4) Mössbauer spectra, which are measured by the specimens pressed at liquid nitrogen bath, differ from that of the undeformed specimens seems to show the different states of Fe solute atoms from the isolated Fe solute atoms in Al matrix, and it has been found that the Mössbauer measurements in a sufficiently dilution for iron atoms are useful methods to detect the some interactions between Fe impurities and the lattice defects, i.e. dislocations, vacancies, stacking faults and some crystalline boundaries.

REFERENCES

1. H. L. Marcus, L.H. Schwartz and M. E. Fine; Trans. A. S. M., 59 (1966) 468.

2. P. M. Gielen and R. Kaplow; Acta Met., 15 (1967) 49.

3. I. Miki and H. Warlimont; Z. Metallkde, 59 (1968) 254.

4. K. Nagahama and I. Miki; Keikinzoku, 20 (1970) 137.

5. J. K. Edgar; Trans. A. I. M. E., 180 (1949) 225.

6. K.Hirano, R. P. Agarwala and M. Cohen; Acta Met., 10 (1962) 857.

7. G. M. Hood; Phil. Mag., 21 (1970) 305.

8. V. V. Memoshkalenko, O. N. Rasumov and V. V. Gorskii; phys. stat. sol., 29 (1968) 45.

9. A. Kelly and R. B. Nicholson; " Precipitation Hardening" in Progress in Material Science, vol. 10, edited by B. Chalmers, (Pergamon Press, New York, 1963).

10. J. Freedman and A. S. Nowick; Acta Met., 6 (1958) 176.

11. H. B. Huntington, G. A. Shirn and E. S. Wajda; Phys. Rev., 99 (1955) 1085.

REFERENCES (CONT.)

12. S. Nasu, M. Nishio, T. Tsuchida, Y. Murakami and T. Shinjo; J. Phys. Soc. Japan, 27 (1969) 1363.

13. R. A. Oriani; Acta Met., 4 (1956) 15.

14. J. W. Christian; "The Theory of Transformations in Metals and Alloys", p. 191, (Pergamon Press, New York, 1965).

15. K. A. Gschneidner, Jr; Solid State Physics, vol. 16, edited by F. Sitz and D. Turnbull, (Academic Press, New York, 1964).

16. R. H. Bush, C. A. Stikels and L. W. Hobbs; Scripta Met., 1 (1967) 75.

17. H. Frauenfelder; "The Mössbauer Effect", (W. A. Benjamin, New York, 1963).

18. G. K. Wertheim; " Mössbauer Effect: Principles and Applications", (Academic Press, New York, 1964)

19. C. A. Wert; J. Appl. Phys., 20 (1947) 943.

20. E. W. Hart; Acta Met., 5 (1957) 597.

CHAPTER III

MÖSSBAUER EFFECT STUDY OF Al-0.01at.%Fe SOLID SOLUTION

III-1. Introduction

The Mössbauer effect of Fe^{57} nucleus has been widely applied to the study of solid state physics and it is well known that the study of the resonant absorption, its temperature dependence, and the temperature dependence of the second-order Doppler shift of the resonant absorption line are directly related to the dynamics of the Mössbauer active nucleus[1].

A considerable body of the theoretical and experimental research has been devoted to the discussion of determination of the Mössbauer recoil free fraction, from which the mean-square atomic displacement of resonant nuclei can be deduced[1]. On the experimental side, however, it is more accessible to measure the change in the peak position of Mössbauer line than that of its intensity as the temperature is varied. Futhermore, the observed total shift of the Mössbauer line resulted from the temperature independent isomeric or chemical shift. The absolute isomeric shift can be only obtained by the deduction of temperature dependent second-order Doppler shift from the observed total shifts[2].

It is the purpose of this CHAPTER to observe the Fe^{57} Mössbauer line in aluminum in the temperature range between 4.2°K and 453°K and to separate the isomeric shift and the second-order Doppler shift of Fe^{57} in aluminum from the observed total shifts.

It is well known that the iron atoms shows a extremely low bulk solubility in aluminum[3] as described in CHAPTER II, and its reason may be able to be interpreted in terms of the electric structure of iron impurity in aluminum and the vibrational properties of iron in aluminum. The electronic structure of transition metal impurities has been the subject of considerable study in recent years[4].

However, the detailed discussion for these behaviour in microscopic stand points have not yet been carried out except the observation of the oscillating electric field gradiants around the impurities using the nuclear magnetic resonance[5] and then it is necessary for the discussion to investigate the vibrational as well as electronic local state of iron atoms in an aluminum lattice. Isomeric shift(it means the temperature independent absolute isomer shift; this description is following in this volume) and second-order Doppler shift which was the results from the Fe^{57} Mössbauer effects in solid aluminum must be shown as a local state of iron atoms in aluminum lattice.

From the metallurgical aspects, Bush et al.[6],

Miki et al.[7] and our previous investigation in CHAPTER II the precipitation phenomena in Al- dilute Fe alloys are reported that, if these specimens (Al-0.01at.%Fe) were not deformed after quenching from a solid solution temperature, any precipitated phase or particles could not yet be observed after short time aging treatment at low temperatures (at least below 500°K).

As above mentioned, it is possible to observe the temperature shift of Mössbauer line using the quenched specimen from the solid solution temperature, since the precipitated particles will not be formed and iron atoms will be isolated in aluminum lattice at the temperature range below 500°K.

III-1-1. Isomeric Shift

The isomeric or chemical shift of the energy levels in either source or absorber nuclei is given by

$$\delta E^i = (2/5)\cdot\pi\cdot Z\cdot e^2\cdot R^2\cdot|\psi(0)|^2, \qquad \text{(III-1)}$$

and a formal expression for the isomeric shift in velocity unit is

$$\Delta S^i = (4\pi Z e^2 R^2 c/5E_\gamma)(\delta R/R)\left[\sum_A|\psi(0)|^2 - \sum_S|\psi(0)|^2\right], \qquad \text{(III-2)}$$

where Z is the atomic number, R is the nuclear radius, $|\psi(0)|^2$ is the electron density at the nucleus, and δR is the difference between the radius of the nucleus in its excited state and in its ground state ($=R_{excite} - R_{ground}$). The sum is taken over the electron density in source and absorber material.

In the absence of phase changes, the value of $\psi(0)$ should not change appreciably with temperature, so that the isomeric shift may usually be regarded as temperature independent. However, it has been suggested that the isomeric shift for Fe^{57} nucleus has a volume-independent temperature-dependent part which cancels to a good approximation the part which varies with the thermal expansion of the crystal[1]. Therefore, at least in the case that the resonant nucleus is Fe^{57}, it appears that we can regard the isomeric shift as temperature independent and separate the value of isomeric shift from the experimental values of center shift.

III-1-2. Second-Order Doppler Shift

It can be predicted that the center of the recoil free peak occurs at $E=E_o$. In fact, a simple argument shows that the center of the peak is shifted slightly from this position[8]. Because of the relativistic equibalence

of energy and mass, in the consideration of the emission processes in which the nucleus decay from its lowest excited stateto its ground state with the emission of γ-ray of energy E_γ, the mass of the emitting nucleus decreases by the amount of

$$\delta m = - E_\gamma / c^2, \qquad \text{(III-3)}$$

where c is the speed of light. This change is given by the expectation value of the crystal Hamiltonian,

$$\delta E^V = \langle \Delta H \rangle = - \langle p_i^2 / 2m^2 \cdot \delta m \rangle = E_\gamma / 2m^2 c^2 \cdot \langle p_i^2 \rangle, \qquad \text{(III-4)}$$

where i labels the emitting nucleus, and "m" is its mass. This energy increase is drained away from the energy of the γ-ray which is shifted by this amounts.

The shift of the γ-ray energy is called the second-order Doppler shift, or the velocity shift, of the Mössbauer peak. Its existence was first pointed out theoretically and demonstrated experimentally by Pound and Rebka[8,9]. The simple derivation of its magnitude was given by Josephson[10].

It is more convenient to express the energy shift as a velocity through the equation for the Doppler shift in the energy due to a change in its velocity,

$$\Delta V/c = \delta E/E_{\gamma} \ .$$

We thus study the velocity shift as a form of

$$\Delta S^{V} = 1/2c \cdot < V_i^2 > \ , \qquad \text{(III-5)}$$

where $< V_i^2 >$ is the mean-square velocity of the resonant nucleus.

A corrsponding shift occurs during the absorption process, so that any experiment measures only $< V_s^2(T_s) > - < V_a^2(T_a) >$. This is not in fact the measured shift, since we have to add to this the isomeric shift.

III-2. Sample Preparation and Experimental Procedures

III-2-1. Sample and Experimental Technique

The tools required for a demonstration of the Mössbauer effect are fundamentally those encountered in γ-ray spectroscopy. The experiments in this CHAPTER were performed in transmission geometry samely in all the CHAPTERS in this volume and required a radio-active source, Co^{57} in Cu plate, an absorber which was made up as a

specimen and a commercial Mössbauer apparatus; T. M. C. set (Gammascope 102, Drive Unit 306 and Transducer 305) operated in a time mode similarly to the CHAPTER II.

An Al-0.01at.%Fe^{57} alloy ingot was prepared by melting from 99.999% Al and metallic Fe^{57} powders.

For the 14.4 KeV γ-ray absorber, this alloy plates were cut from a sheet rolled to a nominal thickness of 0.5 mm, a typical thickness being about 0.03 mg/cm^2 for Fe^{57}. Thickness of this alloy specimen was selected to be the best condition for the amounts of the resonant Fe^{57} nuclei and the attenuation of the 14.4 KeV γ-ray by the specimen. The larger the quantity of the Fe^{57} in absorber, the larger the probability of resonant absorption. The increase in the number of Fe^{57} nuclei in constant alloy composition results in the increase of the thickness of the alloy specimen. But the increase of thickness decreases the intensity of γ-rays which pass through the specimen.

The attenuation of the 14.4 KeV radiation can be calculated from the mass absorption coefficient, μ , and the absorber area density, t (g/cm^2), using the equation:

$$I = I_o \exp(- \mu \cdot t) \ , \qquad \text{(III-6)}$$

$$t = d \cdot \sigma \ ,$$

where d is the thickness of the absorber and σ is the density of the absorber. For the case of the solid aluminum, the values of these factors are given to be[11)]

$$\mu_{Al} = 7.84 \text{ cm}^2/\text{g for 0.015 MeV.}$$
$$\sigma_{Al} = 2.70 \text{ g/cm}^3 .$$

The quantity, $\exp(- \mu \cdot d \cdot \sigma)$, in Eq. III-6 shows the permeability of γ-rays through the specimen. The measurement condition is determined by two quantities; i.e. the number of Fe^{57} atoms in the specimen and the permeability of γ-rays through the specimen.

Figure 14 shows the relationship between the thickness of the specimen (d) and these two quantities, the amounts of Fe^{57} atoms in the specimen(A) and the permeability of γ-rays through the specimen (P). From the value of the products of these two quantities, A·P, the dgree of the condition of good measurement, could be determined, as being shown in Fig. 14. From Fig. 14, 0.5 mm was chosen as the most suitable thickness of the specimen.

A monochromatic source, which was always used at the room temperature, was obtained from the 5 mC of Co^{57} doped into a pure copper foil.

The measured velocity range was relatively narrow

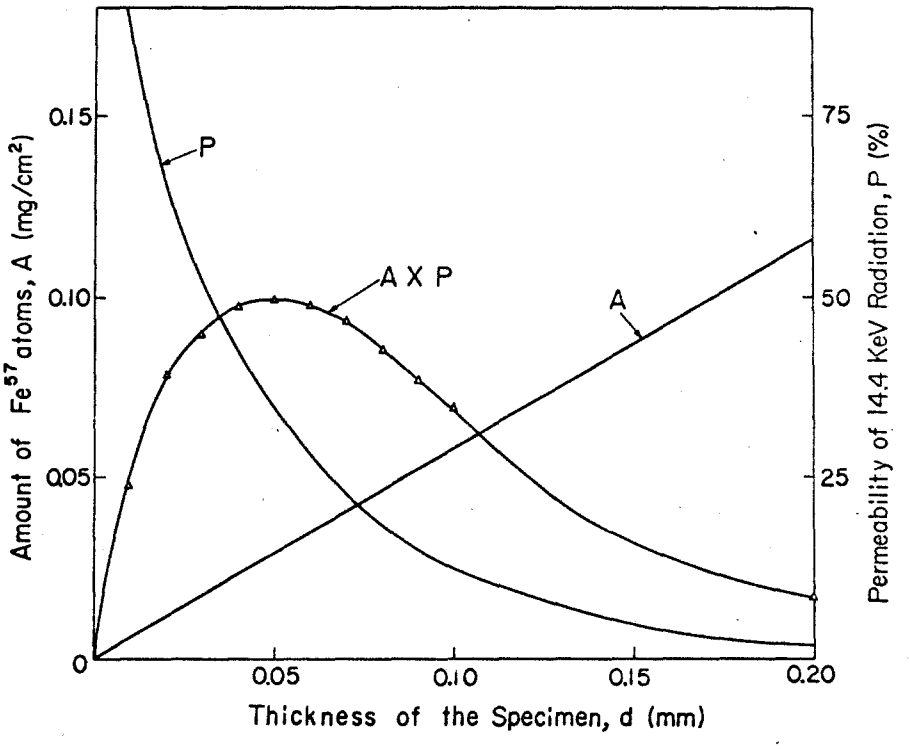

FIG. 14 Relationship between thickness of specimen d and two quantities; amount of Fe^{57} atoms in the specimen, A, and the permeability of gamma-rays through the specimen, P.

because of the observation of accurate center shift and was calibrated by the peak positions obtained from iron foil and stainless steel absorber, and this calibration were carried out always at the room temperature.

Before the performing of the measurements, Al-0.01 at.%Fe^{57} alloy specimens were homogenized in a usual vertical electric furnace for 1 day at 643°C and then quenched into water, since this alloy composition is not solid solution below 600°C; namely the specimens in this CHAPTER show a supersaturated solid solution of Al- 0.01 at.%Fe^{57} alloy.

III-2-2. Cryostats and Furnace

For the measurements from room temperature to 95°K, the absorber was mounted on a copper rod coolant, which was cooled down by liquid nitrogen, of a cryostat as shown in Fig. 1 (see CHAPTER I). The temperature of the absorber was measured by the use of a Cu-AuCo thermo-couple screwed to the frame which holds the specimen absorber.
For the measurement at the liquid helium temperature, the absorber was mounted on the bottom of a liquid helium vessel. The thermal-radiation shield can be obtained by the cooling cap at the liquid nitrogen temperature.
The γ-rays are transmitted through two thin foil windows

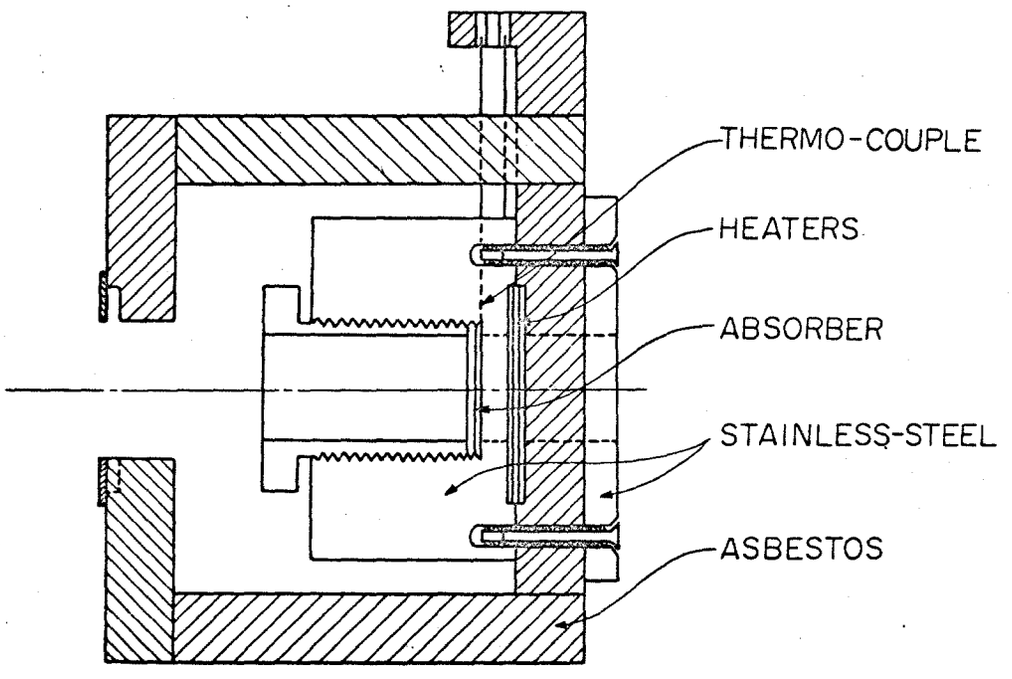

FIG. 15 Furnace used to heat the absorber.

of the cooling cap.

For the measurements at the temperature range from 363°K(90°C) to 453°K(180°C), the HITACHI vertical heating cell for the optical measurements as being shown in Fig. 15 was used as a heater for the absorber. The chromelalumel thermo-couple was used to measure the temperature of the absorber.

III-3. Experimental Results and Interpretations

III-3-1. Experimental Data and Their Analysis

(i) Energy of Gamma-Rays

In the recoilless nuclear resonance absorption of gamma radiation, the energy of the γ-ray emitted from the source nucleus is equal, within the inherent width of its γ-rays, to the energy spent in the resonance absorption process of the other nucleus.

As shown by an illustration in Fig. 16, the energy balance in the recoilless absorption process can be given by

$$E_o + \delta E_s^i - \delta E_s^v + \delta D = E_o + \delta E_a^i - \delta E_a^v , \quad \text{(III-7)}$$

where suffixes s and a show the source and the absorber nuclei respectively and δD is the first-order Doppler shift caused by the mechanical motion of the source matrial. From Eq. III-7, δD is directly derived to be

$$\delta D = - (\delta E_s^i - \delta E_a^i) + (\delta E_s^V - \delta E_a^V). \quad \text{(III-8)}$$

In this present investigation, as described in Sec. II, Co^{57} in copper foil was used as a γ-ray source and Fe^{57} in aluminum plate as an absorber, so that Eq. III-8 gives following form of

$$\delta D = - (\delta E_{Cu}^i - \delta E_{Al}^i) + (\delta E_{Cu}^V - \delta E_{Al}^V). \quad \text{(III-8')}$$

Using the convenient definition of the isomeric shift in α-iron equal to zero, the zero velocity is determined to be identical with the center position in the spectrum which was obtained by the pair of Co^{59} in Cu and Fe^{57} in α-Fe, because the total shift observed by this experiment between Co^{57} in Cu and Fe^{57} in Al can be shown as a total shift relative to metallic α-Fe. Above discussion can be followed by

$$\delta D = - (\delta E_{Cu}^i - \delta E_{Fe}^i) + (\delta E_{Cu}^V - \delta E_{Fe}^V) = 0, \quad \text{(III-9)}$$

$$\delta E_{Fe}^i = 0 . \quad \text{(III-10)}$$

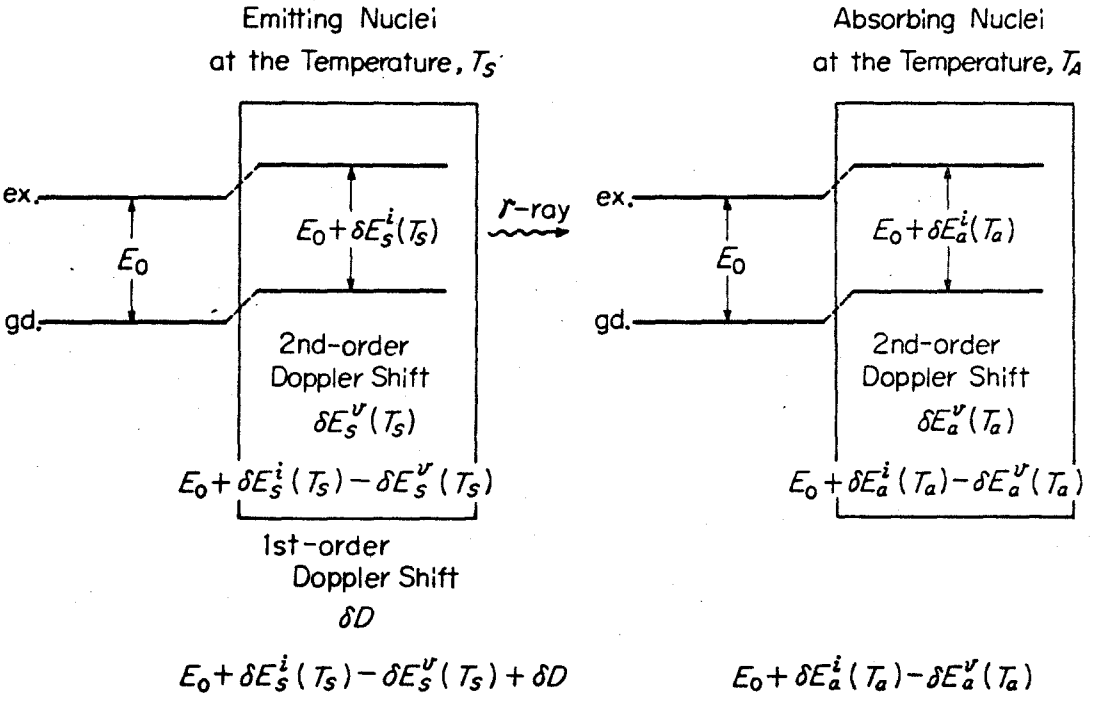

FIG. 16 An illustration for the energy balance between emitted gamma-rays and absorbed one. The notations are in text.

From Eqs. III-9 and III-10, Eq. III-8´ can be rewritten by

$$\delta D = \delta E^{i}_{Al} + \delta E^{V}_{Fe} - \delta E^{V}_{Al} \ . \qquad \text{(III-11)}$$

The first-order Doppler shift in velocity unit, that is, the observed total shift can be given, finally, by

$$\Delta S^{T} = \Delta S^{i}_{Al} + \Delta S^{V}_{Fe} - \Delta S^{V}_{Al}. \qquad \text{(III-12)}$$

Observed total shift, ΔS^{T}, and a second-order Doppler shift, ΔS^{V}_{Al} , are functions of measuring temperatures, T, but the isomeric shift, ΔS^{i}_{Al} , is temperature independent and the second-order Doppler shift of Fe^{57} in α-Fe, ΔS^{V}_{Fe}, shows also constant value for any measuring temperatures, because it was always obtained at room temperature (R.T.), (see Eq. III-9).

Therefore, Eq. III-12 can be shown as

$$\Delta S^{T}(T) = \Delta S^{i}_{Al} + \Delta S^{V}_{Fe}(R.T.) - \Delta S^{V}_{Al}(T). \qquad \text{(III-12´)}$$

The temperature dependence of the second-order Doppler shift in aluminum, $\Delta S^{V}_{Al}(T)$, can be deduced from the temperature variation in the observed total shift, $\Delta S^{T}(T)$, using Eq. III-12´.

(ii) Mössbauer Spectra

Figure 17 shows the typical Mössbauer spectra obtained from the Al-0.01at.%Fe^{57} alloy specimen, 0.5 mm in thickness, at various temperatures. Alloy specimens were homogenized for 1 day at 643°C and then quench into water prior to the measurement of the spectrum.

The peak position of the single Lorentzian spectrum in the velocity unit of abscissa in Fig. 17 can be truely estimated to be the total shift ΔS^T at the temperature, T, relative to α-iron; as described in Sec. III-1-i.

As measuring temperatures go on a increase, the observed total shift, $\Delta S^T(T)$, tends to approach to the zero velocity according to the increase of the second-order Doppler shift, $\Delta S^V_{Al}(T)$, in Eq.Ⅲ-12´ which shows the mean-square velocity of the Fe^{57} nuclei in the aluminum host lattice. The numerical results of the observed total shift at the temperature range between 4.2°K and 453°K were tabulated in Table. 2 and the magnitude of the increase in the temperature dependent shifts relative to to the value at 4.2°K were also shown in the right column of the same Table.

The solid lines in Fig. 17 show least-squre fits of data to single Lorentzian curve obtained by the aid of Kyoto University's KDC-II computer.

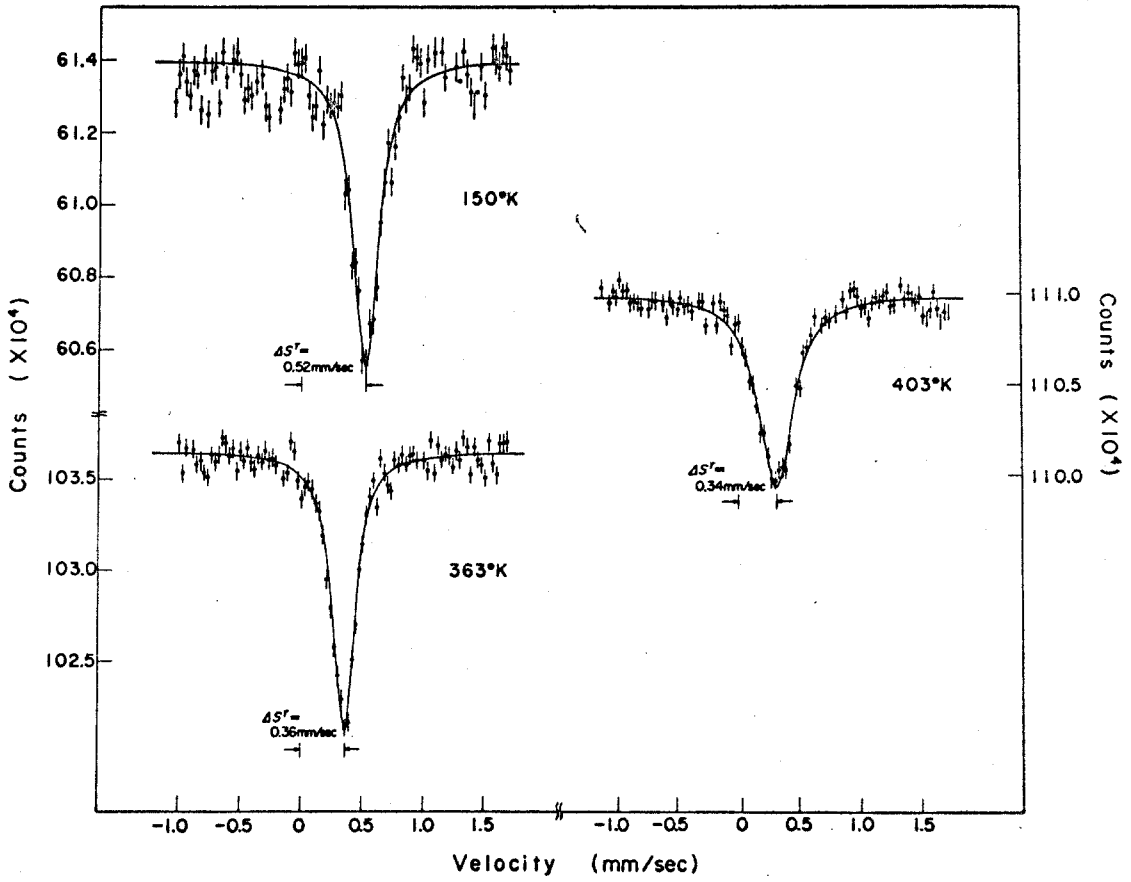

FIG. 17 Typical Mössbauer spectra obtained from a quenched Al-0.01%Fe alloy at various temperatures. $\Delta S^{T}(T)$ indicates the observed total shift at the temperature.

TABLE 2 Numerical results of a observed total shift for a Al-0.01%Fe^{57} alloy plate, 0.5 mm in thickness. The shifts ΔS^T were measured relative to metallic iron and the $\Delta S^T(0)$ is a shift at absolute zero temperature. We assum that $\Delta S^T(4.2°K) \simeq \Delta S^T(0)$.

T (°K)	ΔS^T (mm/sec)	$\Delta S^T(T)-\Delta S^T(0)$ (mm/sec)
4.2	0.57 ± 0.02	~0
95	0.54 ± 0.02	−0.03
150	0.52 ± 0.02	−0.05
293	0.43 ± 0.02	−0.14
363	0.36 ± 0.02	−0.21
403	0.34 ± 0.02	−0.23
453	0.30 ± 0.02	−0.27

The values of the half-width of the Mössbauer spectrum obtained at 453°K in Fig. 17 show to be greater than that of the other low temperature spectra. It provides the existence of the added broadening to the half-width in spectrum. This may be explained from the effect of diffusion coefficient should be estimated from the temperature dependence of its broadening using the relation proposed by Singwi and Sjölander[12].

However, in this present study the magnitude of the broadening of the half-width could not be acculately observed for the comparative low temperature measurements and also the purpose in this study is concentrating to the temperature dependence of the value of the center position in the spectra, that is, truely of the second-order Doppler shift, $\Delta S^{V}_{Al}(T)$.

III-3-2. Second-Order Doppler Shift and Absolute Isomeric Shift

According to the previous descussion in Sec. I, the second-order Doppler shift of Fe^{57} nuclei in the aluminum host was given, as the identical form of Eq. III-5 by

$$\Delta S^{V}_{Al}(T) = 1/2c\langle V^{2}_{Al}(T)\rangle \ , \qquad \text{(III-13)}$$

where $\langle V_{Al}^2(T) \rangle$ shows the mean-square velocity of the Fe^{57} nuclei in an aluminum host lattice at the temperature, T.

Assuming the dynamical properties of the Fe^{57} impurity in an Al host lattice is isotropic and can be discussed by the harmonic approximation, the mean-square velocity of Fe impurity atom in Al matrix, as shown by Maradudin[13] and Mannheim[14], in powers of the temperature is given by

$$\langle V_{Al}^2(T) \rangle = 3kT/M' \cdot \{1 + 1/12(\hbar/kT)^2 \cdot \lambda'/M' \quad , \text{(III-14)}$$

where M' is mass of Fe^{57} impurity atom, λ' shows a force constant between impurity atom and host atom, in this case, Fe^{57}-Al force constant and k, $\hbar(=h/2\pi)$ are usual meaning.

Furthermore, for the case of pure lattice in which the central force is only operated Mannheim et al[14]. suggested the relation between the experimentally known maximum frequency of pure lattice, ω_{max}, force constant in pure lattice, λ, and the mass of pure crystal and shows the relation as

$$\omega_{max}^2 = 2\lambda/M \quad , \qquad \text{(III-15)}$$

Combining Eq. III-14 and III-15 we have

$$\langle V^2(T)\rangle = \frac{3kT}{M'}\{\ 1 + \frac{1}{24}(\frac{\hbar}{kT})^2 \frac{M}{M'}\cdot\omega^2_{max.}\frac{\lambda'}{\lambda} + \ldots.\} \ , \tag{III-16}$$

that is, from Eq. III-13

$$\Delta S^V_{Al}(T) = \frac{3kT}{2M'c}\{\ 1 + \frac{1}{24}(\frac{\hbar}{kT})^2\cdot\frac{M}{M'}\omega^2_{max.}\cdot\frac{\lambda'}{\lambda} + \ldots.\}, \tag{III-17}$$

Substituting Eq. III-17 in III-12´ and also taing a rearrangement, the observed total shift, $\Delta S^T(T)$, can be shown as

$$\Delta S^T(T) + \frac{3kT}{2M'c} = [\Delta S^i_{Al} + \Delta S^V_{Fe}(R.T.)] - (\frac{1}{16}\cdot\frac{\hbar^2}{k}\cdot\frac{M}{M'}\cdot\frac{1}{M'c}\ \omega^2_{max.}\cdot\frac{\lambda'}{\lambda})\cdot\frac{1}{T} + O(T^{-3}) \ , \tag{III-18}$$

where $O(T^{-3})$ shows the terms which is less than three inverse powers of the temperature and can be neglected at high temperatures. Therefore, Eq. III-18 can be approximated to

$$\Delta S^T(T) + \frac{3kT}{2M\ c} = [\Delta S^i_{Al} + \Delta S^V_{Fe}(R.T.)] - (\frac{1}{16}\cdot\frac{\hbar^2}{k}\cdot\frac{M}{M'}\cdot\frac{1}{M'c}\cdot\omega^2_{max.}\cdot\frac{\lambda'}{\lambda})\cdot\frac{1}{T} \ . \tag{III-18´}$$

The second term in left members of Eq. III-18´ is the pure classical limit. At high temperatures the value of λ'/λ can be estimated from the experimental total shift $\Delta S^T(T)$ and the value of $[\Delta S^i_{Al} + \Delta S^V_{Fe}(R.T.)]$ can also be estimated from Eq. III-18´. This not accurate, since the second-order Doppler shift differs only slightly from the pure calssical limit. However at lower temperature quantum corrections become important, so that here it can be hoped to distinguish between force-constant ratio.

The values of the $[\Delta S^i_{Al} + \Delta S^V_{Fe}(R.T.)]$ and λ'/λ can be estimated from the relation between $[\Delta S^T(T) + 3kT/2M'c]$ versus inverted temperature, 1/T, in the Eq. III-18, since the values of ΔS^i_{Al} and $\Delta S^V_{Fe}(R.T.)$ is constant. The straight line in Fig. 18 can be obtained by a least-square fit of data. The least-square fitting of the parameters in Eq. III-18´ to the experimental results for the temperature range 95°K to 453°K gives

$$\Delta S^T + 3kT/2M'c = 0.639 - 0.00244(10^3/T), \qquad \text{(III-19)}$$

that is

$$\Delta S^i_{Al} + \Delta S^V_{Fe}(R.T.) = 0.639 \text{ mm/sec.}$$

According to the results from Preston et al.[15], $\Delta S^V_{Fe}(298°K)$

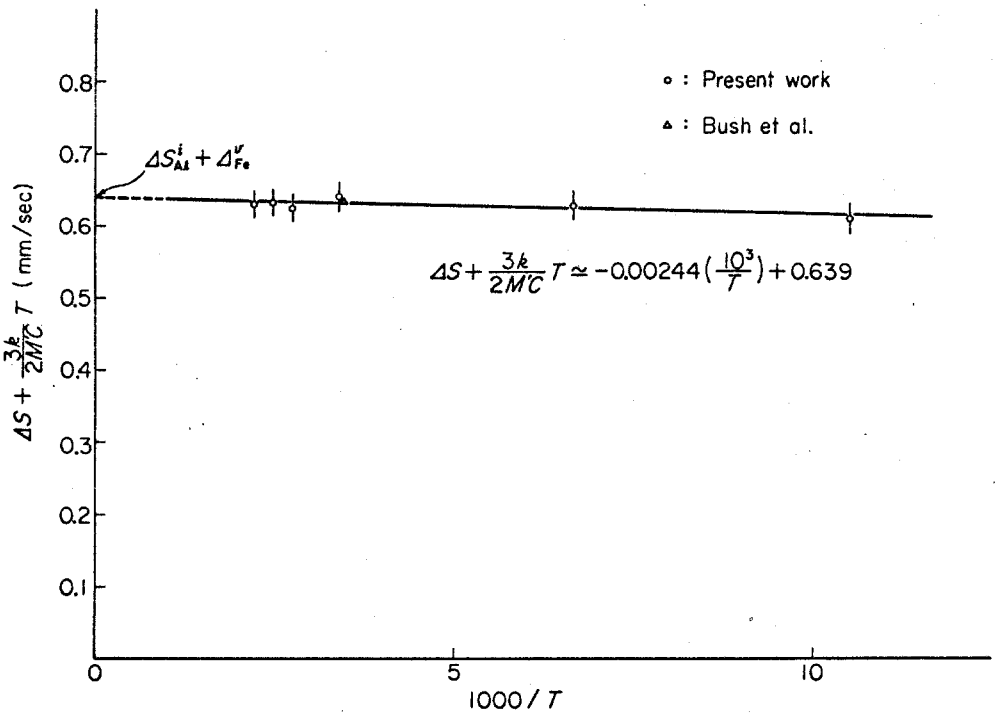

FIG. 6 The variation with temperature of the quantity $[\Delta S^{T}(T) + 3kT/2M'c]$. The straght line shows least-square fit of the data at the temperatures above 95°K.

is 0.118 mm/sec and then the isomeric shift ΔS^{i}_{Al} could be determined to be 0.52 mm/sec relative to metallic α-iron.

Isomer shift has been measured in various materials and a large amount of informations has been obtained for metals and alloys. Walker et al.[16] reported the information of the Fe^{57} Mossbauer isomeric shift in various solid relative to stainless steel and shows the observed isomeric shift as the "Walker Chart" in which the total s-electron density is plotted as a function of the percentage of 4s character for various 3d electron configurations. In the interpretation of observed shifts Walker et al. considered the fact that, is a significant differences in $|\psi_{3s}(0)|^2$ for different configurations with a much smaller change in $|\psi_{2s}(0)|^2$ and $|\psi_{1s}(0)|^2$, from the results of the restricted Hartree-Fock calculation. The variation of the 3s density at the nucleus corresponds to different degrees of shielding by the different number of 3d electrons.

In order to interpret the observed isomeric shift according to "Walker Chart", it is neccessary to convert from the value relative to α-iron to that of relative to stainless steel. The value of Fe^{57} isomeric shift in α-iron relative to stainless steel is known to be 0.09 mm/sec. Therefore, the value of isomeric shift in aluminum matrix relative to stainless steel can be estimated to be

$$\Delta S^{i}_{Al} = 0.61 \text{ mm/sec.}$$

In the "Walker Chart", we could estimate electron configuration of solute Fe^{57} atom in Al to be $3d^{7}4s^{0.7}$ or $3d^{7.2}4s^{0.8}$ assuming the electron configuration of Fe^{57} may be $3d^{7}4s^{x}$ or $3d^{8-x}4s^{x}$ (x=4s electron contribution in per cent).

The importance of this data is not, however, yet fully understood, mostly because the theory of metals and alloys has not been sufficiently developed. However, in the Al-0.01at.%Fe alloy the precipitation of clustering of Fe^{57} solute atoms can be expected after the subsequent aging treatments for the quenched specimen and the change of the isomeric shift will be followed to these type phenomena. This isomeric shift may be good tool for the investigation of the clustering and the precipitation in metals and alloys, since that was mostly changed by the variation of the solute atomic configurations. Especially, it may be able to estimate various electric changes, for example, with dislocations, vacancies and various boundaries.

Figure 19 shows the observed total shift ΔS^{T} as a function of the temperature. Eq. III-18´ is valid only for the results obtained at high temperatures above 50°K. Eq. III-19 gives

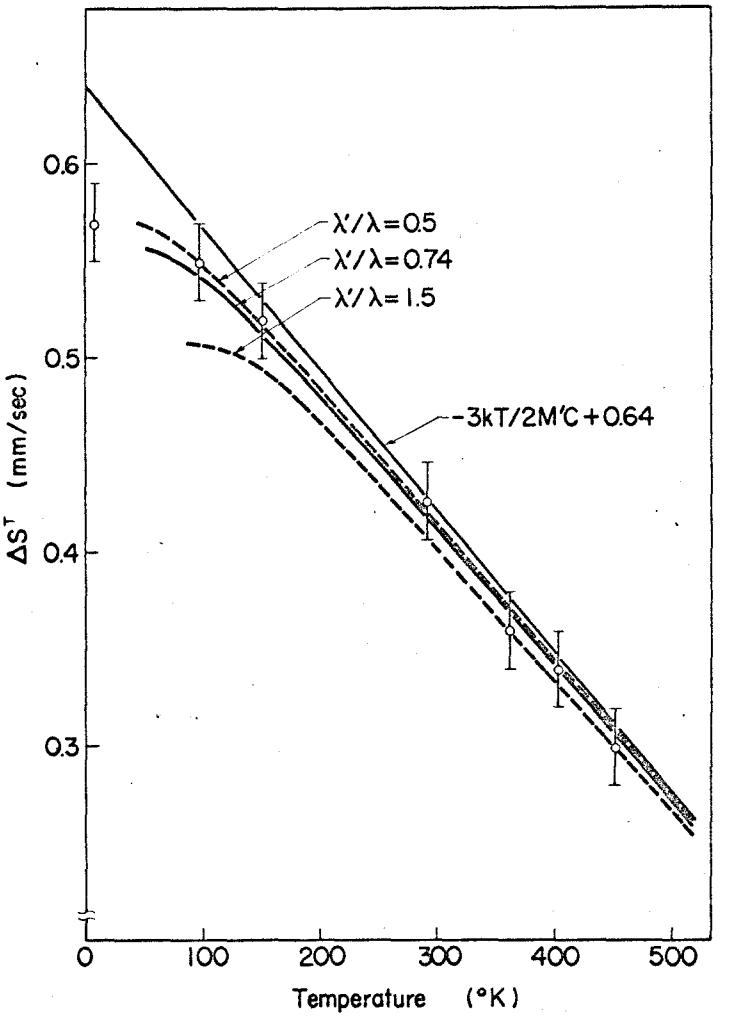

FIG. 19 The observed total shift ΔS^T as a Function of temperatures. The straight line shows the classical limit assuming the value of $[\Delta S^i_{Al} + \Delta S^v_{Fe}(R.T.)]$ is equal to 0.64 mm/sec.

$$\frac{1}{16}\cdot\frac{h^2}{k}\cdot\frac{M}{M'}\cdot\frac{1}{M'c}\cdot\omega_{max.}^2\cdot\frac{\lambda'}{\lambda} = 2.44,$$

where $\omega_{max.}$ is 6.2×10^{13} rad/sec for pure aluminum from the results of Gilate and Nicklow[17] and λ'/λ could be derived to be 0.74 using other numerical constants. The solid line in Fig. 19 shows the curve obtained by the value of λ'/λ to be 0.74. The dolled lines show the predicted curves when λ'/λ are equal to 0.5 and 1.5 respectively.

For the extremely high temperature, $1/T \to 0$, Eq. III-18' can be identical to

$$\Delta S^T(T) = \Delta S^i_{Al} + \Delta S^v_{Fe}(R.T.) - 3kT/2M'c.$$

From the least-square fit of data in the range 293°K to 453°K to straight line the experimental classical limit can be estimated to be about 7.75×10^{-4} mm/sec·°K. It is good agreement with numerical result from Pound et al.[9], that is, 7.32×10^{-4} mm/sec·°K. The classical limit is an expression of the equipartition theorem of statistical mechanics and is independent of the nature of the crystalline forces.

The deviation from the classical limit at low temperatures shows the quantum corrections introduced by the effects of

the force-constant term. As above mentioned, the force-constant ratio in Al-0.01at.%Fe alloy being smaller than unity could be estimated from the experimental results. Since the iron impurity is heavy compared to the host aluminum atoms and the impurity-host binding is also weaker than the host-host binding, a localized mode will be exist within the range of the continuum at low phonon frequency.

Above discussion was carried out by the recent interpretation for the mean-square velocity of solute atoms, but other simple expression for the mean-square velocity can be described by the Debye formula. From the Debye approximation, the energy per one atom in solid is expressed by

$$E = \frac{9}{8} k\Theta_s + 9kT\left(\frac{T}{\Theta_s}\right)^3 \int_0^{\Theta_s/T} \frac{x^3}{e^x-1} dx, \quad \text{(III-20)}$$

where Θ_s is effective Debye temperature. To calculate a mean-square velocity of atom we consider conveniently the equations of motion of the atoms in a linear chain, so that solution of the displacement x_n of n-th atoms at time t can be assumed of the form

$$x_n = u_n \cdot e^{-i\omega t},$$

where it is understood that only the real part of the

right-hand side has any physical significance. And then the velocity of the n-th atom is given by

$$V_n = \dot{x}_n = - i\omega u_n \cdot e^{-i\omega t} = -i\omega x_n ,$$

so that

$$\langle V_n^2 \rangle_{av.} = \langle (\mathrm{Re}\ x_n)^2 \rangle = 1/2 \cdot \omega^2 \cdot u_n^2 .$$

On the other hand the kinetic energy per atom is equal to

$$E = 1/2 \cdot M' \cdot |\dot{x}|^2 = 1/2 \cdot M' u_n^2 \cdot \omega^2 = M' \langle V^2 \rangle .$$

Finally, we have the modefied Eq. III-18′ expressed by the Debye formula of the form

$$\Delta S^V(T) = \frac{9k\Theta_s}{16M'c} + \frac{9kT}{2M'c}\left(\frac{T}{\Theta_s}\right)^3 \int_0^{\Theta_s/T} \frac{x^3}{e^x - 1} dx$$

$$= \frac{3kT}{2M'c} + \frac{3kT}{40M'c}\left(\frac{\Theta_s}{T}\right)^2 + \frac{kT}{1120M'c}\left(\frac{\Theta_s}{T}\right)^4 + \ldots . \qquad \text{(III-21)}$$

For high temperature, the higher order term of Θ_s/T can be neglected and then Eq. III-21 is rearranged to

$$\Delta S^{v}_{Al} = \frac{3kT}{2M'c} + \frac{3kT}{40M'c}\left(\frac{\Theta_s}{T}\right)^2, \qquad \text{(III-22)}$$

Combining Eq. III-22 and III-12, we have

$$\Delta S^{T}(T) + \frac{3kT}{2M'c} = \Delta S^{i}_{Al} + \Delta S^{v}_{Fe}(R.T.) - \frac{3kT}{40M'c}\left(\frac{\Theta_s}{T}\right)^2. \qquad \text{(III-23)}$$

From the experimental results as shown in Eq. III-19, the effective Debye temperature could be estimated to be about 220°K for the Fe^{57} impurity in an aluminum host lattice. Since the Debye temperature is proportional to the cuttoff frequency in the phonon spectrum, one might expect it to vary inversely as the square root of the mass of the impurity atom. The effective Debye temperature of the host crystal by

$$\Theta_{eff.} = (M/M')^{1/2} \cdot \Theta_{host} \quad . \qquad \text{(III-24)}$$

For the case of the Fe^{57} impurity in an aluminum host crystal, the effective Debye temperature could be estimated from Eq. III-24 to be about 260°K whose value is slightly larger than 220°K obtained by a least-square fit in Eq. III-23. Eq. III-24 simple expresses the substitution of the mass of the impurity for the mass of the host atom in the expression

for the Debye temperature and it should be invalid if the forces between the impurity atom and the host atoms are not similar to those between the host atoms themselves. Therefore, in the case of the force-constant ratio λ'/λ is smaller than the unity, the lower Debye temperature is resonable and we choice the effective temperature to be 220°K rather than 260°K.

III-3-3. Zero Point Kinetic Energy

The kinetic energy of the Fe solute atom at 0°K can be obtained from following two methods.

Firstly, it can be estimated from the two experimental total shifts $\Delta S^T(T_1)$ and $\Delta S^T(T_2)$ at the temperatures T_1 and T_2. At the temperatures T_1 and T_2, Eq. III-12′ was shown as

$$\Delta S^T(T_1) = \Delta S^i_{Al} + \Delta S^v_{Fe}(R.T.) - \Delta S^v_{Al}(T_1),$$
$$\Delta S^T(T_2) = \Delta S^i_{Al} + \Delta S^v_{Fe}(R.T.) - \Delta S^v_{Al}(T_2),$$

and then we have next expression combining above equations

$$\Delta S^T(T_1) - \Delta S^T(T_2) = - \Delta S^v_{Al}(T_1) + \Delta S^v_{Al}(T_2),$$

Since the second-order Doppler shift is of cource caused by the mean-square velocity of the Fe solute atom, the above equation is expressed to

$$\langle V^2(T_1)\rangle = \langle V^2(T_2)\rangle + 2c\{\Delta S^T(T_2) - \Delta S^T(T_1)\}. \quad \text{(III-26)}$$

For extremely high temperature, the mean-square velocity of the resonant nuclei is identical from Eq. III-17 to

$$\Delta S^V_{Al}(T) = \frac{3kT}{2M'c},$$

that is,

$$\langle V^2(T)\rangle = \frac{3kT}{M'}. \quad \text{(III-27)}$$

According to Eq. III-26 and III-27, the kinetic energy of Fe^{57} in aluminum at zero temperature can be expressed, substituting the value of T_1 equal to zero and T_2 expressed to extremely high temperature, to the form of

$$\frac{1}{2}M'\langle V^2(0)\rangle = \frac{3}{2}kT_2 + M'c\{\Delta S^T(T_2) - \Delta S^T(0)\}. \quad \text{(III-28)}$$

Secondary, the zero point kinetic energy can be also estimated using the Debye theory. In the Debye theory, the zero point kinetic energy is $9/16 \cdot k\Theta_s$; Θ_s is the effective Debye temperature. This expression simply derived from Eq. III-21 at T=0.

$$\Delta S^{V}(0) = \frac{1}{2c}\langle V^2(0)\rangle = \frac{9k\Theta_s}{16M'c}$$

$$\frac{1}{2}M'\langle V^2(0)\rangle = \frac{9}{16}k\Theta_s \quad . \qquad \text{(III-29)}$$

Using Eq. III-28, the zero point kinetic ecergy of Fe^{57} solute atoms in an aluminum fost lattice could be determined. Numerical results of experimental data in which it was that the $\Delta S^{T}(0)$ is nearly equal to $\Delta S^{T}(4.2°K)$ and the temperatures of 365°K, 403°K and 453°K used as value of T_2, are tabulated in Table 3 comparing with the value resulted from the Debye model in Eq. III-21.

Zero point kinetic energy expresses the internal energy of iron atoms in an aluminum host crystal at 0°K. If the zero point kinetic energy of aluminum atoms themselves could be estimated the increase of the internal energy at 0°K, which resulted from the alloying of iron atoms to the aluminum host lattice, may be estimated from the difference of the zero point kinetic energy between aluminum and solute iron atom.

III-3-4. Conversion from Constant Pressure to Constant Volume

In the above discussion the Maredudin's expression

TABLE 3 Average zero point kinetic energy of Fe^{57} in aluminum. In the Debye theory, the zero point kinetic energy is $9/16 \cdot k \cdot \Theta_s$. $\Theta_s = 220°K$, $T_1 = 4.2°K$.

T_3 (°K)	$\Delta S(T_1) - \Delta S(T_3)$ (mm/sec)	$\frac{1}{2} M' \langle v_0 \rangle^2$ (eV)	$\frac{9}{16} k\Theta_s$ (eV)
363°K	0.21	0.0126	
403°K	0.23	0.0112	0.0126
453°K	0.27	0.0105	

and the Debye formula were discussed under the constant volume, but the experimental data were obtained under the constant pressure. Therefore, it is necessary to convert the observed total shift, $(\Delta S^T)_p$, under constant pressure to, $(\Delta S^T)_V$ at constant volume. The experimental total shifts were converted from constant pressure to constant volume by means of the relation

$$\frac{1}{\nu}\left(\frac{\partial \nu}{\partial T}\right)_V = \frac{1}{\nu}\left(\frac{\partial \nu}{\partial T}\right)_p - \frac{1}{\nu}\left(\frac{\partial V}{\partial \ln V}\right)_T \left(\frac{\partial \ln V}{\partial T}\right)_p ,$$

where ν is the frequency of the γ-ray and we attend to the relation

$$c\frac{\partial h\nu}{h\nu} = \partial(\Delta S^T) \quad ,$$

and then, finally, following equation can be derived as the form of

$$\left(\frac{\partial S^T}{\partial T}\right)_V = \left(\frac{\partial S^T}{\partial T}\right)_p - \frac{c}{\nu}\left(\frac{\partial \nu}{\partial \ln V}\right)_T \left(\frac{\partial \ln V}{\partial T}\right)_p ,$$

In the case of Al-Fe solid solution we have not been able to estimate the value of the correlation term in right-hand side. However, if the value of $\frac{1}{\nu}\left(\frac{\partial \nu}{\partial \ln V}\right)_T$ can be assumed to be nearly equal to the value of the metallic

iron and that of the $(\frac{\partial \ln V}{\partial T})_p$ is identical to the volume expansion coefficient of the pure aluminum, the order of the correlation term at room temperature was estimated to be

$$c\frac{1}{\nu}(\frac{\partial \nu}{\partial \ln V})_T(\frac{\partial \ln V}{\partial T})_p = 0.927\times10^{-4} \text{ mm/sec°K} ,$$

At the temperatures below room temperature, the values of this correlation term are negligble small and at high temperatures 363°K, 403°K and 453°K the magnitude of the correlation term could be estimated to be 0.006, 0.01 and 0.015 mm/sec, respectively.

The magnitude of the error value in experimental data is ±0.020 mm/sec, and it is resonable to be identical the value of $(\Delta S^T)_p$ with that of $(\Delta S^T)_v$.

III-4. Conclusions

Conclusing remarks in this CHAPTER are following: (1) The Fe^{57} Mössbauer spectra in aluminum were obtained in the temperature range of 4.2°K to 453°K, using the Al-0.01at.%Fe^{57} alloy specimen which was quenched from the solid solution temperature. The best condition for the Mössbauer measurement for this alloy could be determined as the function of the specimen thickness and the gamma-ray permeability; and the specimen of 0.5 mm in thickness is best. (2) The second-order Doppler shift and the

isomeric shift of Fe^{57} in aluminum could be separated from the observed total shifts regarding the isomeric shift to be temperature independent. Isomeric shift could be estimated to be 0.52±0.02 mm/sec relative to α-iron using the results in the temperature range 95°K to 453°K. (3) Temperature dependent second-order Doppler shifts were analysed by the Debye formula and the recent Mannheim´s expression. The effective Debye temperature of Fe^{57} solute atom in aluminum and the best fitted force-constant ratio λ'/λ in Mannheim´s expression could be estimated to be about 220°k and $0.5<\lambda'/\lambda<1$, respectively. (4) The zero point kinetic energy for Fe^{57} in Al was obtained by the quantity of the second-order Doppler shift at 4.2°K and various high temperatures, and also estimated using the obtained effective Debye temperature.

REFERENCES

1. A. A. Maradudin; Solid State Physics, vol. 18, p.273, edited by F. Seitz and D. Turnbull (Academic Press, New York, 1966).

2. W. A. Steyert and R. D. Taylor; Phys. Rev., 134 (1964) A-716.

3. J. K. Edgar; Trans. A. I. M. E., 180 (1949) 225.

4. M. D. Daybell and W. A. Steyert; Rev. Mod. Phys., 40 (1968) 380.

5. J. M. Brettel and A. J. Heeger; Phys. Rev., 153 (1967) 380.

6. B. H. Bush, C. A. Stickels and L. W. Hobbs; Scripta Met., 1 (1967) 75.

7. I. Miki and H. Warlimont; Z. Metallkde., 59 (1968) 254.

8. R. V. Pound and G. A. Rebka, Jr; Phys. Rev. Letters, 4 (1960) 274.

9. R. V. Pound, G. B. Benedek and R. Drever; Phys. Rev. Letters, 7 (1961) 405.

10. B. D. Josephson; Phys. Rev. Letters, 4 (1960) 341.

11. G. W. Grodstein; NBS Standard Materials, X-ray Attenuation Coefficients From 10 KeV to 100 MeV.

12. K. S. Singwi and A. Sjölander; Phys. Rev., 120 (1960) 1093.

13. A. A. Maradudin, P. A. Flinn and S. Ruby; Phys. Rev. 126 (1962) 9.

14. P. D. Mannheim and A. Si,opoulos; Phys. Rev., 165 (1968) 845 & 1011.

15. R. S. Preston, S. S. Hanna and J. Heberle; Phys. Rev., 128 (1962) 2207.

16. L. R. Walker, G. K. Wertheim and V. Jaccarino; Phys. Rev., 6 (1961) 98.

17. G. Gilat and R. M. Nicklow; Phys. Rev., 143 (1966) 487.

CHAPTER IV

MÖSSBAUER EFFECT STUDY ON COBALT DILUTE Cu-Co ALLOYS

IV-1. Introduction

In chap. II, we could obtained many fruitful results in the study of iron dilute Al-Fe^{57} alloys using the Fe^{57} Mössbauer effet and the Fe^{57} Mössbauer spectra were measured by the specimen as a γ-ray absorber. However, the electric and magnetic properties for the environments of Co^{57} atoms which were doped into a source material can be also investigated by the Mössbauer measurements, in which the source materials are used as a specimen and the absorber is used as a metal or alloy whose elecric and magnetic properties are well known such as stainless steel, as mentioned at the introductory remarks in Chap. I.

In the Mössbauer study of the Al-Fe alloys, the Co^{57} in pure copper foil was used as a monochromatic γ-ray source. Active Co^{57} nucleus decay to the first excited states Fe^{57*} by the K-electron capture after about 10^{-8} sec and then, also after 10^{-8} sec, decay to the ground states Fe^{57} by the 14.4 KeV γ-ray emission (resonanced γ-ray)[1]. Therefore, the Fe^{57} Mössbauer effect has been observed only after the decay from Co^{57} and its decay time need only about $10^{-7}\sim10^{-8}$ sec without any atomic jumps. If there are any atomic jumps for the resonant nuclei,

the Mössbauer spectra cannot observed because of the not being recoilless for the Fe^{57} resonant nuclei[1].

It is fact that the variations in the Mössbauer spectra as a function of the heat-treatments in source materials which is a specimen in the experiments (on the contrary to the description in Chap.I) indicates the variations of the environments of the Co atoms in that source material[1]. As above mentioned, the radio-active Co^{57} atoms doped into the Cu-dilute Co alloys behave as a solute Co atoms in a similar manner in diffusive motions to the other cobalt atoms previously being existed in these alloys. Therefore, the Mössbauer measurements in the Cu-dilute Co alloys in which the Co^{57} atoms are doped are one of the most powerful methods to investigate the seggregation and precipitation of the solute Co atoms in this alloy, since all of those phenomena are controlled by the diffusive motion of the solute Co atoms.

The aim of this chapter is firstly to observe the Mössbauer spectra using the variously heat-treated Cu-2% Co alloys in which Co^{57} atoms were doped. From the Mössbauer spectra obtained this specimens, we attempt to determine the solubility of cobalt in solid copper using the technique described in Chap. II (Sec. IV-3-1), to observe firstly the superparamagnetism[2] of precipitated Co-rich particles and also determine the size distribution

of the precipitated particles being applyed its superparamagnetic transition (Sec. IV-3-2). In Sec. IV-3-3, we discuss the Mössbauer spectra observed at 4.2°K, since the study for the onset of the precipitation process is the most important subject in the problem of the decomposition of the supersaturated solid solution[3]. The structure of the Co-rich particles precipitated in Cu-Co alloy matrix is expected to be face ectered cubic and the f. c. c. → h. c. p. phase transformation of the particles may be possible to be induced by the plastic deformation of the specimen[4], so that we attempt to observe direct evidence of the phase transformation by the value of the effective hyperfine fields and the magnitude of the effective anisotropy energy by the analysis of the Mössbauer spectra.

IV-2. Sample Preparation and the Experimental Procedure

Cu-1.97 and 3.52at.%Co alloy ingots were prepared by melting from 99.5% cobalt and oxgen-free 99.995% copper. The melting was carried out at vacuum atmosphere or under a innert gas protection. For the Mössbauer measurements, the platellet alloy specimen, 1 mm thick and about 20 mm in diameter, were cut from this alloy ingots. For the gamma-ray source, Co^{57} was electro-plated onto the disk of this alloy specimen. Electro-plating was carried out in a manner illustrated in Fig.21 using $Co^{57}Cl_3 \cdot HCl$ solution.

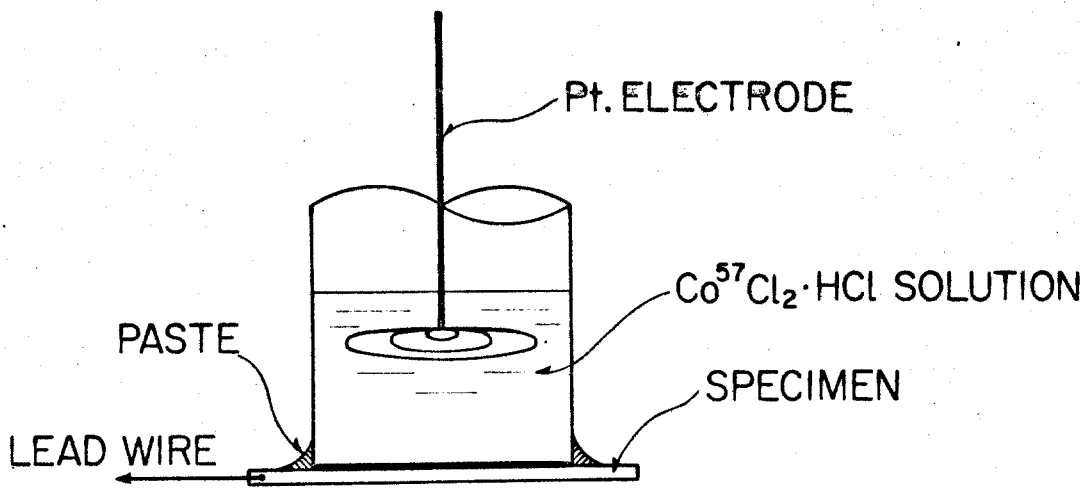

FIG. 21 Electro-plating apparatus for the Co^{57} source on the specimen.

After plating, this source was annealed at about 950°C in hydrogen atmosphere. The activity of the source was about 0.5 mC. Stainless steel foil was always used as a absorber.

Mössbauer measurements were made using a commercial T. M. C. set (Gammascope 102, Drive Unit 306 and Transducer 305) operated in a time mode. For the measurements at room temperature, the specimen used as a source was attached on the Transducer of the T. M. C. set. However, for the low temperature measurements, the specimen was attached on the coolant of the Dewar and the absorber (stainless steel foil) has been given to the Doppler velocity by the Transducer. Experimental geometry for the low temperature measurements are illustrated with the liqid helium Dewar vessel in Fig. 22.

For the solution heat treatment, the specimen was homogenized in an evacuated silica tube for 30 minutes or 1 hour at above 900°C and then quenched into water. Subsequent aging treatments were done for various time at various temperatures, mainly at 600°C, and then quenched into water.

In Sec. IV-3-5, the specimen was gradually reduced in thickness after the aging treatment and the Mössbauer spectra were taken at each stages of rolling. The reduction of thethickness by one pass was 5∿7 per cent.

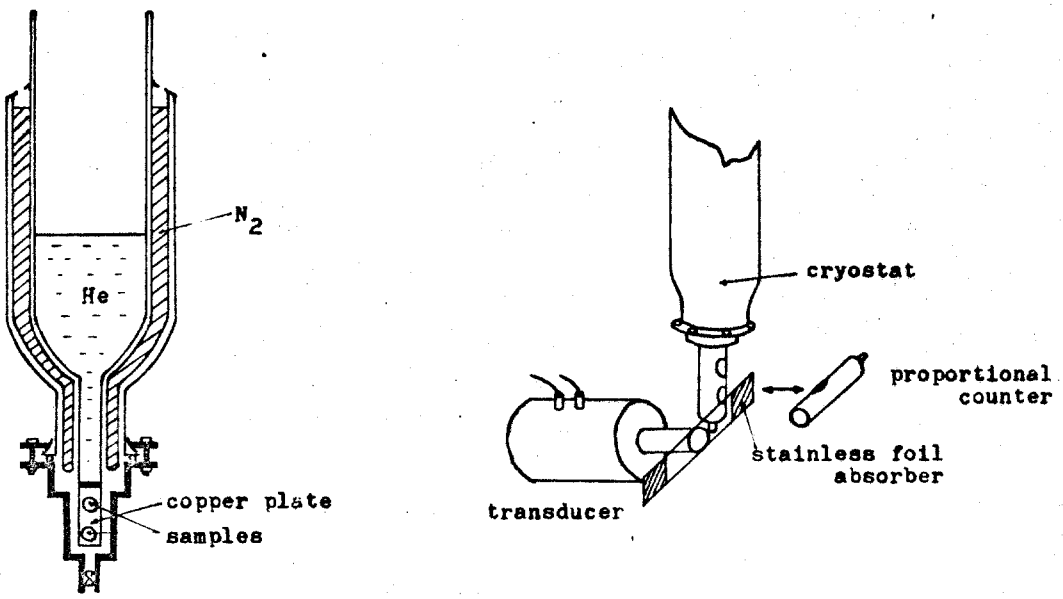

FIG. 22 Glass Dewar for the masurement at liqiud helium temperature.
Illustration for absorber vibration at the Mössbauer measurements.

For the electron microscopic observation, an apparatus of J. E. M. 120 type was used by thin film technique. The electro-thining was performed at -20°C in 50% phosphoric acid solution.

IV-3. Experimental Results and Interpretations

IV-3-1. Solubility of Cobalt in Solid Copper

In Chap. II, the solid solubility of iron in aluminum could be successfully estimated from the analysis of the Mössbauer spectra. In this section, using the similar technique to the Chapt. II we attempt to determine the solubility of cobalt in solid copper as a function of the temperature.

The Mössbauer spectrum of Fe^{57} produced by the decay of Co^{57} represents the environments of the mother nucleus, Co^{57}. If the Fe^{57} nucleus is situated in a sufficiently large Co particles, the spectrum is ferromagnetic (6-line)[5]. On the other hand, it is paramagnetic (single line) when Fe^{57} is dissolved in the Cu matrix or when Fe^{57} lies in a very small Co particles whose magnetization fluctuates faster than the nuclear Larmor precession time and then behaves as superparamagnetic. At room temperature, the

transition from superparamagnetic to ferromagnetic for the spherical f. c. c. Co particles is known to occur at the particle size of about 120 Å in diameter (detailed discussion are presented in next section and also it is noticed in a final CHAPTER)[6]. Therefore, if the specimen containing Co atoms was annealed for a long time enough to grow the precipitated particles above 120 Å in diameter, the Mössbauer spectra of the specimen show the superposition of a single line and a 6-line splitting and then Eq. II-1 is rewritten by

$$Y(X) = \left[\frac{A_o}{1+4(B_o-X)^2/C_o}\right]_{\text{matrix}} + \left[\sum_i^6 \frac{A_i}{1+4(B_i-X)^2/C_i}\right]_{\text{particles}}, \qquad \text{(IV-1)}$$

Using Eq. IV-1, the integrated intensity ratio of a ferromagnetic and paramagnetic components can be estimated and also Co concentrations being existed in the alloy matrix are determined as a function of the annealing temperatures, if the precipitated particles is pure f. c. c. cobalts.

A typecial Mössbauer spectrum of the Cu-1.97at.%Co alloy specimen annealed at 500°C is shown in Fig. 23 and the quantity of the paramagnetic Co components can be estimated to be about 10% (0.19at.%Co in alloy composition). The magnitude of the effective hyperfine field at Fe^{57} nuclei

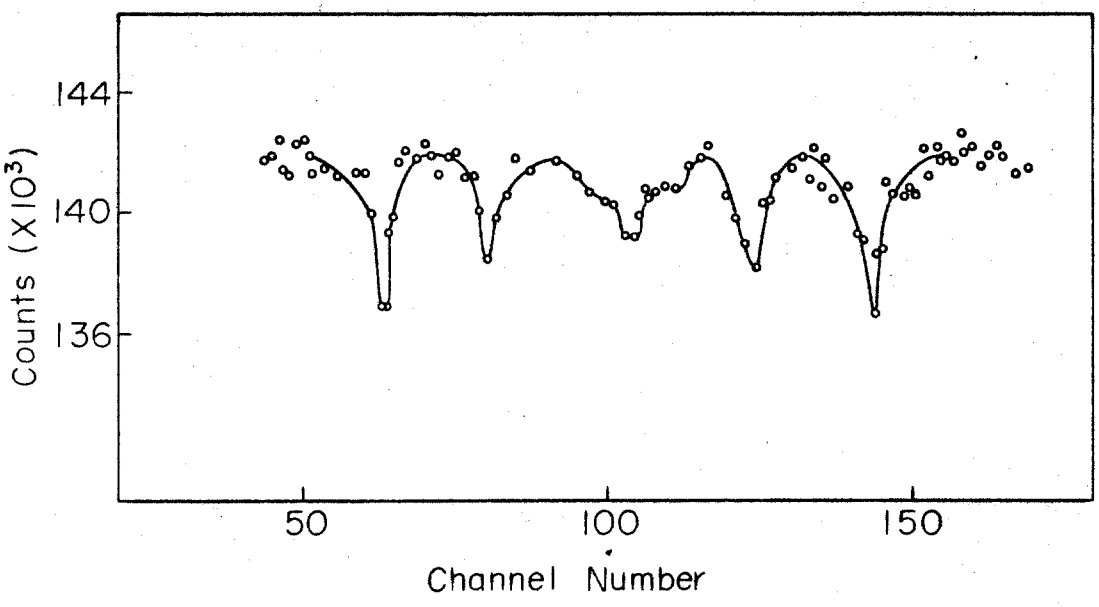

FIG. 23 Mössbauer absorption spectrum for the Cu-1.97%Co alloy at 288°K. Alloy was annealed at 500°C for 5 days after cooled down slowly from 900°C, and then quenched into water.

in precipitated particles can also estimated to be 325±5 KOe by the peak position of the 6-line splitting and fairy agrees well with that of Fe^{57} in f. c. c. Co metal determined by NMR method[7]. Accurate determination of the alloy composition in the precipitated second phase in alloy matrix is probably impossible by the general experimental technique, but we will discuss at later parts in this section its possibility of the analysis of the precipitated second phase in alloy matrix using the value of the effective hyperfine fields at the Fe^{57} nuclei. Accurate estimation for the hyperfine fields at the Co^{59} nuclei and its application for the determination of the alloy composition can be made by the NMR technique and is presented in CHAPTER VI. Assuming the second phase precipitated in alloy matrix are pure f. c. c. cobalt metals, we estimated the values of the solubility of cobalts in solid copper using the integrated intensity ratio in observed Mössbauer spectra. Figure 24 shows the solid solubility of Co in Cu at various temperatures compared with previous results. The present results agree, in general, with previous experiments. It is again proved that the Mössbauer effect being measured by a specimen used as a source is useful tool for the determination of the solubility limits in a solid alloy system, and especially this technique seems to be powerful for the system not containing Fe atoms.

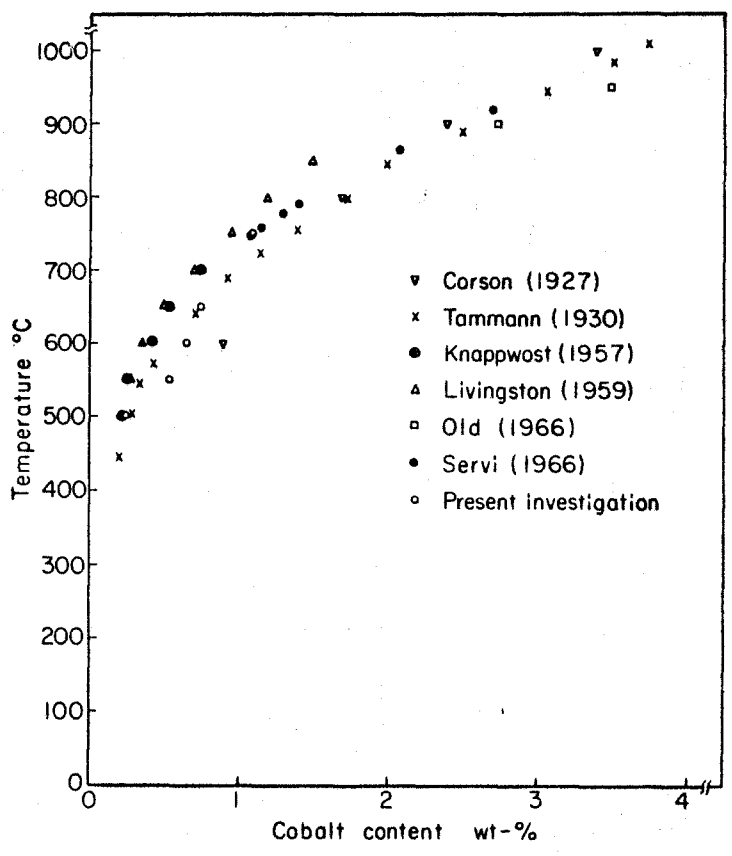

FIG. 24 Temperature dependence of the solubility of cobalt in solid copper.

From the 6-line component of the spectrum the magnitude of the effective hyperfine field was estimated as a function of the annealed temperature and the values were shown in Fig. 25. The variation of the magnitude is thought to be due to the difference of the Cu concentration in the precipitated Co-rich particles, but the quantitative analysis of the Cu concentration from the present results may be very difficult for the not being obtained many accurate values of the Fe^{57} Hyperfine field in Cu-Co alloy system. Applying the NMR technique we will present the new method to determine the Cu concentration in the second phase precipitated from the alloy matrix in CHAPTER VI.

IV-3-2. Size Distribution of Precipitated Co-rich Particles

In previous Sec. IV-3-1, we could estimated the solid solubility of cobalt in copper using the specimens which was annealed for a sufficiently long time enough to show the all of the precipitated particles are ferromagnetic and those particle diameter are above 120 Å. If the specimen contains the precipitated Co-rich particles whose diameter are below 120 Å, the Mössbauer spectra consist of the three components; that is, Eq. IV-1 is rewritten by

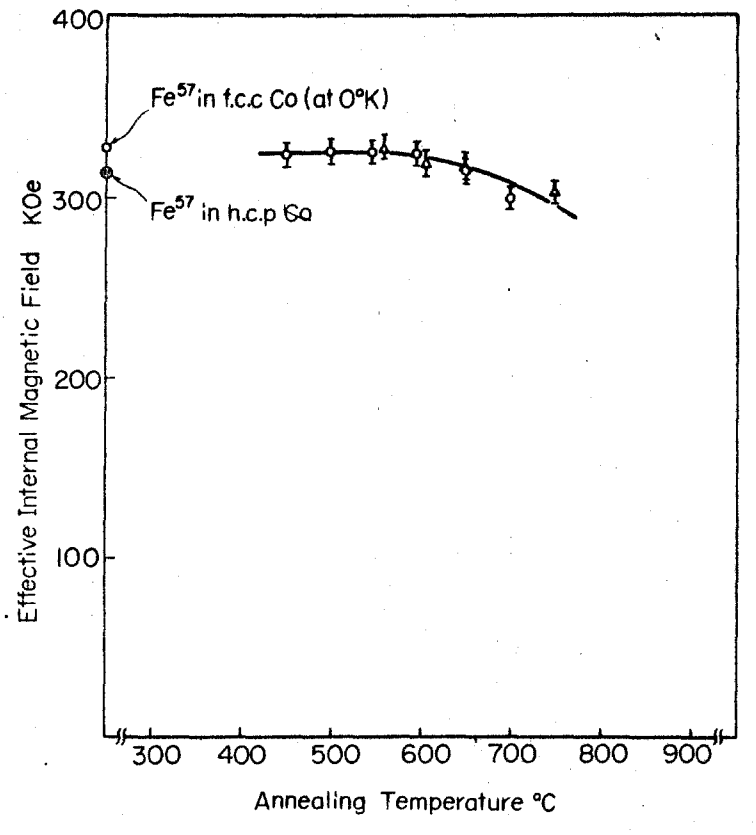

FIG. 25 Effective internal magnetic field at Fe^{57} nuclei in precipitated second phase as a function of annealing temperature.

O : quench and aged

Δ : cooled down and then quenched.

$$Y(X) = \left[\frac{A_o}{1+4(B_o-X)^2/C_o^2}\right]_{\text{matrix}} + \left[\frac{A_o'}{1+4(B_o'-X)^2/C_o'^2}\right]_{\text{superpara.}} + \left[\sum_{i=1}^{6} \frac{A_i}{1+4(B_i-X)^2/C_i^2}\right]_{\text{ferro.}} \quad \text{(IV-2)}$$

The second term in right members in Eq. IV-2 is shown as superparamagnetic components, its Mössbauer profile is same to the first term of paramagnetic component, and the contribution of the second term to the total resonance absorption depend on the test temperatures, if the Mössbauer fraction in each component has a same value. The size distribution of the precipitated particles can be estimated by the quantity of the superparamagnetic component in Mössbauer spectra.

In this section, we attempt to determine the size distribution of Co-rich particles precipitated in Cu-1.97at.% Co alloy from the analysis of the Mössbauer spectra and to compare the results obtained with the observation of thin film electron microscopy.

The Cu-1.97at.%Co alloy specimen, in which Co^{57} was doped as described in Sec. IV-2, was homogenized in evacuated silica tube for 30 minutes at 900°C and then quenched into water. After the solution heat treatment the specimen was aged for 10 hours at 600°C.

Figure 26 shows the Mössbauer spectra measured at various temperatures between 90°K and 350°K. Most of the Mössbauer spectra in Fig.26 consist of ferromagnetic component and paramagnetic one. From the ratio of the area of center single line component to that of 6line splitting, the paramagnetic Co component in Cu matrix was estimated. All of the Co particles precipitated in this alloy behave as superparamagnetic at 335°K.

According to Nee's estimation[8], the relaxation time of the superparamagnetic spin, τ, can be expressed by the following relation;

$$1/\tau = f_o \exp(- KV/kT), \qquad \text{(IV-3)}$$

where f_o is the frequency factor with approximate order of 10^{10} c/s or 10^9 c/s[9], K is the effective anisotropy constant and V the particle volume.

When the relaxation time of the superparamagnetic spin is longer than the Lamor precession time of the nucleus and also longer than the life time of the nuclear levels in Mössbauer resonance, the nuclear levels are are effectively splitted by the nuclear Zeeman effect and the Mössbauer spectrum indicates the 6-line splitting[5,10]. On the contrary, if the relaxation time is shorter, the magnetic hyperfine structure collapsed and the Mössbauer spectrum

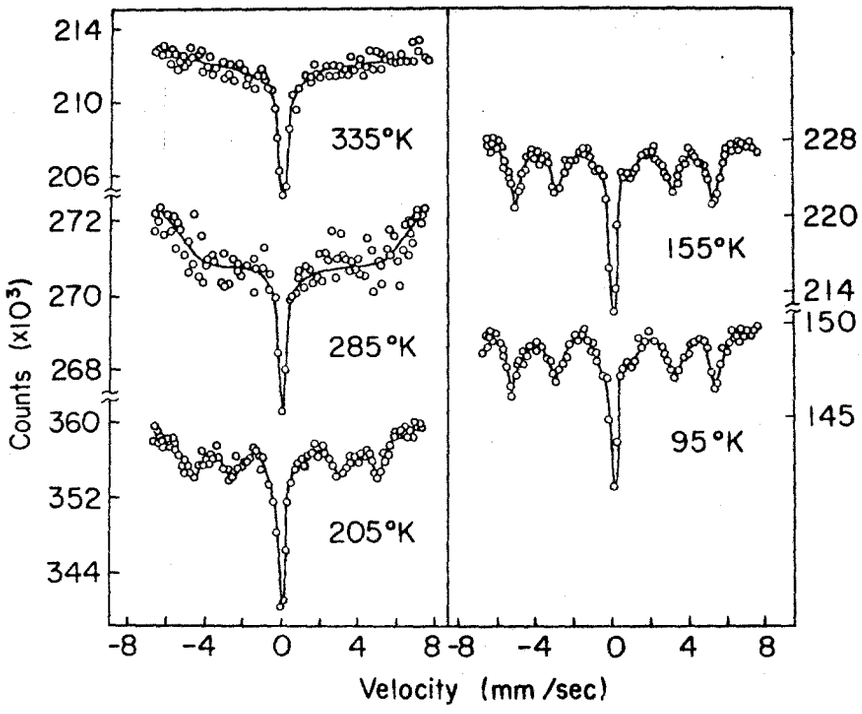

FIG. 26. Mössbauer spectra of Co^{57} in Cu-Co alloy at various temperatures. The sample was aged at 600°C for 10 hours. A stainless steel foil was used as an absorber.

shows the single line[5,10]. The broad line is shown when two values are comparable. The relationship between relaxation time of the superparamagnetic electron spin and the profile of the Mössbauer spectrum is shown in Fig. 27 which was estimated for the effective hyperfine field of 550 KOe by Wickmann et al.[10]. From this investigation, if the relaxation time of electron spin is shorter than 3×10^{-9} sec, the magnetic hyperfine structure is collapsed. Therefore, inserting this value into Neel's equation and assuming $K=2\times10^{5}$ erg/cm^3 for f. c. c. cobalt[11], the critical volume of the superparamagnetic Co particles can be derived as a function of temperature. From the ratio of the area, the volume fraction of smaller precipitates than the critical volume was estimated.

The results obtained from the spectra in Fig. 26 are tabulated in Table 4 and the critical size which shows the superparamagnetic particles in the Mössbauer spectra estimated from the Neel's equation is also tabulated in Table 5. Figure 28 shows the atomic fraction of Co atoms which consist of precipitated particles as a function of the particle diameters.

The size distribution of the particle can be estimated by the distribution of the atomic fraction of the precipitated cobalts percentage and it is calculated by

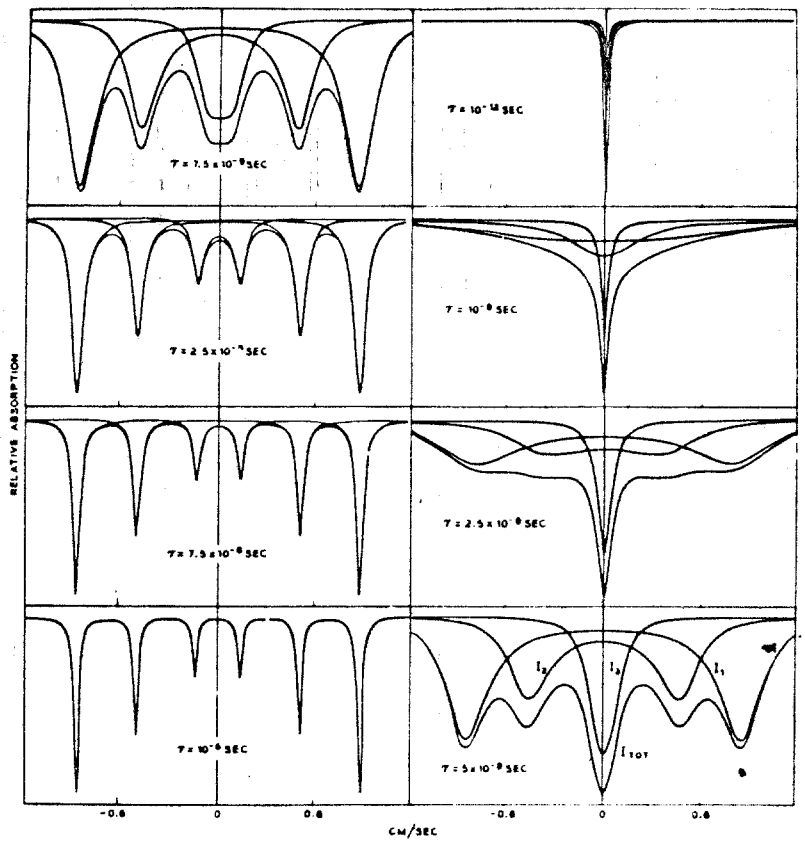

FIG. 27 Relationship between the relaxation time of the superparamagnetic electron spin and the Mössbauer profiles when the hyperfine field is 550 KOe. (after Wickman).

TABLE 4 The percentage of the superparamagnetic fraction in FIG. 26 as a function of the temperature.

Temp. °K	Superparamagnetic %
95	35
155	38
205	52
285	88
335	100

TABLE 5 Critical size of the particle showing the superparamagnetism in the Mossbauer spectrum as a function of the temperature.

Temp. °K	Critical Size Å
95	74
155	87
205	95
288	110
335	125

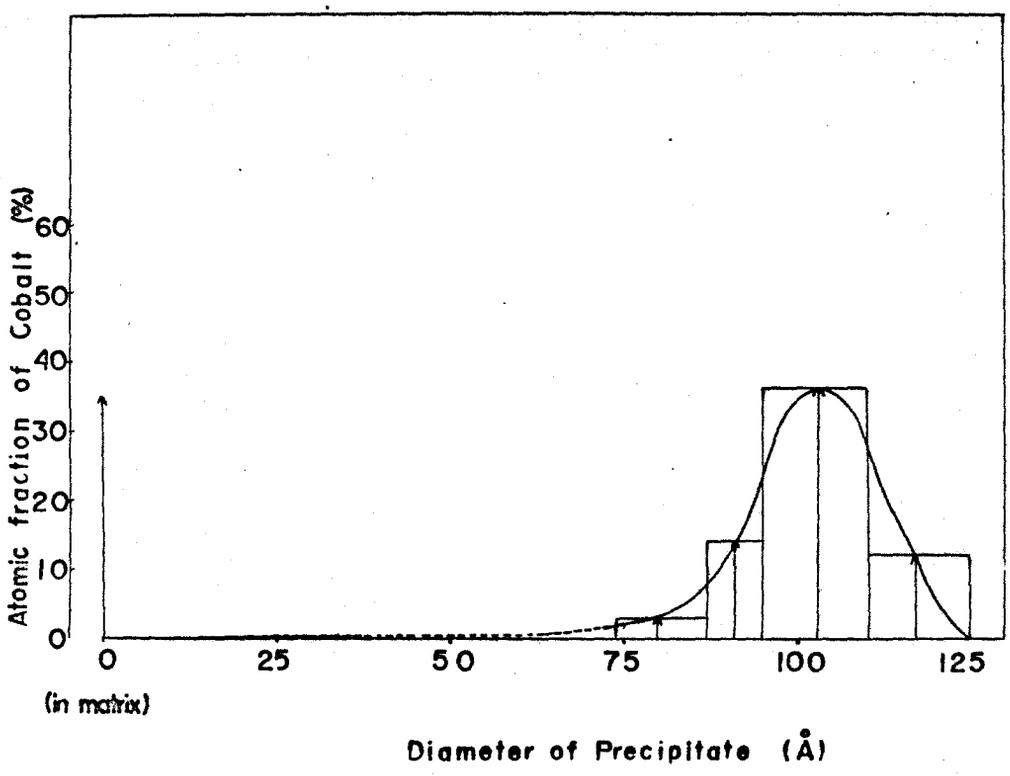

FIG. 28 The distribution of Co atomic fraction as a function of the particle diameter.

$$\Delta N(i) = A(i) / \sum_{i=0}^{\infty} A(i)/V(i), \quad \text{(IV-4)}$$

where $\Delta N(i)$ is the number of particles whose size is "i", N is the total number of precipitated particles, A(i) is the the atomic fraction of the Co atoms which consist of precipitated particles having average diameter of i and V(i) is the volume of a particle whose diameter is "i".

Photograph 1 shows the thin film electron micrograph of the specimen treated samely as that of the Mossbauer measurements. The great coherency strain fields between spherical precipitates and the alloy matrix are shown. It is notable that the size distribution seems to be very narrow and easily estimated.

Figure 29 shows the size distribution of precipitated Co particles in the present study in comparison with the results of electron micrograph. The dotted line was obtained by the Mössbauer spectra and the solid line resulted from the thin film electron micrograph. It is suggested that these two results agree well with each other, if the Neel's frequency factor f_o is equal to be 10^{10} c/s.

IV-3-3. Precipitation Process in Cu-dilute Co alloys

In previous section, we could determine the solid

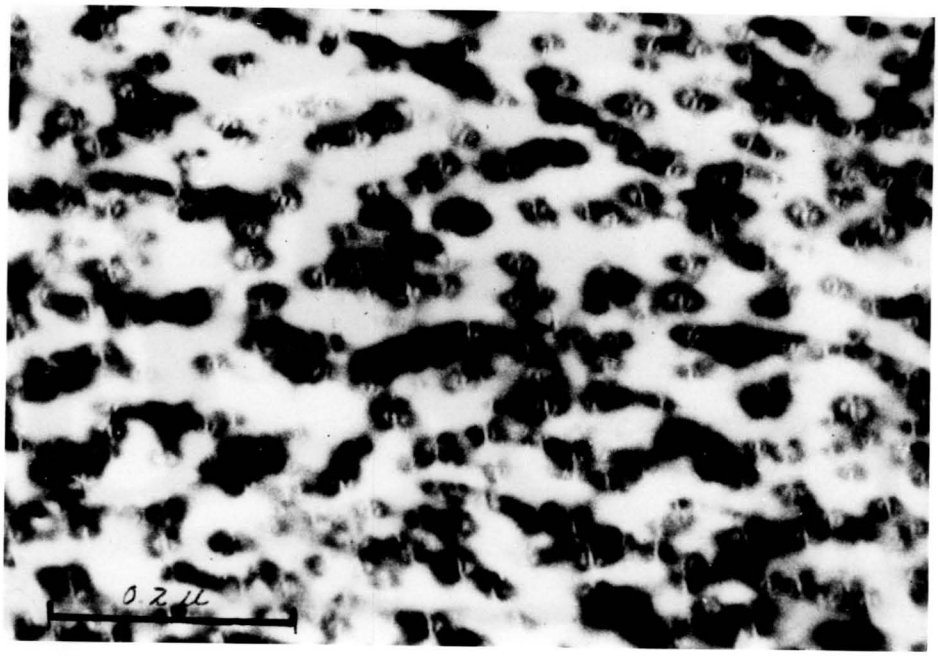

PHOTO. 1 Thin foil electron micrograph of the specimen which was aged for 10 hours at 600°C.

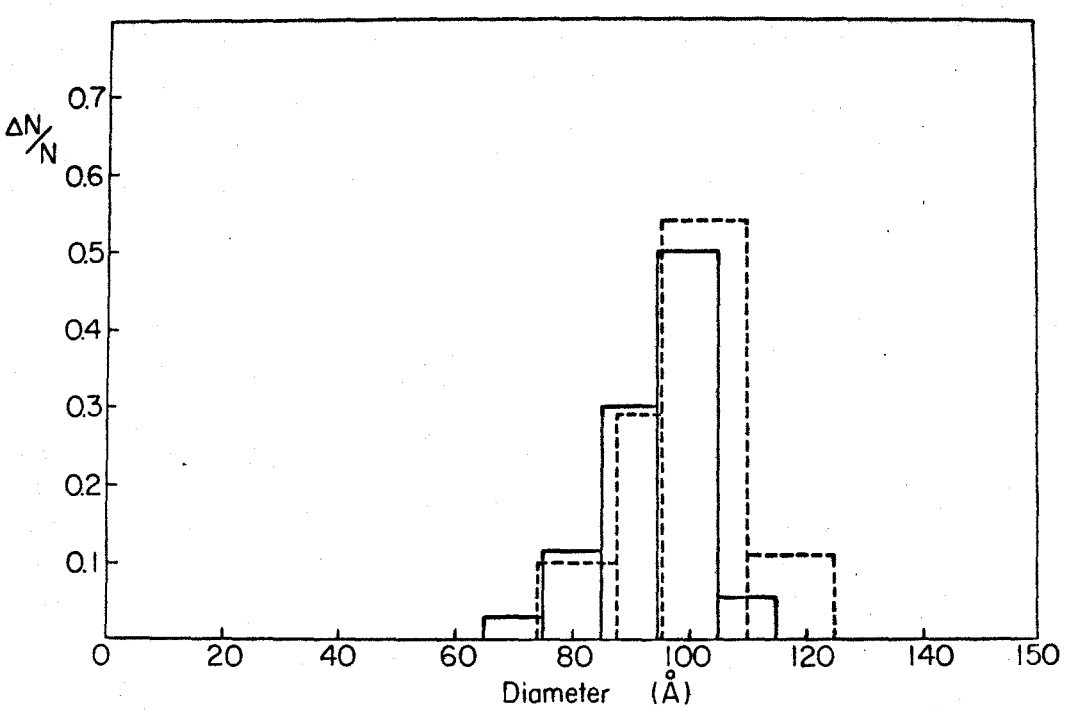

FIG. 29 Statistical distribution of diameter of the spherically precipitated Co particles after isothermal heat treatment for 10 hours at 600°C. The dotted line obtained from Neel's equation, assuming $f_o=10^{10}$ c/s and $K=2\times10^5$ erg/cm^3. The solid line gives the distribution from the electron micrograph.

solubility of cobalt in copper and the size distribution of the precipitated particles in matrix using the Mössbauer technique. In the same way, the precipitation process in the Cu-dilute Co alloys can be discussed by the analysis of the Mössbauer spectra. The decomposition of the supersaturated solid solution of the Cu-dilute Co alloy has been well recognized to be simple[12]; that is, the Co-rich precipitates are firstly spherical in shape and the growth kinetics of the precipitates obeys the general coarsening equation.

In Fig. 30 the variations of the various properties in Cu-1.97at.%Co alloy specimen are shown as a function of the aging time at constant temperature of 600°C. The value of 0.2% proof stress gradually increases with the aging time and reaches to maximum value at 10^3 minutes. This fact implies that the precipitated particle size gradually increase with the aging time. The Co atomic fraction for the precipitated particles does not, however, depend on the aging time and the magnitude of the effective hyperfine fields reaches at constant value of 325±5 KOe after the arrival to the ferromagnetic region (that is, above 120 Å in diameter). The diameter of the precipitated particles increases gradually with the aging time, but the atomic fraction of the precipitates is constant and the alloy composition is also constant for the increase of the aging

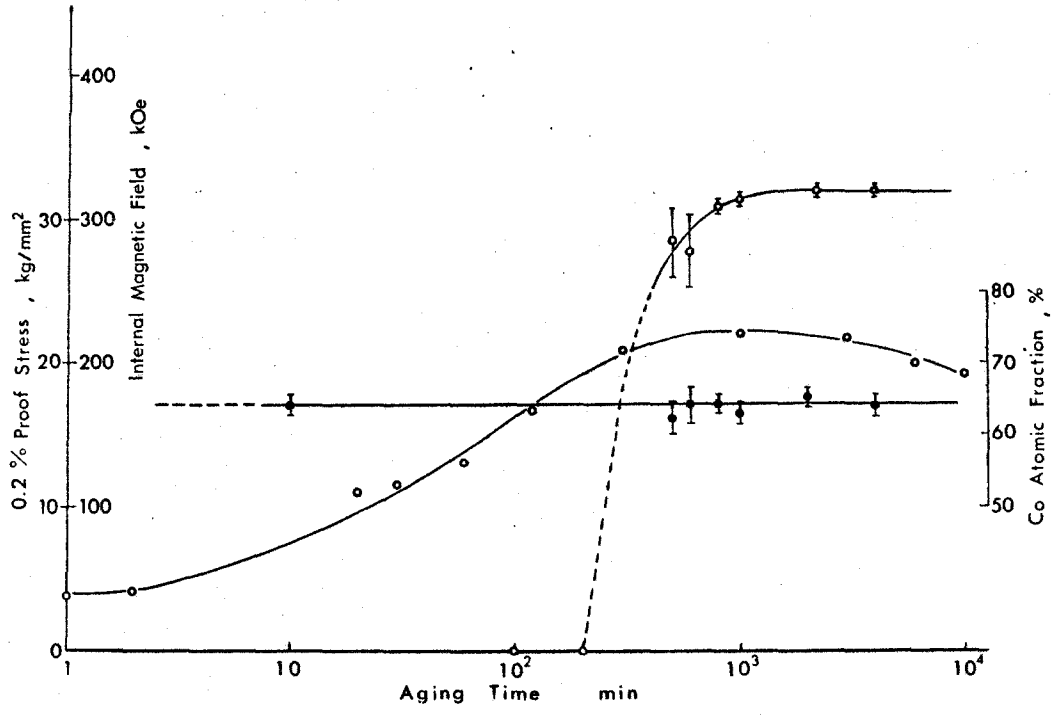

FIG. 30 Variations of the 0.2% proof stress, Co atomic fraction and the effective internal magnetic field in Cu-1.97%Co alloy specimen during 600°C isothermal aging.

time. The kinetics of the precipitation follows the mechanism of so called "coalescence" during the aging treatment at least annealed for above 10 minutes. The knowledge for the onset of the decomposition, in this case the aging time is shorter than 10 minutes, is the most important and then we investigate in this section to discuss the conditions of the solute atoms immediately after the quenching from the solid solution temperature.

There are many investigations for the behavior of the quenched-in vacancies[13,14], but the investigations about the quenched-in cluster of solute atoms (it means a kind of solute atom segragation which caused during the quenching treatment). Becker[15], in 1957, detected the cluster of the solute atoms in the magnetic measurements of Cu-2%Co alloy and estimated the size of the cluster to be about 10 Å in radius at the onset of the aging sequence at 650°C as being shown in Fig. 31. According to the Neel´s estimation, the relation between the superparamagnetic relaxation time and the radius of the Co particles can be estimated at the temperatures of 4.2°K, 95°K and 300°K and is shown in Fig. 32. The precipitated Co particles whose radius are above 10 Å show the ferromagnetic in Mossbauer spectrum at 4.2°K. Figure 33 shows the Mössbauer spectrum at 4.2°K and 95°K obtained by the Cu-3.52at.%Co alloy specimen which was annealed for 1 hour at 1075°C in

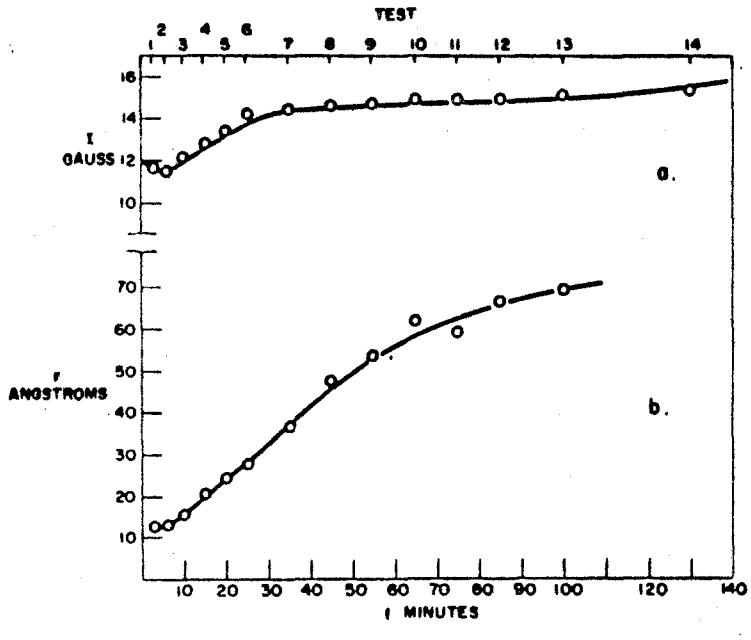

FIG. 31 Graph plots change in saturation and effective particle radius with aging time at 650°C. (after Becker).

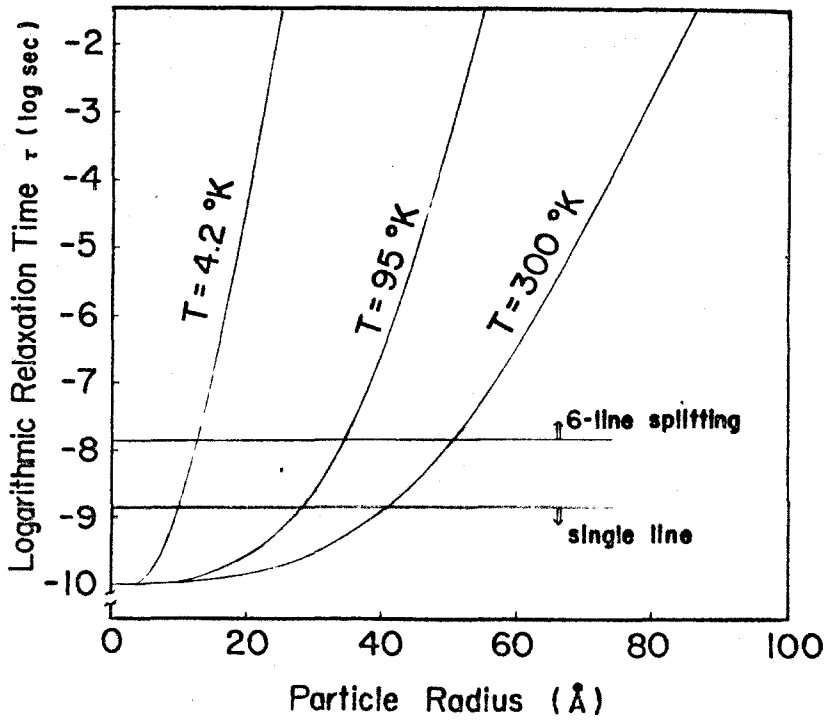

FIG. 32 Relation between the relaxation time of the superparamagnetic electron spin at the temperatures of 4.2, 95, and 300°K, according to the Neel's equation.

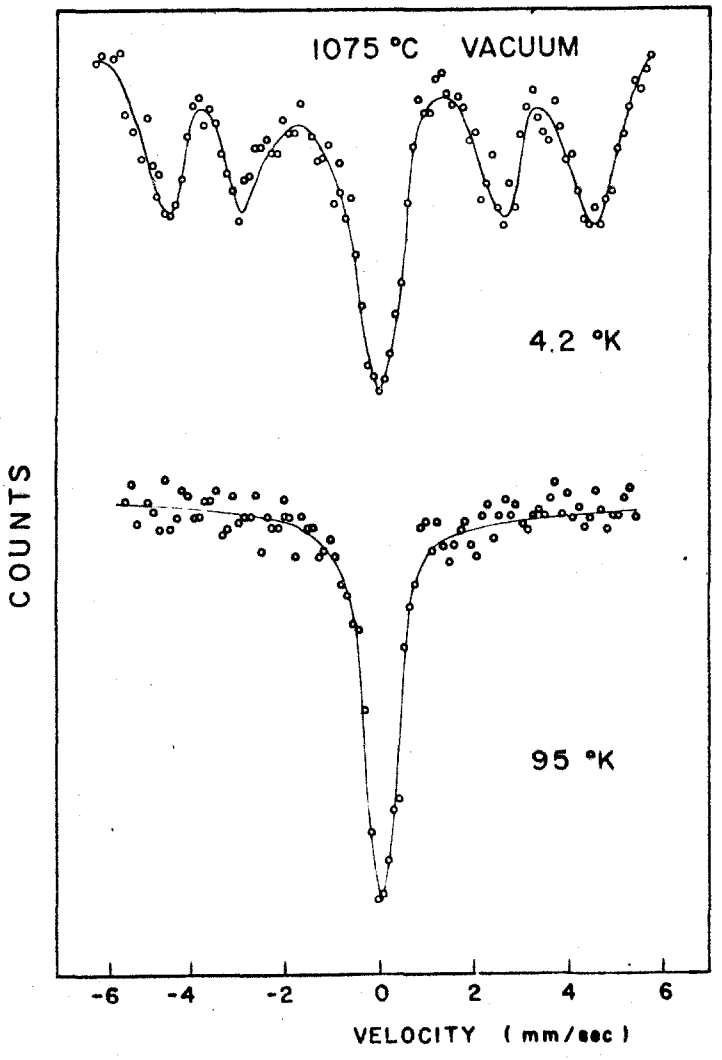

FIG. 33 Mössbauer spectra at 4.2°K and 95°K obtained by the Cu-3.52at.%Co alloy specimen which was annealed for 1 hour at 1075°C in evacuated silica tube and then quenched into 0°C water with the silica tube to obtain slow cooling rato for the specimen.

evaccuated silica tube and then quenched into 0°C water with the silica tube to obtain the slow cooling rato for the alloy specimen. The upper spectrum measured at 4.2°K shows obviously ferromagnetic components, but the lower spectrum measured at 95°K show the complete single line. Using the specimen which was quenched and crushing to obtain the rapid cooling rato, Mössbauer spectrum measured at 4.2°K does not indicate obvious ferromagnetic 6-line splitting, but its spectrum does not also complete paramagnetic single line. These results imply that it is very difficult to obtain the supersaturated solid solution in Cu-3.52at.%Co alloy specimen even if the rapid quenchin g from 1075°C and there are some quenched-in cluster whose size and quantity depends on the cooling rate during the quenching.

IV-3-4. Phase Transformation of Precipitated Co-rich Particles Induced by Cold Rolling

In Neel´s equation, when the particle volume, V, and temperature, T, are constant, the relaxation time of the superparamagnetic spin is a function only of the effective anisotropy constant of the particle, K, so that it is able to discuss the magnitude of the anisotropy constant by observing the Mössbauer spectra. In this section we attmpt

to observe the changes in the structure and the shape of the precipitates with the cold rolling by discussions about the variations of the magnitude of the anisotropy constant, K, according to the change in the Mössbauer profiles.

Figure 34 shows the Mössbauer spectra obtained from the specimens which were unrolled, rolled of 7% reduction in thickness and 97% reduction in thickness respectively. All of the spectra was measured at room temperature. The spectrum of the unrolled specimen shows the broad single line. In the spectra of rolled specimen which was reduced in thickness, the 6-line splitting of ferromagnetic components are appeared. The appeareance of the 6-line components is considered to be arise from the increase of the relaxation time of the superparamagnetic electron spin. The change of the superparamagnetic electron spin relaxation time τ results from the change of the magnitude of the effective magnetic anisotropy constant K in Neel's equation of Eq. IV-3. The integrated intensity ratio of the 6-line components in Fig. 34 to that of the single line was estimated for the rolled specimen which was reduced 7% in thickness to be same as the results from the Mössbauer profile measured by the specimen at 95°K in Fig. 34.

Figure 35 shows the relationship between the relaxation time τ of the superparamagnetic electron spin and the effective magnetic anisotropy constant K when the test temperature T

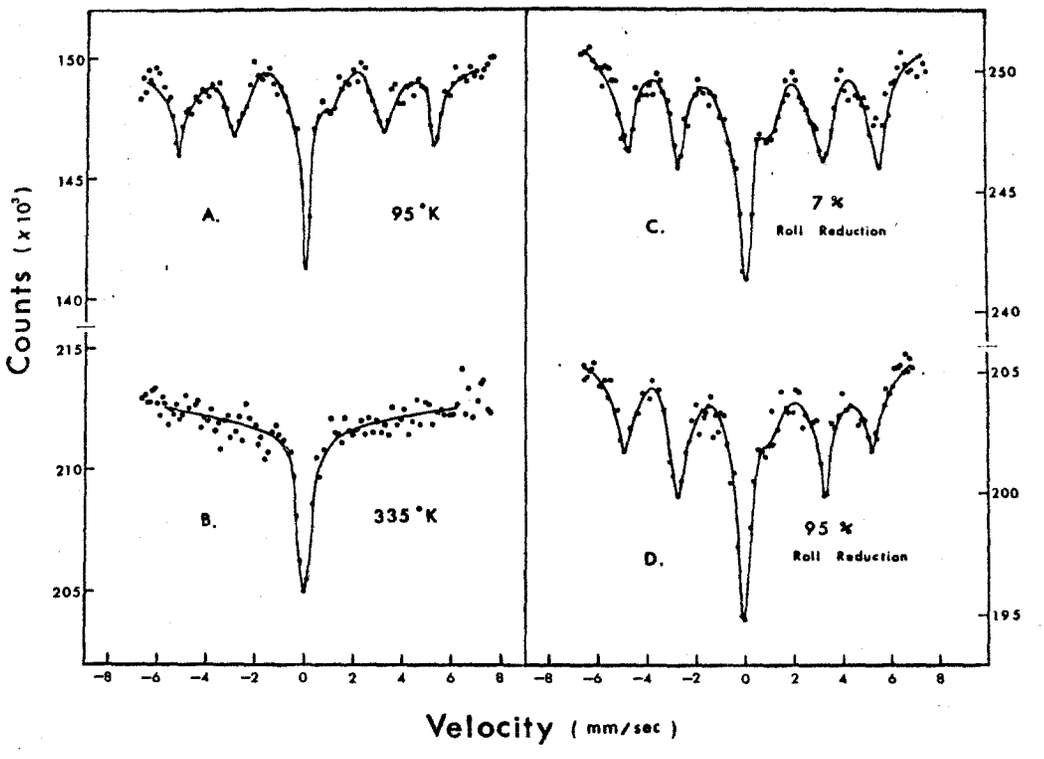

FIG. 34 Mössbauer spectra obtained before and after rolling. A stainless steel foil was used as an absorber.

A : unrolled specimen at 95°K.

B : unrolled specimen at room temperature.

C : rolled specimen reduced 7% in thickness measured at room temperature.

D : rolled specimen reduced 95% in thickness measured at room temperature.

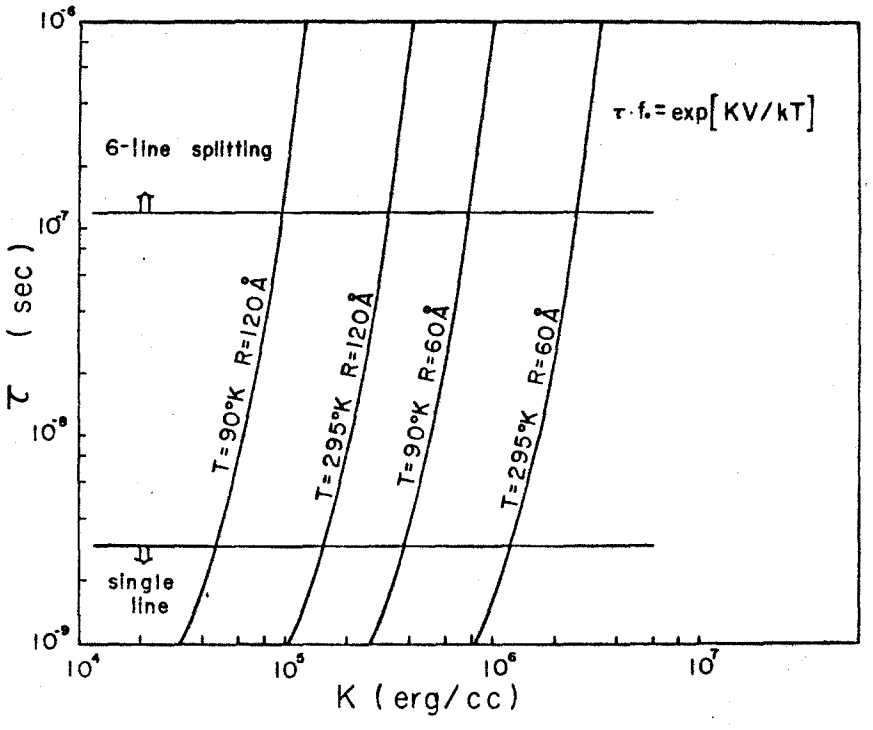

FIG. 35 Relationship between the relaxation time of the superparamagnetic electron spin and the effective anisotropy constant. The solid lines indicate for the particle whose radius are 60 and 120 Å at the temperatures of 90 and 295°K.

and the volume of the precipitated particles V are constant. The magnitude of the magnetic anisotropy constant K has generally three contributions; that is the strain anisotropy, the shape anisopropy and the crystalline anisotropy. The strain anisotropy constant can be expressed by the following equation;

$$K_e = 3/2 \cdot \lambda_m^2 \cdot E,$$

where E is the Young's modulaus and λ_m is the coefficient of magnetostriction. Using the values of $E=2\times10^{12}$ dyn/cm^2 and $\lambda_m=10^{-5}$, the strain anisotropy energy can be estimated to be

$$K_e = 3\times10^2 \text{ erg/cm}^2$$

The magnitude of this anisotropy is not so large enough to explain the transformation of the Mössbauer profile from the paramagnetic single line to the ferromagnetic 6-line splitting as has been estimated in Fig. 35. The shape anisotropy is given by

$$K_s = 1/2 \cdot \Delta N \cdot I_s^2,$$

where ΔN is the difference between the demagnetization

factors in the easy direction and in the hard one. I_s is the saturation magnetization per unit volume of the precipitates. Assuming that the shape of the precipitates are changed to be ellipsoidal in shape by the deformation of the specimen but the saturation magnetization of the precipitates does not change and equal to that of the bulk materials; that is, ΔN at 7% reduction in thickness is 1.4 and I_s is 1200 gauss/cm^3, the magnitude of the K_s for the specimen reduced 7% in thickness could be estimated to be

$$K_s = 10^6 \text{ erg/cm}^3.$$

This value is not also so large enough to explain the experimental results obtained in Fig. 34; that is, the complete transition from the single line to the 6-line splitting involving the precipitate whose diameter is 60 Å. For the f. c. c. cobalt metal, the crystalline anisotropy constant is reprented by[11)]

$$k_1 = 4(E[110] - E[100]),$$

$$k_2 = 27(E[111] - E[100]) - 36(E[110] - E[100]),$$

$$K_{fcc} = E[111] - E[110].$$

K_{fcc} shows the energy barrier for the rotation of the magnetization from a <111> direction to an adjacent one via a <110> direction. At room temperature, the magnitude of the crystalline anisotropy energy was estimated to be

$$K_{fcc} = 2\times10^{5} \text{ erg/cm}^3.$$

On the other hand,

$$K_{hcp} = E[10\bar{1}0] - E[0001]$$
$$= 6\times10^{6} \text{ erg/cm}^3.$$

The structure of the particles precipitated in the unrolled specimen is face centred cubic and show the superparamagnetic single line in the Mössbauer spectra measured at room temperature. Supposing that the precipitated particles indicate h. c. p. in the crystal structure, the 6-line splitting are expected in Mössbauer spectrum as discussed in Fig. 34. The transition from the single line to the 6-line splitting with the cold rolling can be explained by the transformation of the crystal structure from f. c. c. to h. c. p..

Figure 36 shows the change of the magnitude of the effective hyperfine fields as a function of the degree of the thickness reduction. The magnitude of the hyperfine

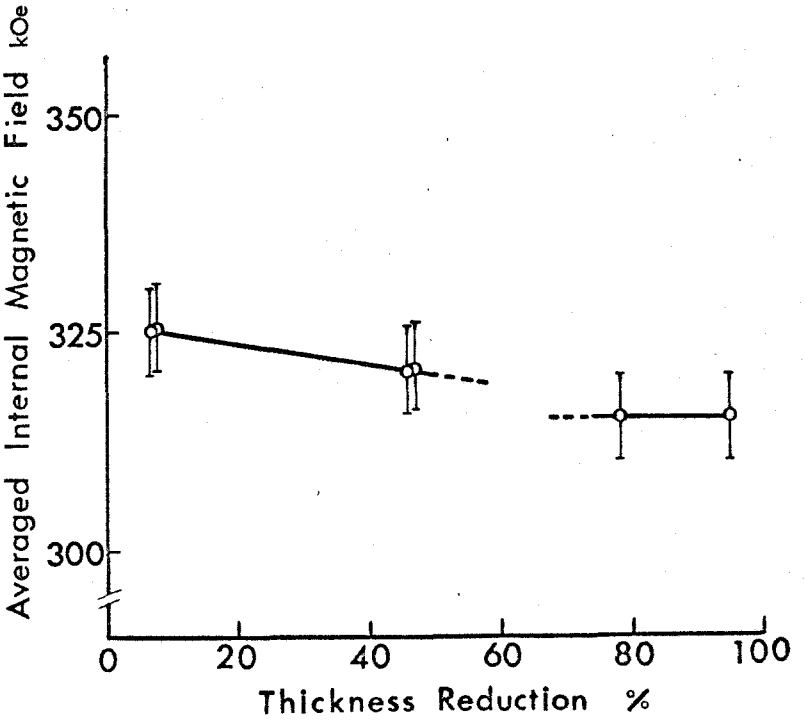

FIG. 36 The average internal magnetic field as a function of the degree of thickness reduction.

field obtained from 7% thickness reduced coincides to that of the f. c. c. cobalt and the magnitude of the hyperfine fields estimated by the specimens which were reduced in thickness over 75% are estimated to be 315±5 KOe and coincide to that of h. c. p. cobalt [7]. It is fact that the transformation of the crystal structure in precipitated particles is induced by the cold rolling.

From the shape of the spectrum obtained from 95% reduction in thickness, it seems that the direction of the magnetic moment of the particles came to be perpendicular to that of the γ-rays, that is, paralell to the rolling plane with the cold rolling. This is explained in Fig. 37 and this fact suggests that the shape of the precipitates was changed from a sphere to a ellipsoid with the heavy cold rolling. When the direction of the magnetic moment of the particles is randomly distributed, the intensity ratio in 6-line splitting of the Mössbauer spectrum is 3:2:1:1:2 :3 and on the other hand, when the direction of the magnetic moment is perpendicular to γ-rays, it is 3:4:1:1:3:4[1].

IV-4. Conclusions

Conclusive remarks in this CHAPTER are following:
(1) The Mössbauer spectra were measured by cobalt dilute Cu-Co alloy specimens in which the radio-active Co^{57} atoms

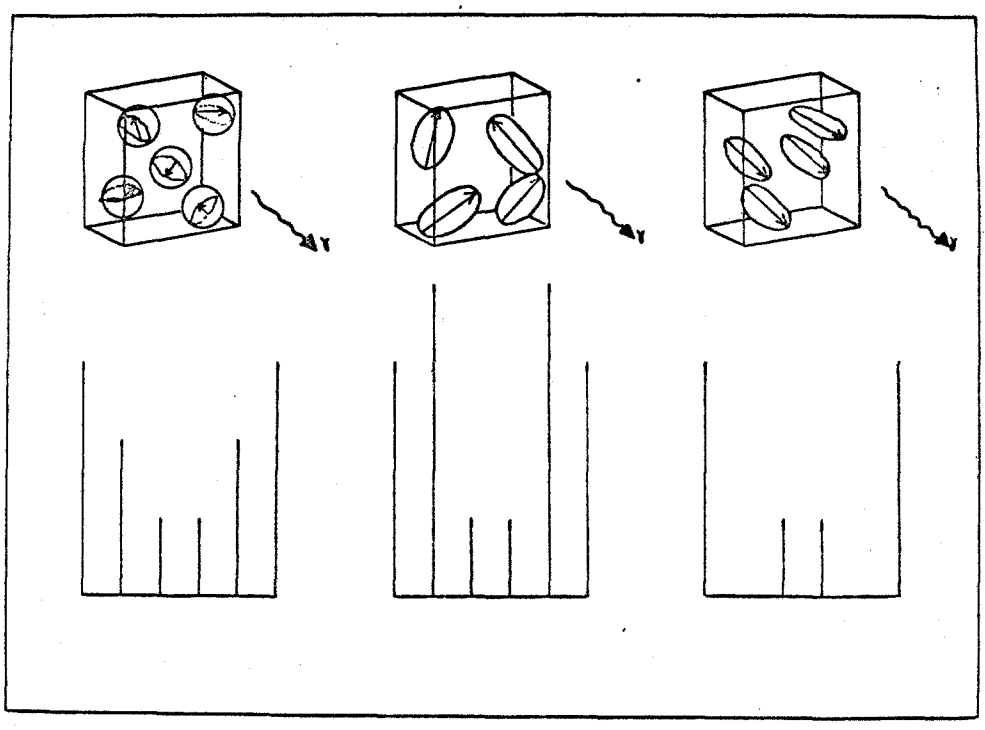

FIG. 37 Relationship between the intensity ratio in the Mössbauer spectrum and the relation indirection between the magnetic moment and the gamma-rays.

were doped and, from the analysis of the spectra, the various situations of Co solute atoms are discussed in Cu-1.97 and 3.52at.%Co alloy. (2) Firstly, the solubility of Co in solid Cu could be estimated at the temperature range of 500 to 800°C. (3) According to the concept of the super-paramagnetism, the size distribution of the Co-rich particles precipitated in Cu matrix could be determined. (4) Process of the precipitation in the Cu-1.97at.%Co alloy is re-examined using the Mössbauer technique and the kinetics of the precipitation follows so called "coalescence" mechanism. However, its nucleation and onset of the precipitation seems to occur during the quenching from solid solution temperatures. (5) Phase transformation of the precipitated Co-rich particles could be detected by the change in Mössbauer profile. Precipitates whose average diameter is 100 Å are transformed from f. c. c. to h. c. p. and also the shape of the precipitates trends to ellipsoidal in shape from spherical by the cold rolling of the specimen.

REFERENCES

1. G. K. Wertheim; "Mössbauer Effect: Principles and Applications," (Academic Press, New York, 1964).

2. C. P. Bean and J. D. Livingston; J. Appl. Phys., 30 (1959) S-120.

3. A. Kelly and R. B. Nicholson; "Precipitation Hardening," in Progress in Material Science, vol. 10, edited by B. Chalmers, (Pergamon Press, 1963).

4. N. Tamagawa and T. Mitsui; J. Phys. Soc. Japan, 20 (1965) 1988.

5. D. W. Collins, J. T. Dehn and L. N. Mulay; "Superparamagnetism and Mössbauer Spectroscopy: a Review and New Results on Iron Dispersion" in Mossbauer Effect Methodology, vol. 3, edited by I. J. Gruverman, (Plenum Press, New York, 1967).

6. S. Nasu, T. Shinjo, Y. Nakamura and Y. Murakami; J. Phys. Soc. Japan, 23 (1967) 664.

7. Y. Koi, A. Tsujimura, T. Hihara and T. Kushida; J. Phys. Soc. Japan, 16 (1961) 1040.

8. L. Néel; Ann. Geophys., 5 (1949) 99.

REFERENCES (CONT.)

9. W. F. Brown; Phys. Rev., 130 (1963) 1677.

10. H. H. Wickman; "Mössbauer Paramagnetic Hyperfine Structure" in Mössbauer Effect Methodology, vol. 2, edited by I. J. Gruverman, (Plenum Press, New York, 1966).

11. W. Sucksmith and J. E. Thompson; Pro. Roy. Soc. London, 225 (1954) 362.

12. V. A. Phillips; Trans. A. I. M. E., 230 (1964) 967.

13. C. Panseri and T. Fedrighi; Phil. Mag., 2 (1957) 374.

14. K. Furukawa; Dr. of Eng. thesis, Kyoto University, Kyoto [Department of Metal Science and Technology, Faculty of Engineering, Kyoto, 1966].

15. J. J. Becker; Trans. A. I. M. E., 209 (1957) 59.

CHAPTER V

MÖSSBAUER EFFECT STUDY OF SMALL ADDITIONAL Co ELEMENT IN Cu - 2wt.%Be ALLOY

V-1. Introduction

It is well known that the Cu-Be alloys are very strongly hardened by the aging treatments and the decomposition of α supersaturated solid solution of Cu-2wt.%Be alloy is also recognized, in general, to be following; α supersaturated solid solution → intermediate γ´ precipitates → equilibrium γ (CuBe) phase. To obtain high strength in Cu-Be alloy, it is necessary to form the γ´ precipitates within the grain boundaries. However, it is fact that the preferential precipitation of the equilibrium γ phase at the grain boundaries which is so called discontinious precipitation occured easily by the aging treatments for the formation of the intermediate γ´ precipitates and then the strength of this alloy fall into weakness. The mechanism and the origin of the discontinous precipitation have been studied by many investigators[1~6], but they have not yet been made clarify.

It is also recognized that small additional Co element restricts the discontinous precipitation in this

alloy, so that the commercial Cu-Be alloy contains small amounts of Co atoms. Many investigators have discussed the role of Co atoms for the aging characteristics and the discontinious precipitation in this alloy and interpreted for the role of Co atoms concerning the change of the aging sequence as well as the mechanism of the discontinous precipitation, but the role has not yet also been made clear completely.

In order to discuss the effects of small amounts of additional Co elements in Cu-Be alloy, it is necessary to investigate the local state of the Co atoms in each stages of Co atoms, the Fe^{57} Mössbauer measurements will be good tool, since the diffusive motion of Co^{57} resont nuclei is similar to the additional Co elements and the Fe^{57} Mossbauer spectra obtained after the decay of Co^{57} indicate truely the microscopic informations for the local states of the Co atoms[7] as being discussed at previous CHAPTERS.

It is the purpose in this CHAPTER to investigate the local states of the Co atoms by the Fe^{57} Mössbauer effect using the specimen doped by Co^{57}. It is also recognized that the Fe^{57} Mössbauer effect is a good tool for the study of solid state physics; especially, for the measurements of the magnetic properties of the materials. There exist two main physical properties obtained by the apllication of the Mössbauer effect, one is the internal magnetic field

acting on the resonant nuclei and other is the isomer shift which indicates the apparent energy shift between nuclear energy levels. Magnetic hyperfine structure is arising from the interaction of the nuclear magnetic dipole moment with the magnetic field due to the atom's own electrons and in the case of Fe-Ni[8] and Cu-Ni[9] alloys the magnitude of the magnetic field acting on Fe^{57} nuclei fall on a single straight line as a function of the magnetizations of the alloy solid solutions . Therefore, the amounts of non-magnetic atoms in these alloy solid solutions can be deduced approximately by the magnitude of the internal magnetic fields acing on the Fe^{57} nucleus. The isomer shift is caused by the difference in the electrostatic energy of the nucleus in twodifferent states of excitation which differ in nuclear radius, and also caused by the difference of the test temperature and/or the effective Debye temperature between the source material and the absorber one in Mössbauer measurements. The values of the Fe^{57} isomer shifts in metals and alloys are observed at various kind of solvent atoms[10,11] and the measurement of isomer shift is used as the investigation of the local electronic states of Fe^{57} solute atoms and from its temperature dependence the effective Debye temperature of Fe^{57} atoms in various metals and alloys can be determined. The value of isomer shift resulted from Fe^{57} Mössbauer effect using the Cu-Be alloy specimen

in which Co^{57} was doped with additional Co elements must give some informations about local states of the small additional Co elements in this specimen.

V-2. Sample Preparation and Experimental Procedure

V-2-1. Sample

A Cu-12.6at.%Be-0.2at.%Co-0.1at.%Zn alloy was prepared by melting in vacuum furnace from 99.99% copper and a commercial mother alloy of Cu-4wt.%Be; samely as described in previous investigations[1,2]. Chemical composition of the specimen is tabulated in Table 6. For the gamma-ray source, Co^{57} was electro-plated using the $Co^{57}Cl_2 \cdot HCl$ solution onto the platellet alloy specimen (as has been illustrated in Fig. 21 at CHAPTER IV) which was cut from the sheet of the rolled specimen, about 1 mm in thickness. After electro-plating the specimen was annealed in hydrogen atmosphere for the diffusion of Co^{57} into the alloy. Previous investigations for the Cu-dilute Co alloy (CHAPTER IV) shows that Co atoms doped in the alloy behave identically as the other additional Co elements which are previously exist in the specimen[12,13].

TABLE 6 Chemical composition of the specimen

	Cu	Be	Co	Zn	Fe	Si
Charged Composition (at %)	87.6	12.6	0.2	0.1	—	—
Chemical Composition (wt %)	bal.	1.83	0.19	~0.1	0.08	0.05

V-2-2. Mössbauer Apparatus

For the Mössbauer measurement, a set of T. M. C. 400 channel PHA and Elron 5011 driving unit operated in Research Reactor Institute of Kyoto Univ. Osaka, was used[14]. For the absorber, a stainless steel foil is always used at room temperature. Calibrations of the velocity range were carried out by the pair of Co^{57} source in Pd or in stainless steel and Fe^{57} absorber in α-iron. The magnitude of isomer shifts was estimated to be relative to metallic α-Fe. The magnitude of internal magnetic fields was determined by the 6-line splitting in α-Fe whose value is 330 KOe.

V-2-3. Heat Treatments

Solution heat treatments at high temperatures were carried out in hydrogen atmosphere using the ususl vertical electronic furnace and the isothermal aging treatments of the specimen were carried out in salt bath. Subsequent aging treatments after solution heat treatments for the formations of G. P. zone, γ′ precipitates and equilibrium γ phase are individually tabulated in Table 7. It can be negligible that the effect of the aging at room temperature after water quench and the aging during the Mössbauer

TABLE 7 Subsequent aging treatments after water quench from 780°C.

G.P. zone	aged for 30min. at 250°C
γ' precipitate	aged for 30min. at 250°C and then aged for 30min. at 350°C
γ phase	aged for 30min. at 450°C

measurement at room temperature, since the formation of any precipitates cannot be mostly occured by the aging treatment at room temperature, in the case of the Cu-Be alloy specimen containing small amounts of Co atoms[1].

V-2-4. Electron Microscopy

Transmission electron micrographs were observed by thin foil technique, using the J. E. M.-6A type electron microscopy operated at 100 KV accelation voltage. The thin foil specimens were obtained by the electron thining in ususl elecrolyte of phosphorus-chromium acid solution.

V-3. Experimental Results and Interpretations

V-3-1. Mössbauer Spectrum Obtained by the Furnace Cooled Specimen

Figure 38 shows the Mössbauer spectra at room temperature obtained for the specimen which was cooled down slowly in the furnace from 750°C to 450°C and then quenched into water. Upper spectrum in Fig. 38 shows the total absorption consisting of the superposition of large component and small ferromagnetic component. Large paramagnetic component indicates

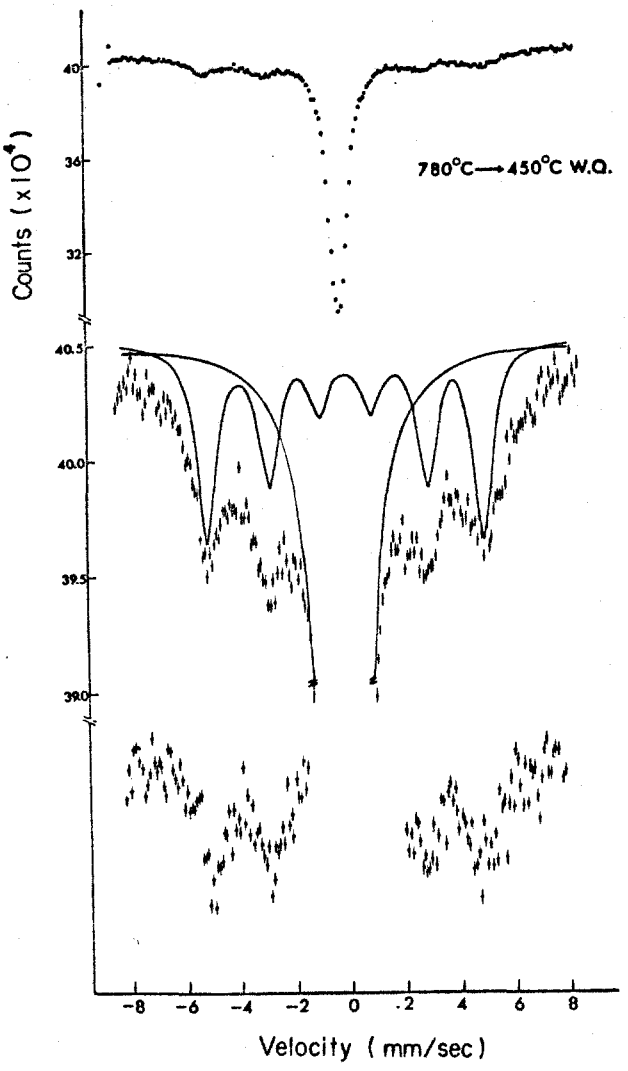

FIG. 38 Mössbauer spectra obtained by furnace cooled specimen. Upper spectrum shows the total absorption. The second spectrum is an expanded profile of the total absorption. Solid lines indicate the single line and the 6-line components. Lower spectrum indicates only the ferromagnetic component.

that the most of Co atoms are dissolved in Cu matrix behave paramagnetically at room temperature. The value of isomer shift for the paramagnetic component in Fig.38 can be estimated to be -0.28±0.06 mm/sec. The second spectrum shows the profile expanded at the background of the total absorption shows obviously a superposition of the 6-line splitting and a single line absorption. The 6-line splitting in the spectrum shows the existance of the ferromagnetic phase in the specimen at room temperature. Solid lines in the second spectrum indicate a single Lorentzian curve and a superposed 6-line Lorentzian curves respectively, which show paramagnetic component and ferromagnetic components individually.
To illustrate the Lorentzian curves, the values of half-width are approximated to be same in all of components. In the analysis of the superposed Mössbauer spectrum, if the recil free fraction(Mössbauer fraction)[7] indicates same value in either a paramagnetic Fe^{57} component or ferromagnetic Fe^{57} components (this is identified as having a same Debye temperature in both phases and it is considered usually to be good approximation), the totl absorption indicates the amounts of additional Co element, that is, 0.2at.%Co in alloy specimen and the ratio of the paramagnetic Co component to the ferromagnetic Co component can be determined from the relative integrated intensity ratio in the spectrum.
From the relative integrated intensity ratio in the spectrum

obtained from the furnace cooled specimen in Fig. 38, the amounts of the ferromagnetic Co components can be estimated to be 20% of the total absorption; that is, the 0.04at.%Co atoms in the specimen from the ferromagnetic particles. The lower spectrum in Fig. 38 indicates only the ferromagnetic (6-line) components which were taken off the paramagnetic components from the total absorption. The magnitude of the hyperfien field estimated from the 6-line component can be determined to be 315±10 KOe whose value is nearly equal to that of the internal magnetic field of Fe^{57} in Co-rich particles precipitated coherently in Cu matrix[13].

The 6-line absorption and a single line absorption indicates the Co components in ferromagnetic Co particles and a paramagnetic component ofCo atoms dissolved in Cu matrix and/or in superparamagnetic Co particles, respectively. Mossbauer spectra obtained for various heat-treated specimens are shown in Fig. 39 and 40. Mössbauer spectra are measured at the each stages of the aging sequence in the alloy, namely, they were observed after the following heat treatments; for the formation of G. P. zones the specimen was aged for 30 minutes at 250°C, for the γ' precipitates the specimen was aged for 30 minutes at 350°C and also for the equilibrium γ phase the aging treatment of the specimen was carried out for 30 minutes at 450°C. In the individual observation of each spectrum of paramagnetic components and

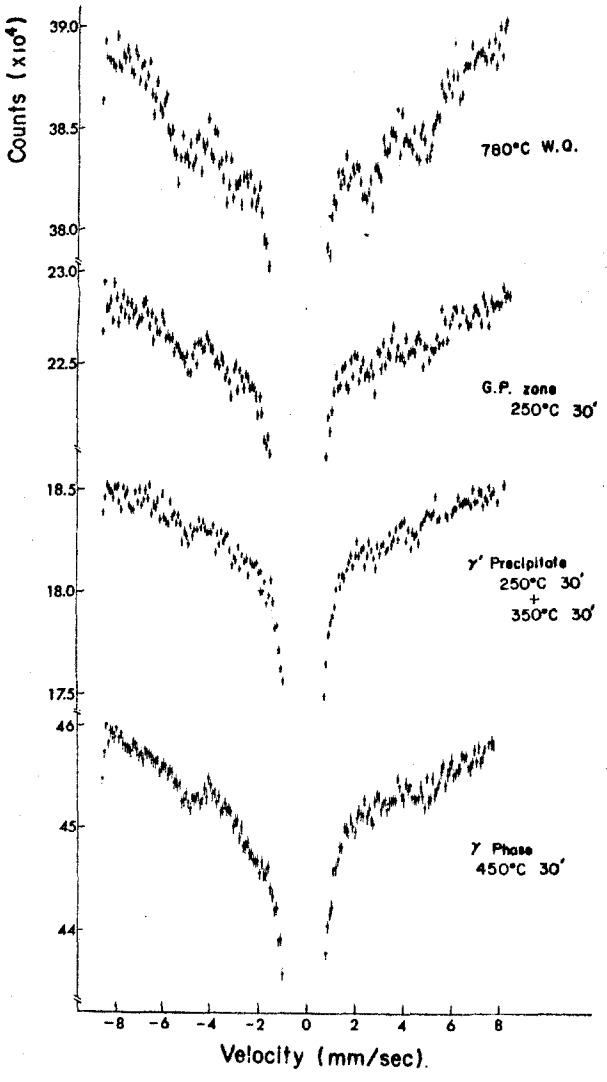

FIG. 39 Mössbauer spectra obtained for various heat-treated specimens. Individual spectrum indicates the superposition of paramagnetic (single line) component and ferromagnetic (6-line) components.

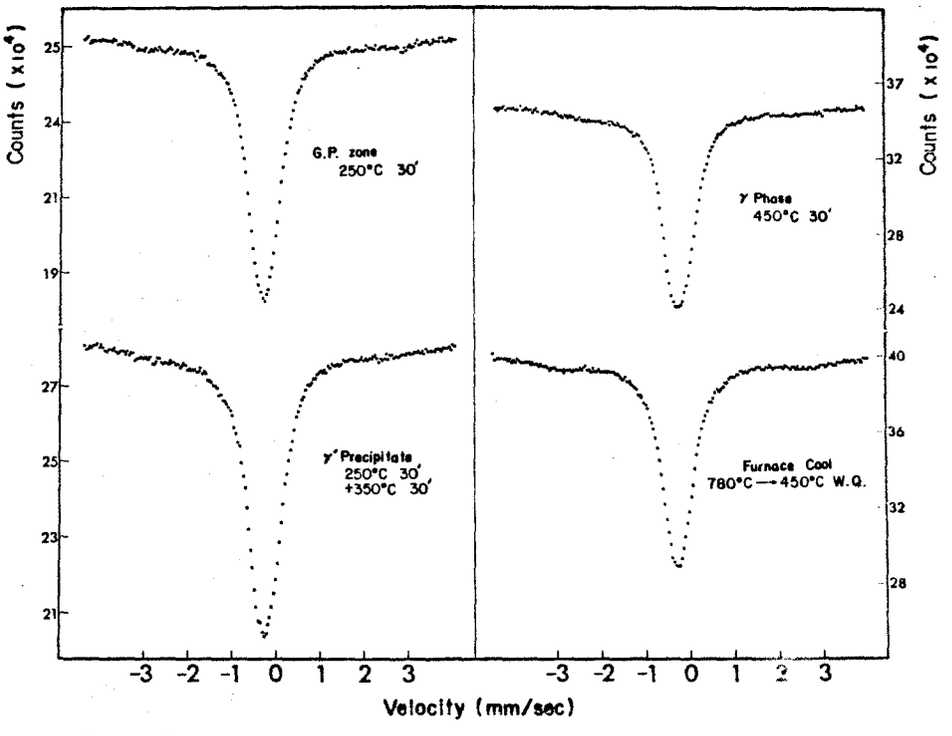

FIG. 40 Mössbauer paramagnetic absorption obtained by aged specimens.

ferromagnetic components obtained for the various heat-treated specimens, the situation of the small additional Co elements in this alloy specimen were discussed.

V-3-2. Paramagnetic Co Components

(i) Isomer Shifts

In Fig. 39 the Mössbauer spectra obtained for the variously aged specimens are shown to expand in relatively narrow velocity range in order to estimate the detail profile for the discussion of the situation of paramagnetic Co atoms. Table 8 tabulates the values of the isomer shifts obtained from the paramagnetic single line which were measured at various aging sequences of the specimen, that is, at the time after quenching, at the formation of G. P. zones, γ' precipitates and the equilibrium γ phase. Most of the values in Table 8 are nealy constant even at any aging stages and indicate the approximate value to -0.226±0.01 mm/sec[10] of Fe^{57} in pure Cu rather than the value of -0.120 ±0.02 mm/sec[10] in pure Be. From this results, it is suggested that the most of Co atoms dissolved in Cu-Be alloy matrix in any stages of aging sequence. However, the detailed estimation of the values of isomer shift shows the following fact that the smallest value of -0.31±0.06 mm/sec

TABLE 8 Isomer shift (mm/sec)

After quench from 780°C	G.P. zone 250°C 30min.	γ' precipitate 250°C 30min. +350°C 30min.	γ phase 450°C 30min.	Furnace cool 780°C–450°C W.Q.
−0.31±0.06	−0.28±0.06	−0.28±0.06	−0.26±0.06	−0.28±0.06

was obtained for the quenched specimen, the largest value of -0.26±0.06 mm/sec was obtained for the specimen containing γ phase and the constant values of -0.28±0.06 mm/sec were obtained for the specimens containing G. P. zones and γ′ precipitates and for the furnace cooled specimen. The difference in the value of isomer shift between the value of the quenched specimen and the other specimens may be interpreted for the difference in the atomic configulations at the nearest neighbor sites of Co atoms, since the alloy matrix is a supersaturated solid solution containing 12.6at. %Be in the quenched specimen and the Co atoms have at least one beryllium atom in its nearest neighbor sites. In a supersaturated solid solution containing 12.6at.%Be, Co atoms have a few Be atoms in its nearest neighbor sites and the value of isomer shift trend to differ from -0.226±0.01 mm/sec resulted from Co atoms having no Be atoms in its nearest neighbor sites according as the difference in electron density at the nucleus and the different Debye characteristic temperatures. For the specimen containing equilibrium γ phase the isomer shift is estimated to be nearly equal to that of Co atoms having no Be atoms in their nearest neighbor sites, since the atomic fraction of Be atoms associated with the nearest neighbor site of Co atoms may be smallest in the aging stage for the formation of the equilibruim γ phase. For the specimens containing G. P. zones and γ′ precipitates

and also for the furnace cooled specimen, the values of isomer shift indicate to be identical to that of Co atoms which may be dissolved in Cu-Be alloy matrix and it could be suggested that the situation of the paramagnetic Co components does not depend on the aging sequence such as G. P. zone and γ' precipitates.

(ii) Half-Width

If the recoil free fraction (Mössbauer fraction) of Fe^{57} decayed from Co^{57} in this Cu-Be alloy specimen is always constant, the variations of the half-width estimated from the resonance absorption lines should be discussed in terms of the distribution among the values of isomer shift. For the discussions about the distribution of the isomer shifts, the values of half-width obtained by the various heat-treated specimens are tabulated in Table 9. The isomer shift of the most of paramagnetic Fe^{57} Mossbauer line in the Cu-Be alloy can be deduced to be identical to the observed values listed in Table 8, since there is any deviations in the distribution of the values in Table 8. The values of the isomer shift obtained from the paramagnetic Co components is estimated to be nearly equal to the value of that in pure Cu matrix and they show hardly different values in each stages of the aging sequences. If the

TABLE 9 Half-width obtained by variously heat-treated specimens (mm/sec).

After quench	G.P. zone	γ' precipitate	γ phase	Furnace cool
0.90 ± 0.1	0.85 ± 0.1	0.85 ± 0.1	0.90 ± 0.1	0.85 ± 0.1

additional Co elements play the nucleation sites for the formation of the G. P. zones, γ' precipitates and γ phase, the isomer shifts of the Fe^{57} in those precipitates and phases should be estimated to be the different values according to the Be-rich cluster, meta-stable CuBe precipitates and the CsCl type CuBe compound. As above mentioned, it is obvious that the small additional Co elements in this alloy have not been dissolved in Be-rich cluster, the meta-stable CuBe precipitates and CsCl type CuBe compound but dissolved in Cu-Be alloy matrix.

The detailed discussion about the recoil free fraction and the values of the isomer shift obtained for the Fe^{57} dissolved in G. P. zones and any precipitates may be played an important part of the investigations for the physical properties of precipitates. Detailed investigations payed attention to this matter have not yet been carried out. The number of Co atoms located at grain boundaries and dislocations can be deduced to be too small to affect on the values of isomer shift and the half-width.

V-3-3. Electron Micrograph

Photograph 2 shows the thin foil electron micrograph using the specimen aged for 5 minutes at 350°C after solution heat-treated of 20 minutes at 780°C in order to form the γ'

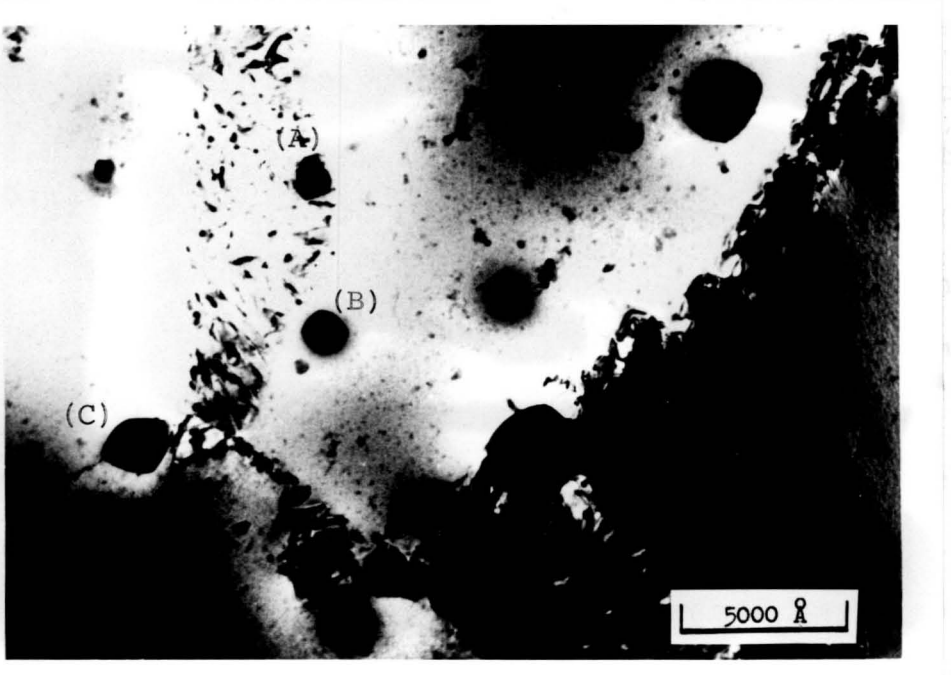

PHOTO. 2 Electron micrograph of a thin foil of Cu-12.6%Be-0.2%Co-0.1%Zn alloy, water quenched from780°C and aged 5 minutes at 350°C.

precipitates in this specimen. The black massive particles in Photo. 2 can be always observed for the specimen containing Co atoms but connot be observed for high pure specimens not containing Co atoms. This massive particles can be considered to be Co-rich particles, since they have different mophology relative to the particles (CoBe, Co_5Be_{21}) observed by usual optical micrograph and the Fe^{57} Mossbauer spectrum of this massive particles can be shown as a ferromagnetic rofile for the reson that their particle size could be estimated to be 200∿2000 Å. The massive particles in Photo. 2 could be observed in various regions, for example, the region (A) in which the discontinous precipitation occurs, the region (B) in which the γ' precipitates are formed and the region (C) located on the grain boundaries. The mophology and the size of the particles do not change greatly themselves during the aging sequence of the alloy and it can not seem for the particles to play an important parts of the kinetics of the alloy decompostion.

V-3-4. Effects of Solution Heat Treatment Temperature

The Mössbauer spectra were measured by the specimens which were annealed at various solution heat treatment temperatures in order to estimate the effects for the ferromagnetic Co components. In Fig. 41 the Mossbauer

spectra at room temperature are shown as a function of temperatures of the solution heat treatments in which the water quenching after the annealing for 20 minutes at 780°C and 840°C respectively is contained. The amounts of the ferromagnetic Co components do not change greatly but the effective internal magnetic field remarkably differ in each other. The magnitude of the effective magnetic field, obtained for the specimen being annealed at 840°C can be estimated to be 260±10 KOe and its value is obviously smaller than that of 300±10 KOe for the specimen at 780°C.
The values of the effective hyperfine fields are tabulated in Table 10. If the magnitude of the effective internal magnetic fields fall on a straight line in a similar manner to the Fe-Ni alloy[8] and Cu-Ni alloy[9] according to the effective electron concentration of the alloy and the ferromagnetic Co-rich particles are also conjugate solid solution with non-magnetic Cu and Be atoms, it can be deduced that the concentration of the Cu and Be at 840°C in the ferromagnetic Co-rich particles may be greater than that of the particles annealed at 780°C. It implies that the ferromagnetic Co-rich particles contain some Cu and Be atoms and the solid solubility of Cu and Be in the particle at 840°C is larger than that of being at 780°C. However if it was assumed that the ferromagnetic Co particles contain only Cu atoms as non-magnetic impurities, the Cu contents in the

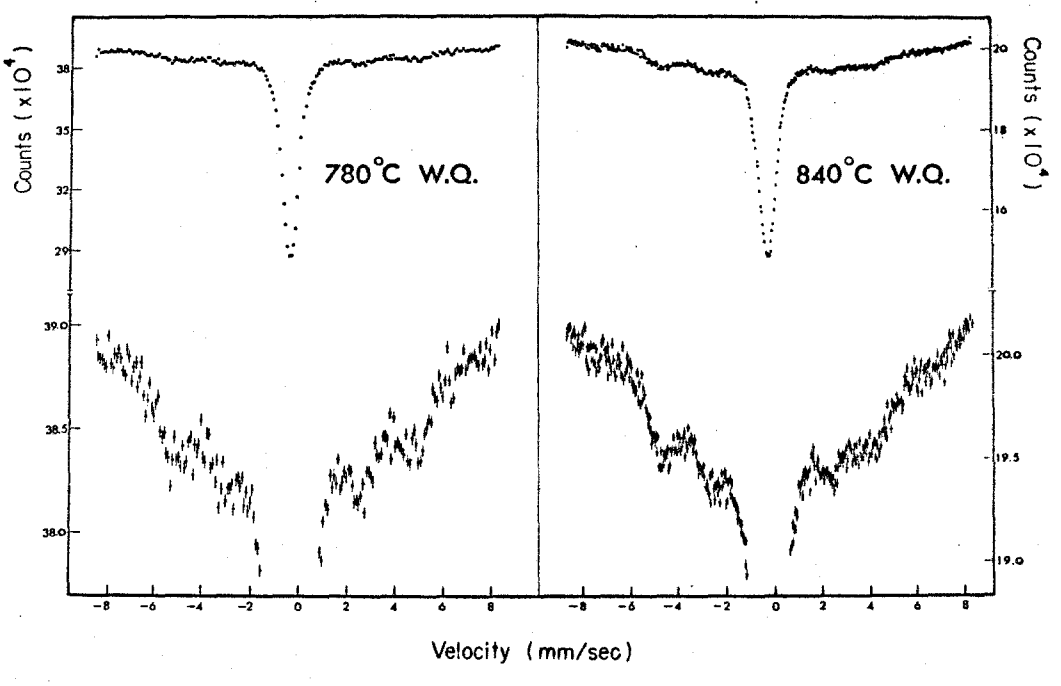

FIG. 41 Mössbauer spectra obtained for quenched specimen. Specime was quenched in water from 780°C and 840°C.

TABLE 10 Average internal magnetic field.

After quench from 780°C	300±10 kOe
After quench from 840°C	260±10 kOe

in the Co-rich particles indicate the large value as large as 20∿40 per cent in order to decrease the effective internal magnetic fields of the Fe^{57} in the particles. The Be atoms in fact dissolved into the particles and seem to make large efficiency of the decrease in the magnitude of the hyperfine fields. Large amounts of experimental determination of the internal magnetic fields on Fe^{57} nucleus in metals and alloys have been carried out by many investigators, especially for the prosecution of magnetic studies[15]. The values of the internal magnetic field on Fe^{57} in all sorts of metals and alloys have not yet been determined especially for the case of precipitates. Moreover there are some investigations in which the magnitude of the internal magnetic fields are reported not to fall on the straight line according to the increase of additional non-magnetic elements[16].

It is still impossible to detect the accurate contents of the non-magnetic impurities according to the magnitude of the effective internal magnetic field. In the present study, Co contents forming the ferromagnetic particles are estimated to be about 0.04% in the specimen. According to the observation of the electron micrograph, the particle density of the ferromagnetic particles can be determined to be 10^{5}∿10^{8} /cc which is smaller than 10^{15} ∿10^{19} /cc[17] for the γ' precipitates and the equilibrium γ phase and they do not play the nucleation sites of these

precipitates and phase. In the aging sequence of this alloy the ferromagnetic particles play the important parts for the decrease of the degree of the supersaturated of Be atoms in the matrix and the increase of the number of vacancy sinks.

V-3-5. Role of the Additional Co Element

Many investigations have studied about the role of small additional Co element in the Cu-Be alloy and interpreted it in terms of isolated Co atoms dissolved in alloy matrix. However there have been no evidence for their interpretations and the present Mossbauer study indicates the direct evidence to the contrary of their interpretations. It is also well known that the additional Co element have the effects to delay the formation of G. P. zone at the low temperature aging. The small additional 0.2at.% Co atoms, whose number is larger than that of excess vacancies introduced by the quenching from the solution heat treatment temperature, decrease the number of the vacancies by whose assistance the Be atoms can be diffusive in the alloy and delay the formation of G. P. zones[2,18], since the binding energy between Co atoms and vacancy is large and a Co atom-vacancy pair seems to be less mobile than the other elements. Above interpretation is resonable for the present results

from which the most of the additional Co element is dissolved in Cu matrix and show the paramagnetic single line in Mossbauer spectra. Futhermore, the effective number of vacancies make to decrease by the increase in the density of vacancy sinks such as the interface between the ferromagnetic Co-rich particles and the alloy matrix. The present Mossbauer study indicates the direct evidence to the contrary of the interpretations which suggest that the additional Co atoms plsy the parts of nucleation sites for the formation of γ' precipitates and the equilibrium γ phase. Previously, one of the reason to restrict the discontinous precipitation was suggested by Thomas[4], in which the additional Co atoms dissolved into the alloy matrix to relax the coherency strain of the lattice and make easy to form the γ' precipitates. Kuntze and Wincierz[5] proposed so called "Umweg diffusion model" for the diffusion of the Be atoms around the Co atoms in interpretations of the role of additional Co elements. Present Mössbauer results do not produce the direct evidence but does not produce a counterevidence for their model. The small additional Co elements are previously recognized to have the effect to make the fine grain size in Cu-Be alloy. For the fine grain size, the interpretations may be discussed in terms of the ferromagnetic Co-rich particles. If more detailed discussions for the paramagnetic Co components resulted from Mössbauer study in Cu-Be alloy will develope

in future, the many problems in this alloy will make to be clear.

V-4. Conclusions

Conclusive remarks obtained from this CHAPTER are summarized as following terms: (1) All of the small additional 0.2at.% Co atoms in Cu-2wt.%Be alloy do not dissolve in the alloy matrix even at the solution heat treatment temperatures and about 10∿20 per cent cobalts of the total number of Co atoms form the ferromagnetic Co-rich particles. The Co contents of the ferromagnetic particles depend on the solution heat treatment temperature. These ferromagnetic particles are estimated not to be CoBe, and Co_5Be_{21} which can be usually observed in optical micrograph and have the efficiency to make a fine grain size in the alloy. The composition and the magnitude of the ferromagnetic component have independence on the various aging sequences of the Cu-Be alloy, for example, after quenching, at the formation of G. P. zones, γ' precipitates and equilibrium γ phase. The ferromagnetic particles do not directly play the important parts for the precipitation process of Be atoms. (2) The isomer shifts obtained for

the paramagnetic Co components are estimated to be nearly equal to the value of the Fe^{57} in pure Cu lattice. The paramagnetic Co components exist in the Cu-Be alloy matrix and do not dissolve in γ' precipitates and equilibrium γ phase. About 80 $\sim$ 90 per cent in total additional Co elements show the paramagnetic at the situation of the solid solution and affect to the precipitation kinetics of Be atoms under the isolated Co atoms in alloy matrix.

REFERENCES

1. Y. Murakami, H. Yoshida, T. Kawashima and S. Yamamoto; J. Japan Inst. Metals, 30 (1966) 508.

2. Y. Murakami, H. Yoshida and S. Yamamoto; Trans. J. I. M., 9 (1968) 11.

3. P. A. Beck; J. Appl. Phys., 20 (1949) 666.

4. H. Thomas and U. Wilke-Dörfurt; Z. Metallk., 50 (1959) 466.

5. G. Kunze and P. Wincierz; Z. Metallk., 56 (1959) 421.

6. H. Kimura; Bulletinof Japan Inst. Metals, 5 (1966) 690.

7. see, H. Frauenfelder; "Mössbauer Effect", (W. A. Benjamin, Inc., New York, 1963). and G. K. Wertheim; "Mössbauer Effect: Principles and Applications", (Academic Press, Inc., New York, 1964).

8. C. E. Johnson, M. S. Ridout, T. E. Cranshaw and P. E. Madsen; Phys. Rev. Letters, 6 (1961) 450.

9. G. K. Wertheim and J. H. Wernik; Phys. Rev., 123 (1961) 775.

REFERENCES(CONT.)

10. A. H. Muir Jr., K. J. Ando and H. M. Coogan; "Mössbauer Effect Data Index, 1958-1965" p.26, (North American Aviation Science Center Thousand Oaks, California, 1966).

11. S. M. Qain; Proc. Phys. Soc., 90 (1967) 1065.

12. S. Nasu, T. Shinjo, Y. Nakamura and Y. Murakami; J. Phys. Soc. Japan, 23 (1967) 664.

13. S. Nasu, Y. Murakami, Y. Nakamura and T. Shinjo; Scripta Met., 2 (1968) 647.

14. see, Y. Maeda; J. Phys. Soc. Japan, 24 (1968) 151.

15. W. Marshall and C. E. Johnson; in "Metallic Solid Solution, A Symposium on their Electronic and Atomic Structure", 1963.

16. H. L. Marcus and L. H. Schwartz; Phys. Rev., 162 (1967) 259.

17. S. Yamamoto; Private communication.

18. A. Lawly, K. F. Luckens, H. Kimura and R. Maddin; Trans. A. S. M., 16 (1967) 516.

CHAPTER VI

NUCLEAR MAGNETIC RESONANCE OF Co^{59} NUCLEI IN PRECIPITATED COBALT PARTICLES

VI-1. Introduction

Since the first successful nuclear magnetic resonance (NMR) observation of Co^{59} nuclei in ferromagnetic f. c. c. cobalt metal, the NMR of nuclei in magnetic atoms has become one of the most powerful methods for investigating magnetic materials[1]. Utilizing the NMR technique, it become possible to study the static and dynamic character of local atomic system in ferromagnetic particles not easily obtained by other means. Perhaps this is best illustrated in the NMR technique where high precision measurements of the distribution of the frequency for resonance or the hyperfine field in metals and alloys are made possible, from which it would be able to determine the local magnetic and atomic characters of substances.

On the problem of the precipitation phenomena, it is expected to study the microscopic nature of the precipitated particles in alloy matrix for better understanding of kinetics of the precipitation process. Our motivation is simply to apply the NMR technique to this problem and to clarify the precipitation process from the microscopic standpoint.

There will be our concern in this article.

There are many alloy systems, for example Cu-Co, Au-Co and Cu-Ni-Co, to be suitable for the NMR studies of the precipitation phenomena an ferromagnetic Co-rich particles. Among these alloy systems, dilute Cu-Co alloys were attracted our attention as the first application of the NMR technique, because that the process of the precipitation have been extensively studied by other means and believed to be relatively simple[3,4].

The transmission electron micrograph of the Cu-Co alloy foil has been investigated by Phillips[4] and Tanner[5] and it was concluded that in the early stage of the precipitation process the precipitated Co-rich particles are entirely coherent with the Cu matrix and spherical in shape. Increasing the period of aging treatment the particle size gets large by the usual nucleation and growth process and the particles have a tendency to loose the coherency and to change its shape toward ellipsoidal and octahedron. For the magnetic properties of these precipitated Co particles of the order of 20 $\sim$ 1000 Å in diameter, it is well known that there are three categories as follows[6]. (1) Particles large to contain many ferromagnetic domains which magnetize initially by the motion of domain walls. (2) Smaller particles find it energitically undesirable to contain domain boundaries. They are always spontaneously saturated,

that is single domain particles, and reverse their magnetization only by rotation of entire magnetic moment. (3) Particles which are still smaller continue to be single domain, but the direction of their magnetization fluctuate thermally, that is so called superparamagnetic particles.

In the application of the NMR technique for the studies of magnetic and atomic properties in fine ferromagnetic particles, there now exists two distinct NMR studies; one of this is associated with multi-domain particles. However, the NMR signal associated with nuclei in domain wall is almost unbelievably enhanced by the initial susceptibility due tothe wall displacements[1)]. For this reason, most of the NMR studies in ferromagnetic metals and alloys have been worked out using multi-domain particles. In the present study, the observation of NMR signals was also limited the those in precipitated particles greater than the single domain.

Section VI-2 describes the sample preparation used in this experiment and the determination of the precipitated Co-rich particle size by the magnetic granumetry method. In Sec. VI-2 the transient NMR technique is also described. Our experimental results and an interpretation are given in Sec. VI-3. In the final section, conclusive remarks for the nature of the precipitation process emerged from the NMR studies are summarized.

VI-2. Sample Preparation and Experimental Procedure

VI-2-1. Sample Preparation and Determination of the Precipitated Co-rich Particles

Present NMR studies have been carried out using dilute Cu-3.52at.%Co alloy powders. The alloy ingot was prepared by the electrical induction from the Cu-2%Co and Cu-4%Co alloy in high pure alumina crucible under inert gas protection. The Cu-2%Co and the Cu-4%Coalloys were prepared by melting from the electrolytic cobalt and oxgen-free copper for several times in high vacuum electric furnace.

After the alloy ingot was filed, these alloy powders were mixed with fine alumina powders to avoid sintering at high temperature annealing. These powders were subsequently sealed in a evacuated silica tube and given a solution heat treatment consisted of one hour annealing at 1050°C without sintering and finally followed by a quench and crush in the water bath. The subsequent aging treatment was done in a silica tube contained one of portions of solution heat-treated alloy powders at constant temperature of 600°C, and then quenched into water. These alloy powders were sealed off in glass tubes and placed inside the inner finger of the Deqar for the NMR measurements. Measurements of the magnetization curve for the estimation

of the particle size were carried out at room temperature using the same sample powders.

The precipitated particles size were estimated using the technique similar to those described by Becker and Liveingston[7]. The magnetic measurements of particle size are limited to diameters below about 120 Å of which magnetic properties are superparamagnetic. In the precipitation kinetics of the dilute Cu-Co alloy system, however, the particle size measured by Livingston[8] can be fitted fairly well to a coarsening equation suggested by Greenwood [9], Lifishitz[10] and Wagner[11]. The kinetc equation for the particle growth of the average size is

$$\bar{r}^3 - \bar{r}_o^3 = k \cdot t, \qquad \text{(VI-1)}$$

where $\bar{r}$ is the average radius at time t, and $\bar{r}_o$ is the average particle radius at the onset of the coasening. The rato constant k is given by

$$k = 2\gamma \cdot D \cdot C_e \cdot V_m^2 / (\rho_c^2 \cdot R \cdot T) \qquad \text{(VI-2)}$$

where γ is the interfacial free energy of the particle matrix interface, D is the coefficient of the diffusion of the solute in the matrix, C_e is the concentration of solute in equilibrium with a particle of infinite size, V_m is the

molar volume of the precipitates, ρ_c is a numerical constant related to the distribution of particle size (theoretically $\rho_c=3/2$), and R T has its usual meaning.

The precipitated particle size in Fig. 42 is measured by the analysis of the magnetization curve obtained from the short time aged specimen which contains superparamagnetic particles (40∿100 Å in dia.), and the straight line was extrapolated using the Eq. VI-1, assuming that the growth kinetics of the multi-domain particles are similar to that of the superparamagnetic one. This assumption is resonable for the stage of keepin the coherency between the precipitaed particles and the alloy matrix and not being remarkably change in the distribution of particle size. If the discontinous precipitation occured at some grain boundaries in this alloy, above assumptions become to be unreliable. However, the measurements of NMR signals presented here carried out with form of alloy powders and its size are very small about 100 μ. Each alloy particles could be assumed to contained few grain boundaries and the amount of the discontinous precipitation is very small and could be negligible.

Recent Co^{57} Mössbauer effect investigation on the Cu-3.52at.%Co alloy plate suggests in CHAPTER IV that the existence of the quenched-in cluster of Co solute atoms. It was also reported by Jacobs[12] and Van Der Berg[13] that

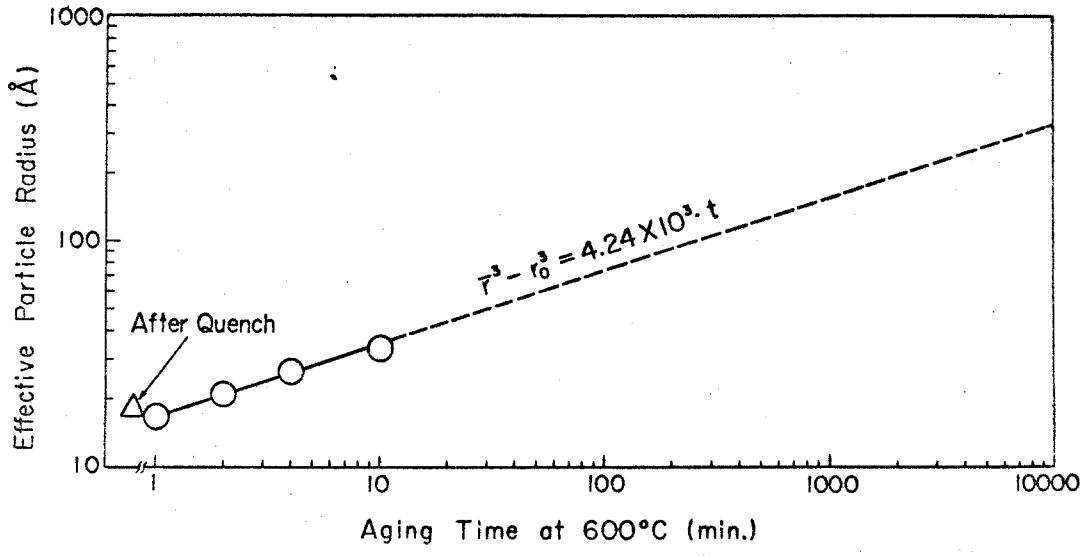

FIG. 42 Change in average precipitated particle size with aging time at 600°C for the Cu-3.52%Co alloy. The straight line was obtained by the extrapolation in Eq. VI-1.

there is an evidence that magnetic moments seems to exist at relatively high concentration specimens (>2%) which indicates the clustering of Co solute atoms.

Certainly, the magnetization curve obtained by the specimen after quench did not show the complete paramagnetic one, and the effective particle size was estimated to be about 20 Å in diameter whose value was identified to the nearly same after 1 minute aging, but the total magnetization at high appled field per sample 1 cc was less than that of the aged samples. Their result indicates the existence of the quenched-in cluster whose volume fraction is still less than precipitated particles. The particle size obtained from the subsequent aging periods more than 1 minutes increases gradually and can fit to the Eq. VI-1, so that the precipitation process in Cu-3.52at.%Co alloy can be consider to be the coarsening stage even for 1 minute aging at 600°C.

VI-2-2. Experimental Method of the Pulsed NMR Technique

For the observation of NMR signal, there are now two different type of techniques; one is contineous wave (steady state) excitations of nuclear spins and the other is transient (pulsed) excitations[1]. These two methods have different merit depending on what the nature of

observing signal is, particularly the broadness of NMR lines. In dense alloy system, however, it is generally accepted that the line width usually becomes broad due to many crystallographic effects[14] (e.g. disordered lattice, faulted planes, dislocations and so on), hence, the transient NMR method is suitable to detect its NMR signals. Therefore, the transient NMR method was utillized and so called "spin-echo" nuclear signal was observed. The technique of transient excitation of nuclear spins in ferromagnetic materials is by now well established[1], and has been fully described by many resonance workers. It consists of creating a nuclear spin-echo by applying to the sample two consecutive pulses of rf excitation and measure the amplitude of spin-echo as a function of frequency across the inhomogeneously broadened nuclear resonance line.
After ajusting the reciever system, including the tuning circuit in which the sample was placed, to a particular frequency, the pulsed rf frequency was tuned to a maximum echo signal. For the measurement of the echo amplitude, a pulsed calibrator signal produced by a standard signal generator was externally put on, and the amplitude of the of the calibrator signal was made equal to the amplitude of the echo signal, both being observed on the oscilloscope. The calibrator signal voltage was then taken as the amplitude of the nuclear signal at that frequency. The calibration

voltage accuracy was estimated to be less than 10%.

The separation between the rf pulses was kept (6μsec) small enough so that the echo decay to transverse relaxation negligible. In order to compensate for any change in exciting condition, the rf level was kept constant and the pulse width was ajusted at each point so that the echo siganal was a maximum. The strength of rf pulse field was typically order of 20 Oe and about 0.5∿∿2.0 μsec rf pulse width was used. The block diagram of the apparatus used in this study is shown in Fig. 43.

The NMR signals in precipitated Co-rich particles were observed below room temperature. The interpretations of the data were mostly made at 77°K. For the low temperature measurements, a exposed-tip liquid nitrogen and helium Dewar were used. The finger of the Dewar fitted inside of the tuning sample coil which is coupled to the rf transmiter and the receiver by low impeadance cables. The alloy powders were sealed off in glass tubes and placed inside of the finger of the Dewar. The sample tube (under a helium-gas atmosphere for the 4.2°K measurements) was about 10 mm in diameter for 77°K measurements and was about 7 mm in dia. for the 4.2°K measurements.

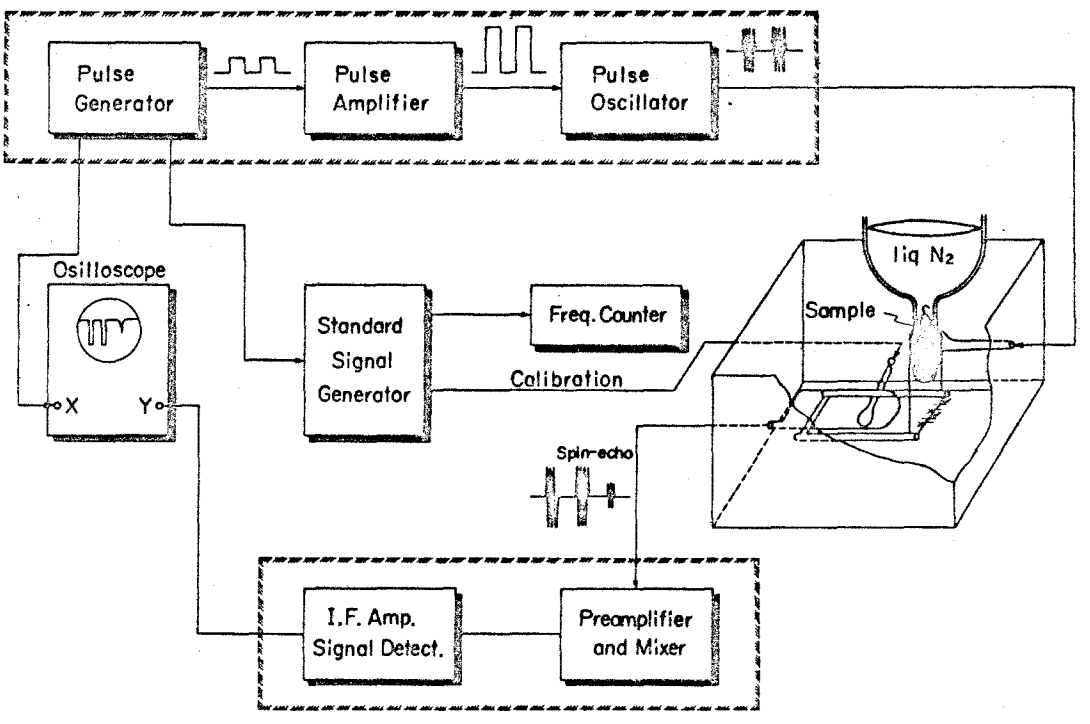

FIG. 43 Block diagram of the pulsed NMR system.

VI-3. Experimental Results and Interpretations

The Co^{59} NMR signals of precipitated Co-rich particles in Cu-3.52at.%Co alloy have been observed at temperatures below 300°K. Since essential features were not changed with temperature, the interpretation was mostly made for the data taken at 77°K.

VI-3-1. Frequency for Resonance and Spectra

The Co^{59} spin-echo signals were observed in samples whose precipitated particle size is greater than 100 Å. In the alloys, we found resonance spectra which consist of a main intense sharp line (M) and a weak somewhat broad line (N). Typical examples are shown in Fig. 44 for alloys aged for 100 minutes, 10 hours and 1 week at 600°C after solution heat treatment, respectively. In this figure, the observed spin-echo intensities were normalized at 217 MHz. The integrated spin-echo intensity was increasing with increasing the aging period, as a consequence of growing the precipitated size. This means, as a matter of cource, that the number of particles contributing to observe the spin-echo signal in multi-domain particles is increasing with increasing the aging period.

The main resonance peak has been observed in the

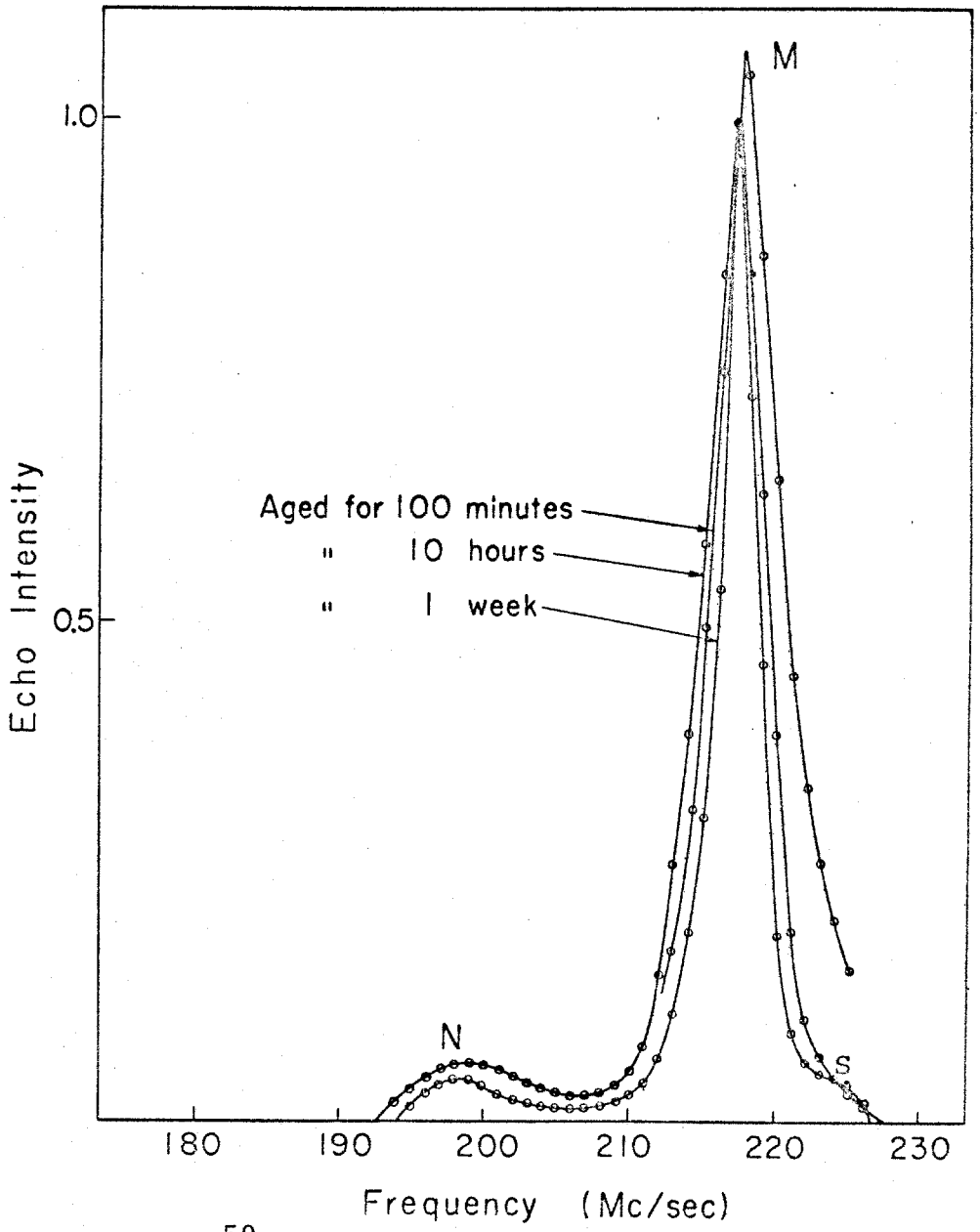

FIG. 44 The Co^{59} (spin-echo) resonance spectra in Cu-3.52%Co alloys which were aged at 600°C. Spectra were observed at 77°K. M : the Co^{59} resonance to the pure f.c.c. Co. N : the Co^{59} resonance which are nearest neighbor sites to the Cu impurity. S : the Co^{59} resonance in stacking faults. Data are uncorrected for the frequency dependence of signal amplitude. The observed echo intensity was normalized at 217 MHz.

frequency range 217 ∿ 219 MHz at 77°K for all aged samples. Since the observed frequencies are considerably lower than that of h. c. p. Co (227 MHz at 77°K[1]) and almost agree with that of pure f. c. c. Co (217 MHz at 77°K), the observed siganl was attributed to the resonance in f. c. c. particles. The reason for the slightly higher frequencies depending on the aging time in precipitated particles will be discussed as due to the internal stress in the following section (VI-3-2). It is then confirmed that the crystal structure od the precipitated particles is undoubtedly face centered cubic phase.

A satellite resonance line has been observed at lower frequency side (198 MHz at 77°K) than that of the main line in samples aged more than 155 minutes. The origine of satellite lines in ferromagnetic dilute Co alloys has been worked out for bulk materials and it is concluded that the lower frequency satellite is due to the Co atoms which are perturbed by the addition of the impurity[15]. Here, the discussion of the hyperfine field acting on the nucleus of Co atom disturbed by the nearest neighbor of an impurity is summarized. This should be worthwhile to give, since in the precipitated Co particles some Cu atoms are expected to be dissolved and it makes a possibility for the origine of the observed satellite resonance line.

In general, the hyperfine field, H_n, of a Co nucleus

is proportional to the local magnetization of itself and that of its nearest neighbor. The field at the Co atom at the i-th position is

$$H_n^{(i)} = a \cdot \mu_i + b \cdot \sum_{n.n.} \mu_{n.n.}, \qquad \text{(VI-3)}$$

where μ_i and $\mu_{n.n.}$ are the moments on the i-th and each of the nearest neighbor atoms respectively, and a and b are constants of proportionality determined empirically to be a=-39 KOe/μ_B and b=-7.3 KOe/μ_B. The magnetic moment of the Co atoms on the nearest neighbor sites of an impurity is given by

$$\mu_{n.n.} = 1.7 + (d\bar{\mu}/dc + 1.7)/12, \qquad \text{(VI-4)}$$

where $d\bar{\mu}/dc$ is the decrease of the average moment of the alloys with the concentration of the impurities. Then the field at the Co nucleus which is the nearest neighbors of an impurity in the f. c. c. lattice is given by

$$H_n = a \cdot \mu_{n.n.} + b \cdot (4\mu_{n.n.} + 7\mu_o + \mu_i), \qquad \text{(VI-5)}$$

where μ_o is the moment of Co which has no impurity in its nearest neighbor sites and so is $1.7\mu_B$ and μ_i is the moment of the impurity.

For the Co-Cu alloys, $d\bar{\mu}/dc$ was recently determined to be $-2.25\ \mu_B$/(Cu atom) by Crangle[16] and the magnetic moment of impurity Cu atom, μ_i^{Cu}, should be zero. Using Eq. VI-5, the value of hyperfine field of the Co nucleus which is the nearest neighbors of the Cu impurity is estimated to be -199 KOe. This value corresponds to the frequency for Co^{59} resonance of 199 MHz which agrees well with the frequency of the observed satellite line. Consequently, it is concluded that the observed satellite line is due to the Co^{59} resonance associated with the Co atoms which are nearest neighbor sites to the Cu impurity atoms dissolved in the precipitated particles. Once the resolved satellite line in the experimental spectrum is assigned to a given configuration of nearly the impurities, the ratio of the intensity of the main line in a perfectly random alloy is easily calculated statistically for f. c. c. lattice as

$$I' = N/M = 12(1 - c)^{11}c/(1 - c)^{12}, \quad \text{(VI-6)}$$

where c is the atomic concentration of the Cu impurity atoms. From the experimental integrated intensity ratio I' of the satellite to the main line, the concentration of the Cu atoms dissolved in the precipitated Co particles was estimated to be about 0.5%. Here we ignored the contribution of the

interface between precipitated particles and the alloy matrix to the resonance spectrum, since the Co atoms in the interface region has many impurity atoms in its nearest neighbors and the resonance frequency of such atoms will be distributed widely by the variety of configurations. The solubility of the Cu atom in the precipitated particle estimated from the NMR technique is extremely small compared to that expected from the equilibrium phase diagram, i.e. 10% at 600°C[17]. Any interpretations for the difference seem to be difficult, it should neverthless be pointed out that the precipitation process does not obey the usual equilibrium phase diagram and there is a tendency of the precipitation to for almost pure f. c. c. Co particles.

It was also found that the slight copper concentration in the precipitated particles is independent on the aging periods and/or the precipitated particle size within the experimental error. This suggests that the alloy composition of the precipitated particles does not change during the aging, since the stable phase is precipitated firstly.

As is seen in Fig.44 still more broad satellite line has been observed between 220 ∿225 MHz for 1 week aged sample. This line could be identified to due to the Co^{59} resonance in stacking faults and agree well to that of deformed Co powders observed previously[14]. The f. c. c. → h. c. p. transformation of the Co-rich particles in Cu matrix could

be induced by the heavy cold work[18, 19] as has been described in CHAPTER IV. The NMR technique may be a good tool for the study on the transformation of these precipitated particles.

VI-3-2. Particle Size Dependence of the Center Frequency

In this section, our attension will be concentrated to the particle size dependence of the center frequency of the main line. For all aged samples used in this study, the center frequency was slightly higher than that of the free f. c. c. cobalt metal and depends on the aging periods and/or the particle size. The experimental results obtained at 77°K and 4.2°K are shown in Fig. 45. The particle sizes in abscissa were obtained from the extrapolation of the kinetic Eq. VI-1.

For the interpretation of the experimental results, we can recall the pressure dependence of the Co^{59} resonance frequency in f. c. c. Co. It has been studied and the pressure dependence of the resonance frequency was determined to be[20]

$$\partial\nu/\partial p = +0.135 \text{ MHz/Kbar.} \qquad \text{(VI-7)}$$

From this pressure studies of free f. c. c. Co, the shifts of the center frequency in Fig. 45 was attributed to the

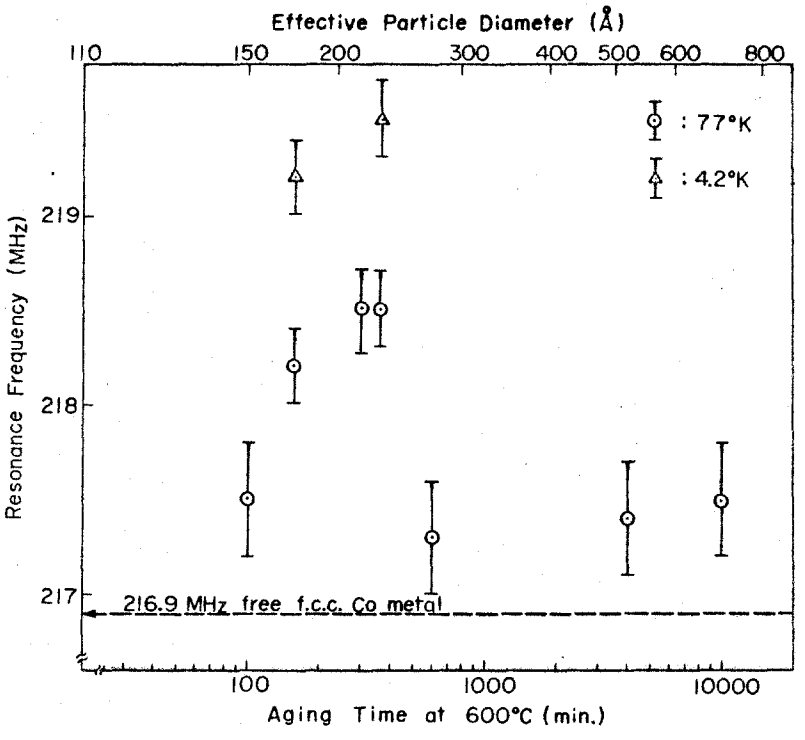

FIG. 45 Aging periods and/or particle size dependence on the center frequency of the main line.

effect of internal stress acting on the precipitated particles. The value of the effective pressure increased gradually with the aging periods from 100 minutes to 300 minutes, and then reached at maximum value which was estimated to be about 12 Kbar from Eq. VI-7. The most interesting feature of this study is that after the arrival to the maximum value of the internal stress, it was abruptly diminished at the particle size of about 300 Å and became independent on particle size. This effect may be attributed to the loss of full coherency between the precipitates and the Cu matrix. The electron microscope analysis of Servi[5] and Phillps[4] is indicating this effect at the particle size of 400∿600 Å in diameter and fairly agrees with present results. However, we beleive that present NMR detection of this effect should be much sensitive than the electron microscope technique.

VI-4. Conclusions

The most important result in this CHAPTER is that a nuclear magnetic resonance signal is observable in precipitated particles in Cu-Co alloy matrix with a relatively weak satellite in lower frequency side. The frequency of the main line is about the same as that of the free f. c. c. Co. This reveals immediately that the crystal structure of the precipitated particle is face centered cubic. The weak

satellite line was attributed with the Co atoms being the nearest neighbor sites to the dissolved Cu atoms.

From the intensity ratio of the main line to the satellite line, the Cu concentration in precipitated Co particles was estimated to be about 0.5% which is suprisingly small compared to that expected from the phase diagram. It is also found that the concentration is independent of the aging period of aging treatment, that is, independent of the particle size.

Careful measurements of the particle size dependence of the center frequency of main line yields a maximum value of the internal stress acting on the precipitated particles of about 12 Kbar. The stress was abruptly diminished at the particle size of about 300 Å as a result of lossing of full coherency between the precipitates and the Cu matrix.

A much weak and broad satellite line associated with Co^{59} nuclei in stacking faults was also observed in long period aged samples at higher frequency side of the main line.

The present work described in this CHAPTER is probably the first example to data where NMR sgnals have been observed and provided some informations from the microscopic standpoints in precipitated particles.

REFERENCES

1. A. M. Portis and R. H. Lindquiat; "Magnetism, vol. II Part A", edited by G. T. Rado and H. Suhl (Academic Press, New York, 1965).

2. A. Kelly and R. B. Nicholson; "Progress in Materials Science, vol. 10", edited by B. Chalmers (Pergamon Press, 1961).

3. J. D. Livingston; Trans. A. I. M. E., 215 (1959) 566.

4. V. A. Phillips; Trans. A. I. M. E., 230 (1964) 967.

5. L. E. Tanner and I. S. Servi; Acta Met., 14 (1966) 231.

6. C. P. Bean and J. D. Livingston; J. Appl. Phys., 30 (1959) S-120.

7. J. J. Becker; Trans. A. I. M. E., 209 (1957) 59.

8. J. D. Livingston; Trans. A. I. M. E., 215 (1959) 566.

9. G. W. Greenwood; Acta Met., 4 (1956) 243.

10. J. M. Lifshiftz and V. V. Slyozov; J. Phys. Chem. Solids, 19 (1961) 35.

11. C. Wagner; Z. Elektrochem., 65 (1961) 581.

REFERENCES (CONT.)

12. I. S. Jacobs and R. W. Schmitt; Phys. Rev., 113 (1959) 459.

13. G. J. Van Der Berg, J. Van Herk and B. Knook; "Proceedings of the 10th International Conference on Low Temperature Physics, Moscow, 1966, vol. 4", p.272.

14. R. Street, D. S. Rodbell and W. L. Roth; Phys. Rev., 121 (1961) 84.

15. S. Kobayashi, K. Asayama and J. Itoh; J. Phys. Soc. Japan, 21 (1961) 65.

16. J. Crangle; Phil. Mag., 46 (1955) 525.

17. M. Hansen and K. Anderko; "Constitution of Binary Alloys, vol. 1", (Mcgraw-Hill, 1958).

18. N. Tamagawa and T. Mitui; J. Phys. Soc. Japan, 20 (1965) 1988.

19. S. Nasu, Y. Murakami, Y. Nakamura and T. Shinjo; Sripta Met., 2 (1968) 647.

20. D. A. Anderson and G. A. Smart; J. Appl. Phys., 35 (1964) 3043.

APPENDIX

SUPERPARAMAGNETIC PARTICLES

The energy of a single domain particle with uniaxial anisotropy as a function of the angle α between the magnetization and the easy direction is given by

$$F_T = K \cdot V \sin^2 \alpha \ ,$$

where K depends on the anisotropy but is a constant for a given particle. It follows that for shape anisotropy $K=1/2 \cdot \Delta N \cdot I_s^2 = (D_b - D_a) \cdot I_s^2$, for crystalline anisotropy $K=K_1'$, whereas for strain anisotropy $K=3/2 \cdot \lambda^2 \cdot E$. The dependence of the energy F_T on α is shown graphically in Fig. 46. Either $\alpha=0$ or π is obviously a direction of minimum energy, and these directions are separated by an energy barrier of height KV. The magnetization will remain stable and lie along the direction defined by $\alpha=0$ or by $\alpha=\pi$ unless some perturbing force exists that can take the magnetization over the energy barrier. Thermal agitation may provide such a pertubation. This process is most likely to occur if the volume V of the particle is small, so that the height of the energy barrier is lowered, or if the temperature T is high. Particles whose magnetization changes spontaneously are analogous to paramagnetic atoms, except that their magnetic moment is much larger. Such particles are said to exhibit

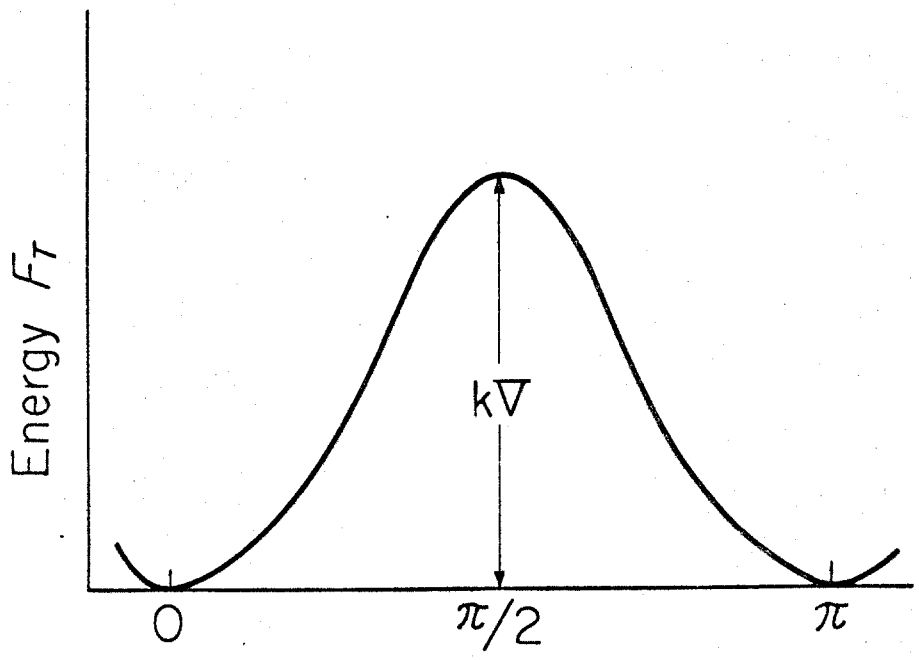

FIG. 46 The energy F_T of a single domain particle with uniaxial anisotropy as a function of the angle α between the magnetization and the easy direction.

superparamagnetism; their existence was first predicted by Néel.

The process may be characterized by a relaxation time τ. For exsample, consider a powder of uniaxial particles whose easy directions all lie along the z-axis. Now $1/\tau$ is the probability per second for a single transition of the magnetization from a +z- to a -z-direction, plus that for the transition from -z to +z. Thus $1/\tau$ must be proportional to the Boltzmann factor $e^{-KV/kT}$, since KV is just the activation energy for a transition. The constant of proportionality may be estimated from the following argument. The upper limit for $1/\tau$ must be given by the frequency of precession from a +z- to a -z-direction, namely $\gamma H_{crit.}/2\pi$, where $H_{crit.}$ is the eqivalent applied field necessary to produce a magnetization reversal in a stable particle. Thus $H_{crit.}$ is given by K/M, regardless of the type of anisotropy present. Since $\gamma \simeq 10^7$, the order of magnitude of $\gamma K/2\pi M$ is 10^9 or 10^{10}.

Thus we have

$$1/\tau = (10^9 \text{ or } 10^{10}) \cdot \exp(-KV/kT).$$